ISSN: 2708-7956

الأكاديمية
للهندسة والعلوم

Academic
For Engineering and Science

مجلة علمية محكمة فصلية
تصدر عن نقابة الأكاديميين العراقيين
المجلد (4) العدد (3)
آب - السنة 2022

رقم الإيداع في الدار الوطنية
2422 لسنة 2020

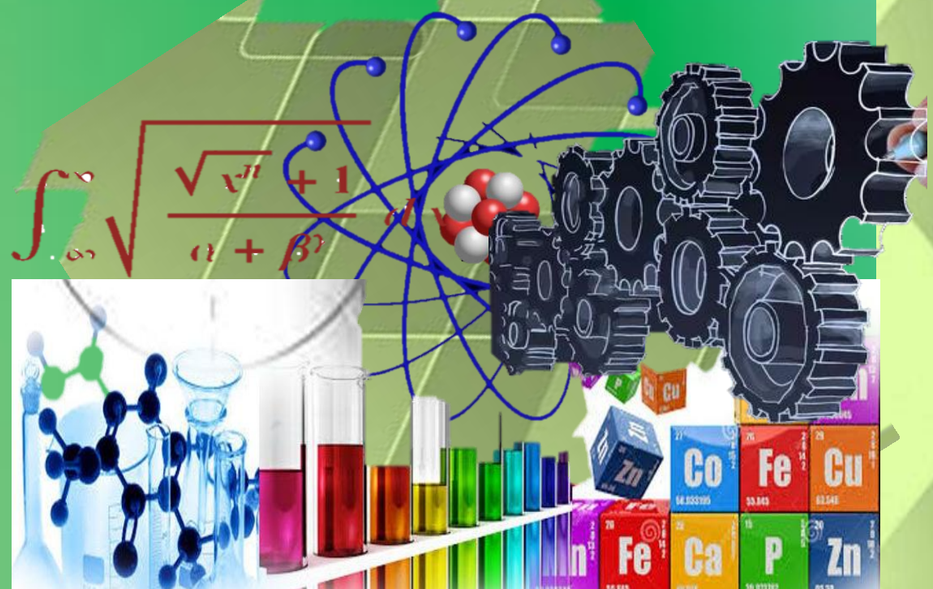

الأكاديمية للهندسة والعلوم
http://aphjournal.iraqiacademic.com
ISSN: 2708-7956 DOI prefix: 10.47719

الأكاديمية

للهندسة والعلوم

Academic

For Engineering and Science

مجلة علمية محكمة فصلية

تصدر عن نقابة الأكاديميين العراقيين

المجلد (4) العدد (3)

2022 /8/ 15

هيئة التحرير

الهيئة الاستشارية

كـــلمة العدد (3) لسنة (2022)

يسعدنا ان نقدم لكم **العدد الثالث/ السنة 2022** لمجلة **الأكـاديمـية للهندسة والعلوم**. أود أن اسجل شكري الجزيل للجهود الكبيرة لكل من ساهم في إظهار هذا العدد. كما أتقدم بالشكر لجميع الباحثين الذين دعموا المجلة من خلال نشر أبحاثهم فيها، خاصاً بعد حصول المجلة على الرقم المعّرف **DOI** في عام 2020.

ضم هذا العدد، بحوث في مختلف المجالات العلمية، هي: الهندسة، والفيزياء، والاستشعار عن بعد، التحليل الإحصائي والرياضيات.

نأمل أن تحقق مجلة الأكاديمية للهندسة والعلوم، من خلال هذه الطبعة، تطلعات الباحثين والمهتمين، وأن نسعى، بعون الله تعالى، إلى تطوير مجلتنا نحو الأفضل، وأن يكون لها حضورا علميا متميزا إقليمياً وعالمياً، ونتطلع ان تكون المجلة في التصنيفات العلمية الدولية.

مع خالص التقدير

أ. د. أحمد كمال أحمد
رئيس هيئة التحرير
آب - 2022

نبـــــذة عن
نقابة الاكاديميين العراقيين

أسست نقابة الأكاديميين العراقيين بموجب القانون رقم (61) لسنة (2017)، بغية الاهتمام بالملاك التدريسي والأكاديمي (الأكاديمي: التدريسي الحاصل على شهادة الماجستير أو الدكتوراه ويمارس مهنة التدريس أو يعمل بمراكز البحث العلمي في الجامعات).

والارتقاء بمستوى العاملين في هذا القطاع الحيوي وإعداد الخطط والسياسات التي ترتقي بالعملية التدريسية ومن أجل إنشاء مجالس ونقابات تهتم بشؤون الأكاديميين والدفاع عنهم وحفظ كرامتهم وضمان حرياتهم الأكاديمية، ومن أجل رفع سمعة الجامعات والمعاهد العراقية ومساواتها مع مثيلاتها في الدول المتحضرة. ووفقاً للمادة –2– من البند الثاني من قانونها فأنها:

أولاً: تتمتع نقابة الأكاديميين العراقيين بالشخصية المعنوية والاستقلال المالي والإداري يمثلها (نقيب الأكاديميين العراقيين) أو من يخوله.

ثانياً: يكون مركز النقابة في بغداد ولها فتح فروع في المحافظات وحيثما تقتضي مصلحة النقابة إيجاد تمثيل.

ثالثاً: لأعضاء الهيئات التدريسية في الجامعات والمعاهد العراقية المعترف بها من وزارة التعليم العالي والبحث العلمي الانتماء إلى النقابة.

ووفقاً للمادة –3– فأن أهداف تأسيس النقابة هي:

أولاً: الارتقاء بمهنة التعليم العالي والبحث العلمي لتحقيق رسالتها في خدمة الوطن وأجيال الأمة.

ثانياً: التنسيق والتعاون مع وزارة التعليم العالي والبحث العلمي والجهات ذات الصلة بما يحقق مهام النقابة.

ثالثاً: تعزيز أخلاقيات مهنة التعليم العالي والمحافظة على آداب وتقاليد وشرف المهنة.

رابعاً: تشجيع الدراسات والبحوث والنشاطات والمؤتمرات التعليمية وعقد الدورات والندوات لرفع المستوى العلمي والمهني لتدريسي الجامعات والمعاهد العراقية.

خامساً: تعزيز مكانة الأكاديميين في المجتمع والدفاع عن حقوقهم ومصالحهم وكرامتهم.

سادساً: النهوض والارتقاء بالأعضاء مهنياً واقتصاديا وثقافياً واجتماعياً.

سابعاً: تأسيس صندوق للتكافل الاجتماعي لمساعدة أعضاء النقابة، يؤمن لهم ولأسرهم العيش الكريم في حالات العجز الكامل أو الوفاة وتوفير الرعاية الصحية للأعضاء وأسرهم.

ثامناً: التعاون وتوطيد العلاقات مع الاتحادات العربية والدولية المماثلة.

أ. م. د. مهـند الهـلال
نقيب الاكاديميين العراقيين

المحتوى (العدد 3 لسنة 2022)

أهداف ورؤية المجلة Aims and Scope

- تنشر المجلة الدراسات العلمية ذات الأفكار الأصيلة والحديثة والمتجددة، ويحوت الرسائل والأطروحات، التي لم يسبق نشرها أو المساهمة بها في أحد الملتقيات العلمية، وان تكون هذه البحوث مندرجة ضمن أحد المحاور تخصصات الهندسية والعلوم الصرفة.
- كما تنشر المجلة الكتب المؤلفة والمترجمة ضمن التخصصات أعلاه.

الوصول المفتوح للبحوث Open Access Policy

مجلة **الأكاديمية للهندسة والعلوم** هي مجلة مفتوحة الوصول، بالتالي لا توجد رسوم مطلوبة لتنزيل أي منشور من موقع المجلة من قبل المؤلفين والقراء والمؤسسات، وعلى الموقع:
http://aphjournal.iraqiacademic.com/Journal/GetAllVersions

قواعد النشر:

- البحوث المرسلة إلى المجلة يجب أن تكون سليمة من الأخطاء اللغوية والمنهجية والمعرفية، وملتزمة بالأعراف العلمية المتبعة، ولم يسبق نشرها.
- لا ينبغي أن يتحاوز عدد صفحات البحث عن خمسة عشر ورقة من حجم B5.
- في حالة وجود هوامش في اسفل الصفحة ينبغي اعتماد ترقيم آلي يتجدد في كل صفحة.
- يتضمن البحث ملخصين: الأول بلغة البحث، والثاني باللغة العربية أو الإنجليزية.
- تخضع جميع البحوث للتحكيم العلمي على نحو سري، ويخبر الباحث إما بقبول بحثه، أو بالقبول المشروط ببعض التعديلات التي يبلغ بها، أو بالرفض. وفي هذه الحالة الأخيرة؛ فإن المجلة ليست ملزمة ببيان الأسباب.

توصيات تقنية في كتابة البحوث:

- مقاس الورقة والهوامش: الورقة حجم B5، ويترك هامش بمسافة 2 سم من حواشي الورقة. مع مسافة 1 سم بين الأسطر في المتن والهوامش.
- يُعتمد الخط **Simplified Arabic** (البحوث باللغة العربية)/ و **Times New Roman** (البحوث باللغة الإنكليزية)، مقاس 16 غامق عنوان البحث، مقاس 14 غامق العناوين الأساسية، مقاس 12 غامق العناوين الفرعية، وبمقاس 12 في المتن، مقاس 11 غامق لعناوين الأشكال والجداول، 10 في الحواشي.

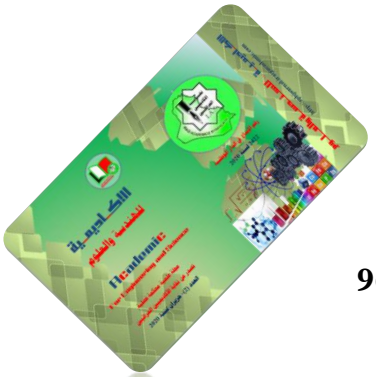

معلومات الاتصال:

- **موقع المجلة:** http://aphjournal.iraqiacademic.com/

ISSN: 2708-7956, DOI prefix: 10.47719

- **البريد الإلكتروني للمجلة:** info@iraqiacademics.iq
dr.ziadmabood@gmail.com

- **أرقام الهواتف: 9647709298631 -9647902746409**

- **رقم الإيداع في الدار الوطنية 2422 لسنة 2020**

Effect of Titanium Doping on the Structural and Optical Properties of ZrO_2 Thin Films Prepared by Spray Pyrolysis Method

Sami Salman Chiad
Department of Physics, College of Education, Mustansiriyah University, Baghdad, Iraq.

Abstract

The inquiry of structural and, optical properties of undoped ZrO_2 and ZrO_2: Ti films deposited by spray pyrolysis method were studied. XRD anaylsis clarifies that undoped undoped ZrO_2 and ZrO_2: Ti films are polycrystalline and preferred orientation is (111). The grain size for undoped ZrO_2 showed an increased from 10.58 nm to 12.13 nm on Titanium doping, whereas the strain (%) parameter decreased from 32.76 to 28.56. Optical transmittance value of ZrO_2 and ZrO_2: Ti films reaches 68 % in the visible regions, which declines as the doping concentration increases. . Optical energy gap for ZrO_2 and ZrO_2: Ti doping with 2% and 4% were 5.22, 5.16 and 5.10 eV respectively. The results of absorption coefficient (α) undoped and Ti -doped ZrO_2 films showed an increase with increasing of Titanium concentration, whereas extinction coefficient and refractive index decreased with increasing of Titanium concentration.

Keywords: ZrO_2, Ti, thin films, structural and optical properties, energy gap.

تأثير التشويب بالتيتانيوم على الخصائص التركيبية والبصرية لأغشية أوكسيد الزركونيوم الرقيقة المحضرة بطريقة التحلل الحراري

سامي سلمان جياد
قسم الفيزياء، كلية العلوم التربية، الجامعة المستنصرية

المستخلص

تمت دراسة الخواص التركيبية والبصرية لأغشية أوكسيد الزركونيوم غير المشوب والمشوب بالتيتانيوم باستخدام تقنية التحلل الحراري . اثبت تحليل حيود الاشعة السينية بان أغشية أوكسيد الزركونيوم غير المشوب والمشوب بالتيتانيوم كانت متعددة التبلور وباتجاه سائد (111). وجدب بان الحجم الحبيبي لأوكسيد الزركونيوم غير المشوب يزداد من 10.58 نانومتر إلى 12.13 نانومتر عند التشويب بالتيتانيوم، بينما قلت المطاوعة المايكروية من 32.76 إلى 28.56. تبلغ نفاذية أغشية أوكسيد الزركونيوم غير المشوب والمشوب بالتيتانيوم ا بحدود 68٪ في النطاق المرئي، والتي تنخفض مع زيادة تركيز التشويب. وجد ان قيمة فجوة الطاقة الضوئية لأغشية أوكسيد الزركونيوم غير المشوب والمشوب بالتيتانيوم بنسبة 2٪ و4٪ كانت 5.22 و5.16 و5.10 الكترون فولت على التوالي .أظهرت النتائج ان معامل الامتصاص لأغشية أوكسيد الزركونيوم غير المشوب والمشوب بالتيتانيوم يزداد مع زيادة تركيز التيتانيوم، بينما انخفض الخمود ومعامل الانكسار مع زيادة تركيز التيتانيوم.

الكلمات الافتتاحية: أوكسيد الزركونيوم، تيتانيوم، أغشية رقيقة، الخصائص التركيبية والبصرية، فجوة الطاقة.

Introduction

Zirconium oxide (ZrO_2) is an important metal oxide [1-3]. It possesses a wide bandgap, high refractive index, high thermodynamic stability, low electrical conductivity, and transparency in the visible region [4-6]. ZrO_2 has three crystal structures, including monoclinic at ambient temperature, tetragonal phase at 1170 °C, and cubic structure at 2370 °C [7]. Zirconia can transfer in a direct or indirect way [8, 9]. It is an important material because of its high corrosion resistance [10]. Zirconia was used in many applications like, It is an important material because of its high corrosion resistance [8, 10]. Optoelectronic devices [11], high power lasers [12], light emitting diodes [13], superconducting coatings [14], and gas sensors [15]. The deposition of zirconia films was

done via a variety of techniques like RF sputtering, electrochemical deposition, lasma spraying, spray pyrolysis, chemical vapour deposition, pulsed laser deposition and sol-gel method [16–20]. The spray pyrolysis method is very suitable for metal oxide thin films [21,22]. This research aims to study some structural and optical of zirconia and Titanium doping with 2% and 4% thin films deposited by SPT on class substrates kept at a temperature of 400 °C.

Experimental

By using the spray pyrolysis method, Undoped ZrO_2 and Ti doped ZrO_2 films were deposited on a glass substrate. 0.1 M of ($ZrCl_2.2H_2O$) was dissolved in deionized water. The obtained doping agent was 0.1 M of TiCl was applied as 2% and 4%. Following many experimental procedures, the following preparation conditions were reached: During the deposition process, the substrate's temperature was maintained at 400°C. The distance between the substrate and the nozzle was maintained at 28 cm [16] while nitrogen was used as the carrier gas. Spraying time, spraying rate and the time interval between two spray process was 9 S, 4 mL/min and 1.5 min accordingly. Film thickness was evaluated by weighing method and was 335± 225 nm, By using an X-ray diffractometer (Shimadzu, model: XRD-6000, Japan), structural coefficients were calculated. Using a UV-visible double beam spectrophotometer, the transmittance and absorbance spectra are captured in the wavelength range (300–900 nm).

Results and discussion

Three XRD patterns of the deposited film are displayed in Figure 1, with the (2θ~31.35°, 34.18°, 49.32° and 54.67°) referred to (111), (200), (220) and (003) planes, respectively. These spectra indicated that the films were polycrystalline and fit well with ICDD card No. no 27-0997. The highest peak intensity of (200) was also observed when ZrO_2 deposition ratios at 2% and 4% Ti.

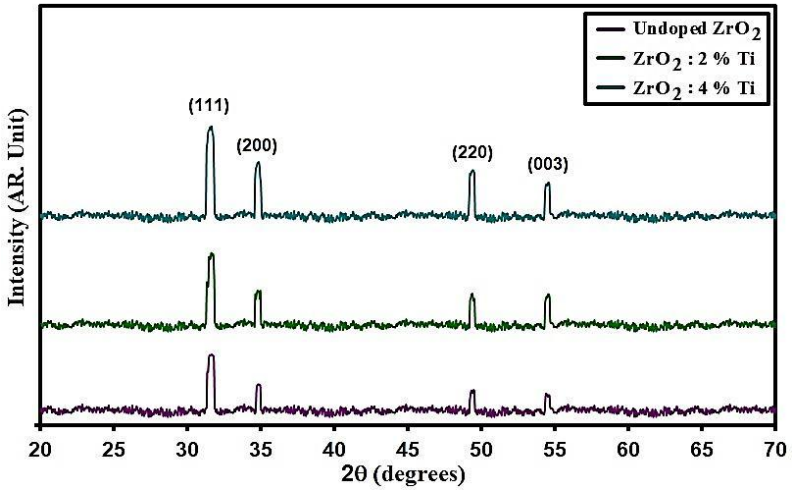

Fig. 1 : XRD-patterns crystalline size of intended films.

Using Scherrer's equation, the average grain size (D) was determined from the highest intensity peaks. [23]:

$$D = \frac{0.9\lambda}{\beta cos\theta} \qquad (1)$$

Where λ is the wavelength of the X-rays (0.1541 nm), β and θ are full width at half maximum (FWHM) and the diffraction angle respectively. The Grain size has been found to vary from 10.58 to 12.13 nm with Titanium concentration as listed in Table. 1

Table 1. Grain size, optical band gap and structural parameters of the prepared films.

Doping (%)	2 θ (º)	(hkl) Plane	FWHM (º)	Optical bandgap (eV)	Grain size (nm)	Dislocations density ($\times 10^{14}$)(lines/m^2)	Strain ($\times 10^{-4}$)
Undoped ZrO_2	31.35	111	0.78	5.22	10.58	89.33	32.76
ZrO_2: 2% Ti	31.32	111	0.73	5.16	11.30	78.31	30.66
ZrO_2: 4% Ti	31.29	111	0.68	5.10	12.13	67.96	28.56

Additionally, dislocation density (δ) and other structural factors like dislocation strain (ε) are assessed. δ gives number of defects in the films, the values of (δ) and (ε) listed in Table. 1 shows the structural parameters estimated from [24]:

$$\delta = \frac{1}{D^2} \qquad (2)$$

$$\varepsilon = \frac{\beta cos\theta}{4} \qquad (3)$$

Figure (2) displays each β, *D*, δ and ε versus doping.

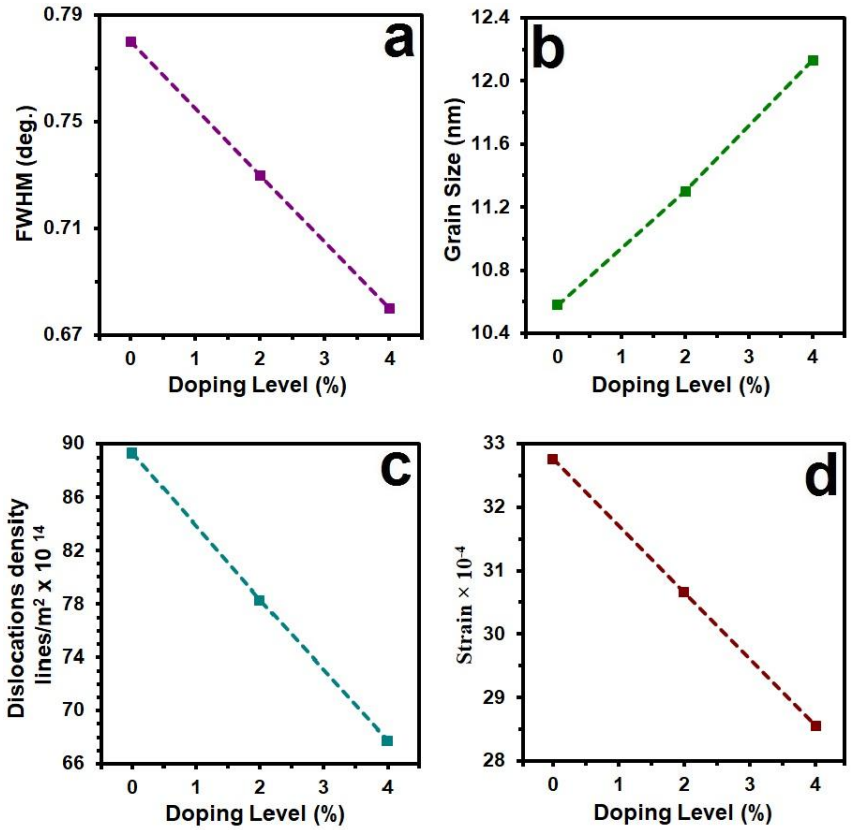

Fig.2. FWHM (a) Grain size (b) Dislocation (c) Strain (d) of the prepared films.

Figure 3 shows the transmittance (T) spectra of the prepared films. All films have more than 70% visible transparency, which guarantees that they are homogeneous and may be the result of crystallinity increase. Low light scattering and increased transparency are achieved by large grains.

Transmittance was shown to decrease when titanium dopants were used [25].

The following equation (4) was used to get the films' absorption coefficient (α) [26]:

$$\alpha = \frac{\ln(1/T)}{d} \qquad (4)$$

Where d is film thickness.

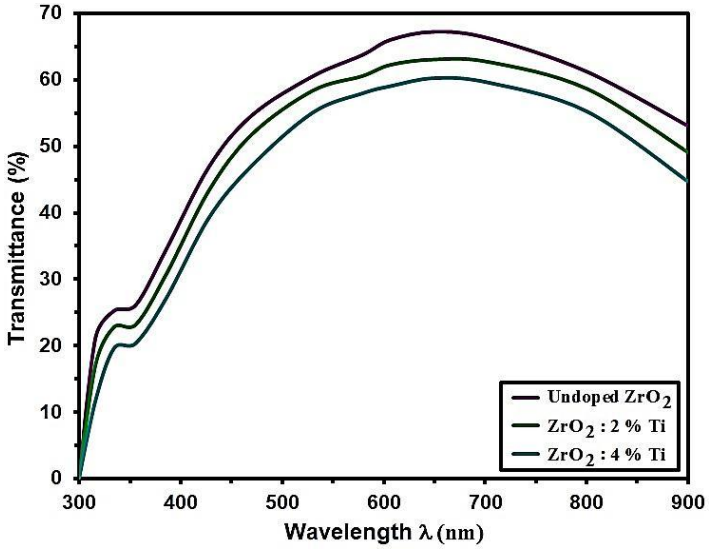

Fig. 3. Transmittance as Function to the Wavelength of deposited thin films by (CSP).

Figure 4 plots the variation of (α) versus against photon energy hv, the absorption coefficient increase with increasing of Titanium concentration.

Equation (5) can be used to estimate the energy gap E_g [27].

$$\alpha h\nu = (h\nu - E_g)^{1/2} \qquad (5)$$

Where, A is a constant. E_g values can be evaluated from the plots of $(\alpha h\nu)^2$ versus energy plots to intercept the photon energy axis [28] (see Figure 5). Energy gap is set to vary among (5.22 -5.10) eV.

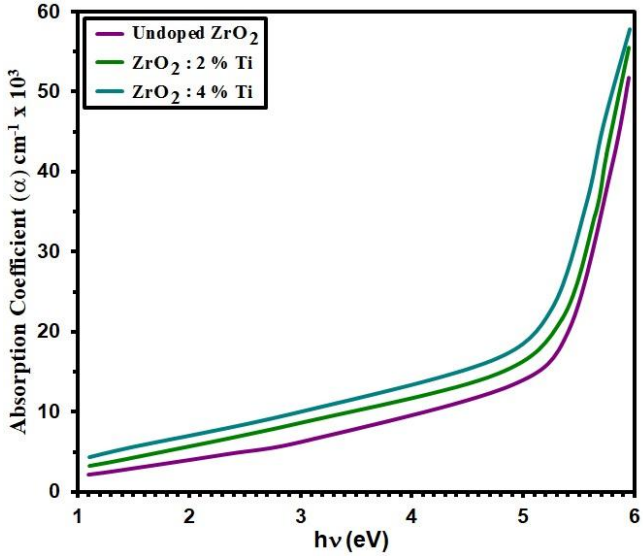

Fig. 4. Absorption coefficient with photon energy $h\nu$ in respectively of deposited thin films by (CSP).

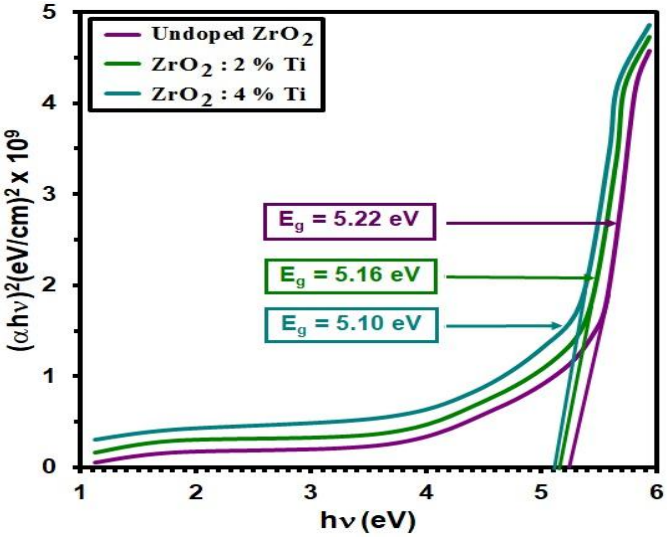

Fig. 5. Shown the energy band gap of deposited thin films by (CSP)

Using the following equation (6), the refractive index (n) can be determined from film reflectance (R) [29].

$$n = \left(\frac{1+R}{1-R}\right) + \sqrt{\frac{4R}{(1-R)^2} - k^2} \qquad (6)$$

Where (k) is the extinction coefficient [30]:

$$k = \frac{\alpha\lambda}{4\pi} \qquad (7)$$

In Figs. 6 and 7, the values of (n) and (k) as a function of wavelength are displayed, and it is clear that Titanium doping causes these two parameters to decreased. High inherent free carrier densities in the conduction band are responsible for this behavior [31].

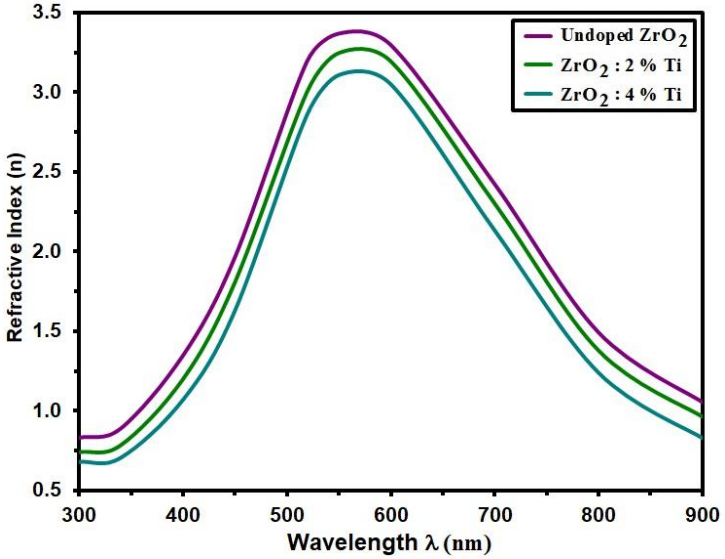

Fig. 6. refractive index of deposited thin films

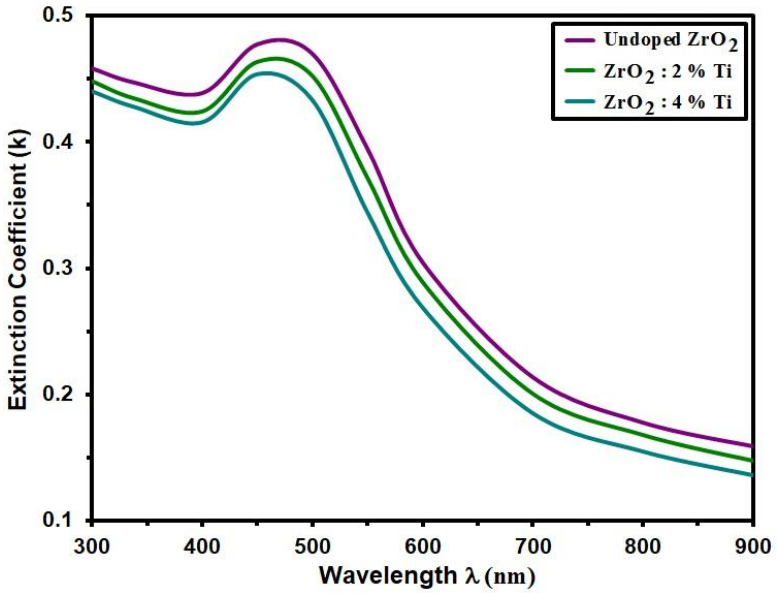

Fig. 7: extinction coefficient of deposited thin films.

Conclusions

Undoped ZrO_2 and ZrO_2: Ti films were prepared by the spray pyrolysis method method. XRD approve that these films were polycrystalline monoclinic structure with a maximum peak at (111) resulting of the Titanium, The Grain size for pure ZrO_2 showed a increased from 10.58 nm to 12.13 nm on doping, whereas the dislocation density an strain (%) parameter decreased from (89.33 to 67.96 and (14.3 to 12.7), transmittance decreased by the increment Titanium doping, Optical bandgap decreased from 5.22 to 5.10 eV with the increasing of Titanium dopants. also The absorption coefficient, refractive index and extinction coefficient decreased via Titanium contents.

References

[1] Li, W., Liu, X., Huang, A., Chu, P. K.: Structure and properties of zirconia (ZrO_2) films fabricated by plasma-assisted cathodic arc deposition. J. Phys. D. Appl. Phys. 40, 2293(2007).

[2] Ma, C.Y., Laspostolle, F., Briois, P., Zhang, Q.Y., " Effect of O_2 gas partial pressure on structures and dielectric characteristics of rf sputtered ZrO_2 thin films," Appl. Surf. Sci. 253, 8718 (2007).

[3] Wong, Y.H., Cheong, K.Y., "Band alignment and enhanced breakdown field of simultaneously oxidized and nitrided Zr film on Si. Nanoscal," Res. Lett.6, 489(2011).

[4] Khojier, K., Savaloni, H., Jafari, F., "Structural, electrical, and decorative properties of sputtered zirconium thin films during post-annealing process," J. Theor. Appl. Phys.7, 55 (2013).

[5] Shen, Y., Shao, S., Yu, H., Fan, Z., He, H., Shao, J., "Influences of oxygen partial pressure on structure and related properties of ZrO_2 thin films prepared by electron beam evaporation deposition," Appl. Surf. Sci. 254, 552(2007).

[6] Rebib, F., Laidani, N., Gottardi, G., Micheli, V., Bartali, R., Jestin, Y., Tomasella, E., Ferrari, M., Thomas, L., " Investigation of structural and optical properties of sputtered zirconia thin films," Eur. Phys. J. Appl. Phys.43,363(2008).

[7] F. Davar, A. Hassankhani, M.R.L. Estarki, Ceram. Int. 39, 2933 (2013).

[8] F. Heshmatpour, R. B. Aghakhanpour, Powder Technol. 205, 193 (2011).
[9] M. Andrieux, P. Ribot, C. Gasquères, B. Servet, C. Garry, Appl. Surf. Sci.263, 284 (2012).
[10] J. Gao, Y. He, D. Wang, "Fabrication and high temperature oxidation resistance ZrO2/Al2O3 microlaminated coatings on stainless steel," Mater. Chem. Phys.123731-736 (2010).
[11] S. Venkataraj et al., "Structural and optical properties of thin zirconium oxide films by reactive direct current magnetron sputtering," J. Appl. Phys.92(7)3599-3607(2002)..
[12] R.W. Lambert et al., "Facet passivation processes for the improvement of Al-containing semiconductor laser diodes," J. Light Technol. 24(2)(2006)956-961.
[13] K. Joy et al., "Effect of sol concentration on the structural, morphological, optical and photoluminescence properties of zirconium thinfilms," Thin Solid Films. 520, 2683-2688 (2012).
[14] Y. S. Yang et al., "Ferroelectricity and electric conduction characteristics of Sr-modified lead zirconium titanate thin film capacitors," J. Appl. Phys. Part I. 36(2) 749-753 (1997).
[15] L. A. Peyser et al., "Photoactivated fluorescence from individual silver nanoclusters," Science.291,103-106(2001).
[16] Zhao, S.; Ma, F.; Xu, K. W.; Liang, H. F. Optical properties and structural characterization of bias sputtered ZrO_2 films. J. Alloy Compd. 2008, 453, 453–457.
[17] Stefanov, P.; Stoychev, D.; Valov, I.; Kakanakova-Georgieva, A.; Marinova, T.S. Electrochemical deposition of thin zirconia films on stainless steel 316 L. Mater. Chem. Phys. 2000, 65, 222–225.
[18] García-Hipólito, M.; Alvarez-Fregoso, O.; Martínez, E.; Falcony, C.; Aguilar-Frutis, M.A. Characterization of ZrO_2:Mn, Cl luminescent coatings synthesized by the Pyrosol technique. Opt. Mater. 2002, 20, 113–118.
[19] Burleson, D. J.; Roberts, J. T.; Gladfelter, W. L.; Campbell, S. A.; Smith, R. C. A Study of CVD Growth Kinetics and Film Microstructure of Zirconium Dioxide from Zirconium Tetra-tert-Butoxide. Chem. Mater. 2002, 14, 1269–1276.
[20] Lee, J.S.; Matsubara, T.; Sei, T.; Tsuchiya, T. Preparation and properties of Y_2O_3-doped ZrO_2 thin films by the sol–gel process. J. Mater. Sci. 1997, 32, 5249–5256.
[21] Godbole B. Badera N. Shrivastav S. B. and Ganesan V, 2009 J. l. of Instrum. Soc. of India 391.
[14] Hadi, E. H., Sabur, D. A., Chiad, S. S., Habubi, N. F., Abass, K. H., Physical properties of nanostructured li-doped zro_2 thin films, Journal of Green Engineering, 10(10), pp. 8390-8400, 2020.
[22] Muhammad, S. K., Dawood, M. O., Ahmed, N. Y., Hassan, E. S., Habubi, N.F., Chiad, S.S., Optical and Structural characterization of spraying ZrO_2 and doped B: ZrO_2 thin films, Journal of Physics: Conference Series, 1660(1), 2020.
[23] Zhu, L.Q., Fang, Q., He, G., Liu, M., Zhang, L. D.: Microstructure and optical properties of ultra-thin zirconia films prepared by nitrogen-assisted reactive magnetron sputtering. Nanotechnology, 16, 2865 (2005).
[24] Yusoh, R., Horprathum, M., Eiamchai, P., Chindaudom, P., Aiempanakit, K.: Determination of optical and physical properties of ZrO_2 films by spectroscopic ellipsometry. Procedia Eng. 32, 745 (2012).
[25] Shen, Y., Shao, S., Yu, H., Fan, Z., He, H., Shao, J.: Influences of oxygen partial pressure on structure and related properties of ZrO_2 thin films prepared by electron beam evaporation eposition. Appl. Surf. Sci. 254, 552 (2007).

[26] Joy, K., Berlin, I. J., Nair, P. B., Lakshmi, J. S., Daniel, G. P., Thomas, P. V.: Effects of annealing temperature on the structural and photoluminescence properties of nanocrystalline ZrO_2 thin films prepared by sol–gel route. J. Phys. Chem. Solids 72, 673 (2011).
[27] Yildiz, K., Akgul, U., Coskun, B., Atici, Y.: Rf-sputtering deposition of nano-crystalline zirconia thin films with high transparency. Mater. Lett. 94, 161 (2013)
[28] Panda, D., Tseng, T. Y.: Growth, dielectric properties, and memory device applications of ZrO_2 thin films. Thin Solid Films 531, 1 (2013).
[29 Balakrishnan, G., Sairam, T. N., Kuppusami, P., Thiumurugesan, R., Mohandas, E., Ganesan, V., Sastikumar, D.: Influence of oxygen partial pressure on the properties of pulsed laser deposited nanocrystalline zirconia thin films. Appl. Surf. Sci. 257, 8506 (2011).
[30] Wang, X.; Wu, G.; Zhou, B.; Shen, J. Effect of crystal structure on optical properties of sol–gel derived zirconia thin films. J. Alloy Compd. 2013, 556, 182–187.
[31] Ehrhart, G.; Capoen, B.; Robbe, O.; Boy, P.; Turrell, S.; Bouazaoui, M. Structural and optical properties of n-propoxide sol–gel derived ZrO_2 thin films. Thin Solid Film. 2006, 496, 227–233.

Design radar absorption materials (RAMs) Based on MgO and AlAs single and double layers structure within 2-18 GHz frequency range

Alaa Jabbar Ghazai
Department of Physics, College of Science, Al-Nahrain University, Baghdad, Iraq.

Abstract:
Radar absorbing materials (RAMs) are dielectric or magnetic materials that has capacity for absorbing electromagnetic waves. In order to increase frequency range (bandwidth) of the absorbance, several structures have been already proposed by several researchers. Objective of this study is to design, fabricate and characterize RAMs based on MgO and AlAs single and double layers structure on Silicon substrate within 2-18 GHz frequency range. For this purpose, Maxwell equations solved and modified characteristic matrix have been used and its programming using Mathlab software. The frequency design is consider to be 10 GHz and 5,8 GHz, The results showed that the MgO and MgO/AlAs single and double layers structure on Si substrate are suitable materials to RAM applications in frequency range from 8 GHz to 12 GHz. In addition, low value of transmittance and reflectivity, and high RAM attenuation value of -39 dB at design frequency of 10 GHz have been obtained in broadband of 8-12 GHz. Finally, the possibility to use MgO and MgO/AlAs single and double layers' structure on Si substrate as materials to RAM in frequency of 5.8 GHz with high effectively is considered.
Keywords: radar, absorption materials, frequency, single and double layers structure.

تصميم مواد ماصة للرادار (RAMs) اعتمادا على تركيب احادي او ثنائي الطبقات من MgO and AlAs ضمن مدى تردد 2-18GHz

علاء جبار غزاي
قسم الفيزياء، كلية العلوم، جامعة النهرين، بغداد، العراق.

المستخلص
المواد الماصة للرادار هي مواد عازلة او مغناطيسية تمتلك قابلية وسعة لامتصاص موجات الاشعة الكهرومغناطيسية. لغرض زيادة مدى تردد (عرض الحزمة) للمواد الماصة، عدة تراكيب اقترحت بواسطة عدة باحثين. الهدف من هذه الدراسة هو لتصميم وتحضير وتوصيف المواد الماصة للراداراعتمادا على تركيب احادي او ثنائي الطبقات MgO وMgO/AlAs على ارضية اساس من السيليكون ضمن مدى الترددات 2-18 كيكاهرتز. لتحقيق هذا الغرض تم استحدام حلول معادلات ماكسويل والمصفوفة المميزة المعدلة وتمت برمجتها باستخدام برنامج الماثلاب. تردد التصميم كان 10 كيكاهرتز و5,8 كيكاهرتز. بينت النتائج ان التراكيب للمواد المستخدمة على ارضية اساس من السيليكون مناسبة جدا كمواد ماصة للرادار ضمن مدى الترددات 8-12 GHz. بالاضافة لذلك تم الحصول على قيم قليلة للنفاذية والانعكاسية وقيم عالية للتوهين -39 dB عند التردد 10 كيكاهرتز، واخيرا تم الاستنتاج بانه بالامكان استخدام المواد المحضرة كطبقة مفردة ومتعددة وبكفاءة عالية ضمن التردد 5.8 كيكاهرتز.
الكلمات الافتتاحية: رادار، مواد ماصة، تردد، تركيب احادي او ثنائي الطبقات.

1. Introduction

Radar is a method for detecting the position and velocity of a distant object, such as an aircraft. Detection is achieved by analyzing the response of high frequency radio waves reflected from the target object. The term RADAR was coined in 1940 by the United States Navy as an acronym for Radio Detection and Ranging [1]. The term not only refers to the detection method, but also refers to the detection system itself.

Despite being found out as a military technology to detect enemy aircraft, nowadays radar technology serves many purposes to humankind. Notable examples include, air, marine and ground traffic control and navigation, short-term weather forecasting and specialized ground-penetrating radars for mapping the composition of Earth's crust [2]. Nevertheless, radar is still a very crucial technology for military applications.

Radar systems are based on transmitting and recieving radio waves which are electromagnetic waves between wavelengths of 1 mm to 100,000 km. Analyzing the

response of the transmitted electromagnetic waves gives information about position, velocity, magnitude and type of the object. The object can be identified from its radar cross section (RCS) which is a footprint of the object in the radar system [3]. Information gained from radar systems are very valuable for the course of military operations, thus giving enourmous advantage to the side which has proper radar systems.

As radar systems came into use, research for reducing the effectiveness of these systems were also began. Research generally focused on reducing the amount of electromagnetic waves reflected from the object by absorbing transmitted waves, achievable through using proper materials and design. These materials defined as Radar Absorbing Materials (RAMs). [4]

Interest at radar absorbing materials and structures began immediately with the discovery of radar systems at World War II. One of the first applications was the using of carbon based radar absorbing materials on submarine periscobes which was developed by Jaumann. But this attempt was greatly reduced by the effect of sea water on the material [5].

In 1971, Naito and Suetake were studied on electromagnetic wave absorber composed of ferrite powder and rubber matrix. The study also investigated the existence of matching frequency, thickness of the RAM for maximizing the bandwith. [6]

In early 80s, the development of RAM was generally based on ferrites or carbonyl iron. First implementation of RAMs was on military applications. One of them was utilized in the development of F-117 Nighthawk, which made its maiden flight in 1981. The aircraft had a paint type absorber, based on both ferrites and carbon particles. In 1983, F-117 fleet was ready for operations for U.S. Air Force. In 1988, the aircraft was announced to public as a “stealth fighter”. The ability of radar wave absorbing generally denoted as “stealth” or “stealth technology” by military and quickly adapted by public [1].

In late 80s, interest for RAMs greatly increased. Knott, Shaeffer and Tuley had written a book about radar cross section which was a concept of footprint of the object exposed to radar waves. Their work also included reducing of RCS, which refers RAMs but also size and shape of the object. [1]

In general, early works on RAMs and were consist of theoretical calculations, simulations and optimizations due to limitations to synthesize the material itself. Studies on Jaumann type absorbers in late 80s and early 90s can be given as an example in which contains simulations and optimizations for resistive sheet configurations and their resistances [7].

RAM studies have been generally based on 0o degree (direct approach) angle of incidence. There were also studies about the performance of RAMs for wide range of angles of incidence. These works indicated that the angle of incidence of radar wave greatly effects the performance. With increasing angle of incidence until 60o reflection coefficient may even increase. However, it was found that above 60o, those value drops significantly.

In early 2000s, studies on lossy RAMs were increased. Both ferrimagnetic based and carbon based dielectric materials were investigated. Carbonyl iron and ferrite powders such as barium hexaferrite have been popular as magnetic RAMs [8]. Studies on dielectric absorbents gained more interest at mid 2000s. These RAMs include graphite, carbon black, single and multi-walled carbon nanotubes, carbon nano fibers which were mixed with epoxy, rubber or silicone matrix [11].

Radar systems generally operates at certain segments of electromagnetic spectrum such as X-band which includes frequencies from 8.2 GHz to 12.4 GHz. (Hill 2007) Thus, absorption of the waves at certain bands can be achievable but more complex materials or designs are needed to prevent all the waves throughout a band reflected. There were additional studies to increase the bandwidth of absorption below certain attuneation (-10 or -20 dB) beyond X-band. These studies focused on broadband absorbers generally aims for combination of X and Ku band or a wider 2-18 GHz range. The electromagnetic spectrum with radio, microwave and visible light spectrums detailed, is illustrated in Figure 1.

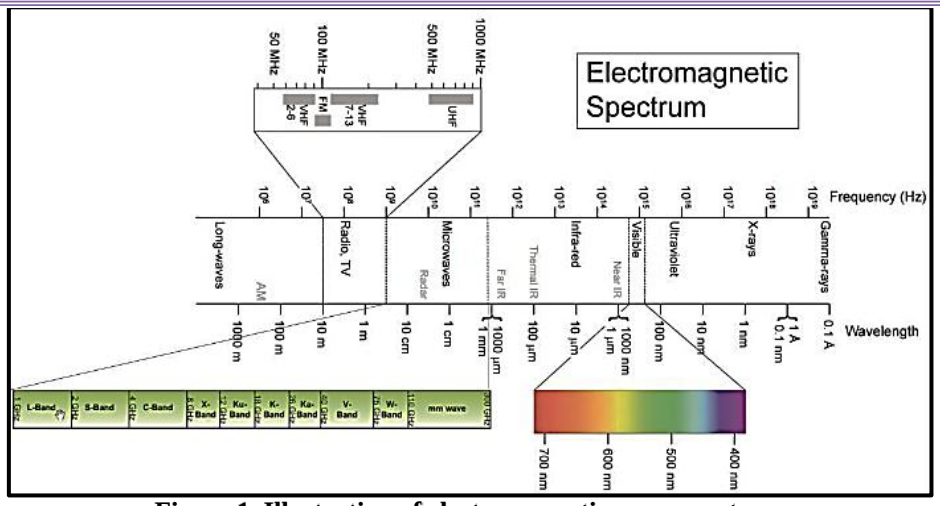

Figure 1. Illustration of electromagnetic wave spectrum

Recent studies concentrate on Radar Absorbing Structures (RAS), which are a combination of RAM and structural design to increase bandwidth and decrease attuneation. Structures have been based on sandwich type structures or continuous fiber reinforced composites. Designs were based on single or multilayer Dallenbach layers which consist a combination of loss materials (D. Micheli et al. 2010), Salisbury screen which is basically a Dallenbach layer including a resistive sheet and Jaumann absorbers which include multiple resistive sheets to increase bandwidth [10].

One of the important advantage of RAS designs is that they are applicaple to several current structures used for vehicles or constructions. Laminated composites and sandwich structures are suited examples for that usage. Vehicle parts such as aircraft wings, or wind turbine blades can be manufactured from materials such as fiber reinforced composites for both structural integrity and radar absorbing properties [11].

In this study radar absorbing materials based on cheap and variables materials have been developed and determine the optimum condition to design the preparation of an anti - reflective coating of a single and double layer of GaAs and MgO to reduce the reflectivity of optical surfaces within the range of X-band frequency of 8-12 GHz, theoretically. In addition, applied these effect and optimization in very interesting applications which is Drone Jammer that helps in control on the Drone plane in frequency of 5.8 GHz. The radar absorbing performance of those structures are measured and compared.

The simplest interference AR coating consists of a single quarter-wave layer of transparent material whose refractive index is the square root of the substrate's refractive index; this, theoretically depend on modified characteristic matrix which presented by Mathlab program as shown later in Figure (2) which gives zero reflectance at the center wavelength and decreased reflectance for wavelengths in a broad band around the center.

The most common type of substrate which used in like these purpose is Silicon (Si), which has an index of refraction of about 3.4. An optimum single layer coating would have to be made of a material with an index of about 1.7. Unfortunately, there are no solid materials with such a low refractive index. The closest materials with good physical properties for a coating are magnesium Oxide, MgO (with an index of 1.8), MgO on a Si substrate surface gives a reflectance of about 1%, compared to 30% for uncoated silicon.

Now, the reflectance of uncoated substrate at F=10GHz, have been calculated as shown below:

1- for glass: n_s=1.52

$$\text{Runcoated} = \left(\frac{n_0 - n_s}{n_0 + n_s}\right)^2 = \left(\frac{1 - 1.52}{1 + 1.52}\right)^2 = \left(\frac{-0.52}{2.52}\right)^2 = (-0.206)^2 = 0.04$$

$$\text{Rcoated} = \left(\frac{n_0 n_s - n_1^2}{n_0 n_s + n_1^2}\right)^2 = \left(\frac{1*1.52 - (1.38)^2}{1*1.52 + (1.38)^2}\right)^2 = \left(\frac{1.52 - 1.9044}{1.52 + 1.9044}\right)^2 = \left(\frac{-0.3844}{3.4244}\right)^2$$
$$= (-0.112)^2 = 0.012$$

$$n_1 = (n_0 n_s)^{1/2} = (1 * 1.52)^{1/2} = 1.23$$

2- for Ge: n_s=4

$$\text{Runcoated} = \left(\frac{n_0 - n_s}{n_0 + n_s}\right)^2 = \left(\frac{1 - 4}{1 + 4}\right)^2 = \left(\frac{-3}{5}\right)^2 = (-0.6)^2 = 0.36$$

$$\text{Runcoated} = \left(\frac{n_0 n_s - n_1^2}{n_0 n_s + n_1^2}\right)^2 = \left(\frac{1*4 - (2.3)^2}{1*4 + (2.3)^2}\right)^2 = \left(\frac{4 - 5.29}{4 + 5.29}\right)^2 = \left(\frac{-1.29}{9.29}\right)^2 = (-0.138)^2$$
$$= 0.019$$

$$n_1 = (n_0 n_s)^{1/2} = (1 * 4)^{1/2} = 2$$

3- for Si: n_s=3.4

$$\text{Runcoated} = \left(\frac{n_0 - n_s}{n_0 + n_s}\right)^2 = \left(\frac{1 - 3.4}{1 + 3.4}\right)^2 = \left(\frac{-2.4}{4.4}\right)^2 = (-545)^2 = 0.29$$

$$\text{Runcoated} = \left(\frac{n_0 n_s - n_1^2}{n_0 n_s + n_1^2}\right)^2 = \left[\frac{1*3.4-(1.73)\text{^}2}{1*3.4+(1.73)\text{^}2}\right] = \left[\frac{1*3.4-(1.73)\text{^}2}{1*3.4+(1.73)\text{^}2}\right]_{\text{^}2} =$$

0.063

$$n_1 = (n_0 n_s)^{1/2} = (1 * 3.4)^{1/2} = n_1 = (n_0 n_s)^{1/2} = (1 * 3.4)^{1/2} =$$ 1.84

Calculation refractive index and thickness for Si substrate:-
n1=MgO =1.737
n2 = n1 *(ns/n0)^0.5
n2 =1.737*1.84 = 3.06
n2=ALAs =3.16

n*d = m*λ /4
for 10[GHz]
d1=0.03/4*1.737 = (935)/4 nm = 234 nm
d2 = 0.03/4*3.16 = (2375)/4 nm = 594 nm
for 5.8 [GHz]
d1=0.051/4*1.737 =760 nm
d2 =0.051 /4*3.16 = 403 nm

Figure (2) shows the transmission measurements of the RAM of MgO and MgO/ AlAs single and double layers structure on Si substrate in frequency range of 8 to 12 GHz which the low value of transmittance at design frequency of 10 GHz are observed and fluctuation values over all range of frequencies.

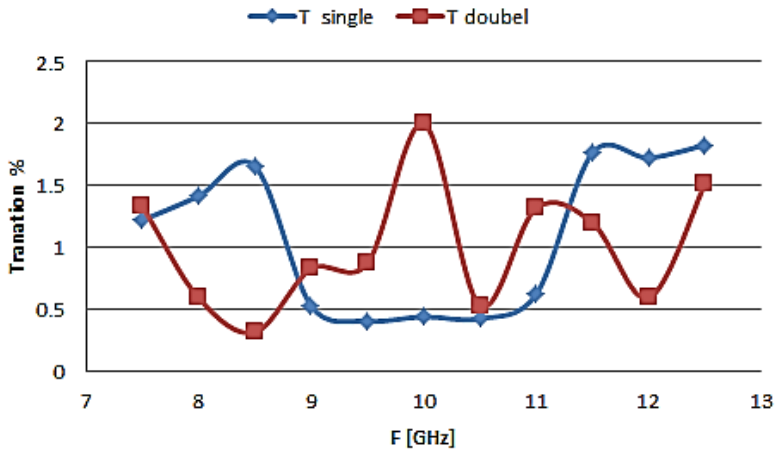

Fig. (2): Transmission spectra as a function of the wavelength for MgO single layer and MgO/AlAs double layers structures on Si substrate at Frequency 10 GHz

Figure (3) shows the reflectivity measurements of the RAM of MgO and MgO/AlAs single and double layers structure on Si substrate in frequency range of 8 to 12 GHz which the low value of reflectivity at design frequency of 10 GHz are observed. Samples with double layers present lower lower value at this frequency in compared with single layer, but nearly constant in frequency more than design frequency range.

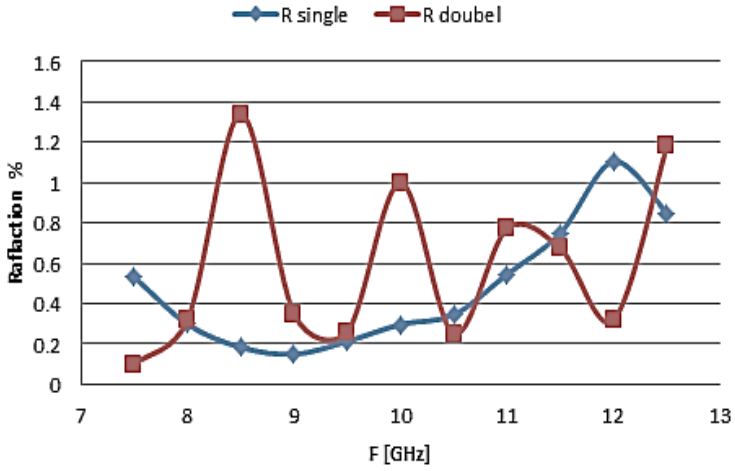

Fig. (3): Reflectance spectra as a function of the wavelength for MgO single layer and MgO/AlAs double layers structures on Si substrate at Frequency of 10 GHz

The maximum absorption value of the RAM of MgO and MgO/AlAs single and double layers structure on Si substrate in frequency range of 8 to 12 GHz where absorption values close to 99% in all cases in are observed. The absorption values have been showed as attenuation in dB in our work which reflect the real behavior of RAM as shown in Figure (4). These data confirm the dependence of attenuation with the number of layers which mean the increased of the sheet resistive of structure and thus, the increasing in the reflection losses.

The low attenuation values of -39 dB are the beat results were founded as our best knowledge and these results show that MgO and MgO/AlAs single and double layers structure behave more efficiently as RAM absorbers.

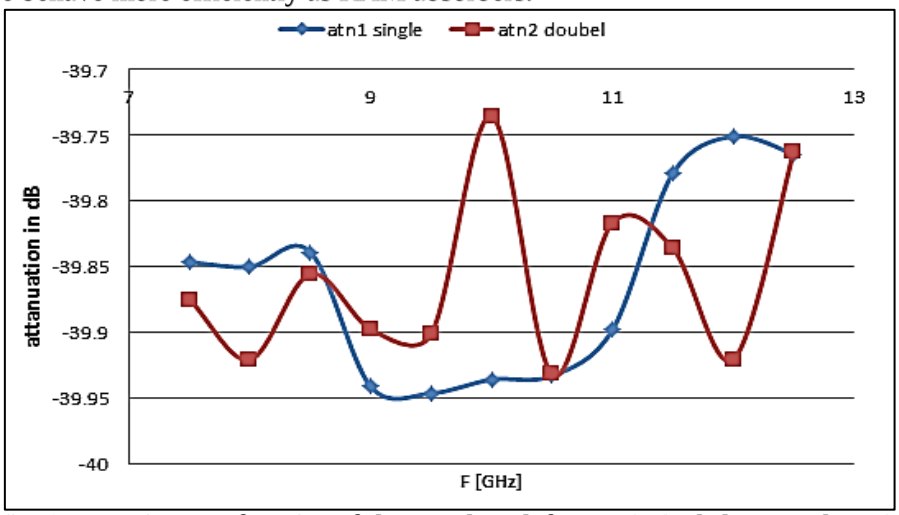

Fig. (4): Attenuation as a function of the wavelength for MgO single layer and MgO/AlAs double layers structures on Si substrate at Frequency 10 GHz

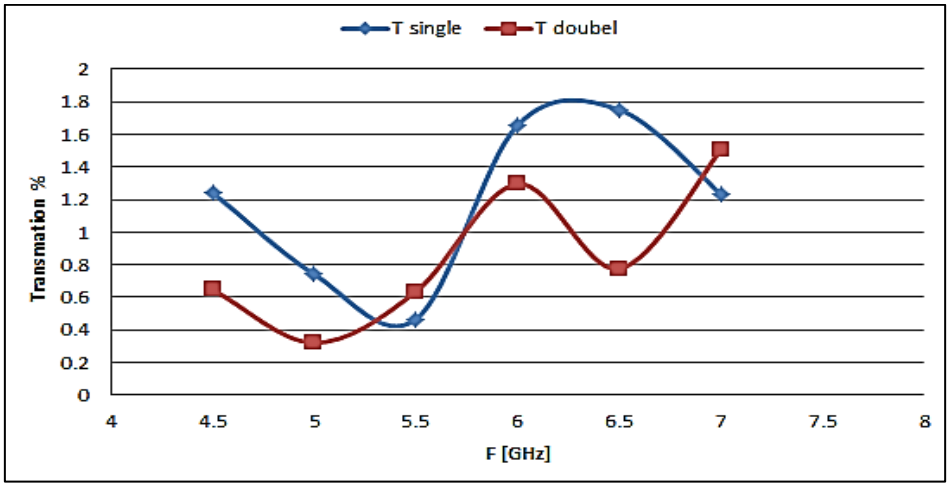

Fig. (5): Transmission spectra as a function of the wavelength for MgO single layer and MgO/AlAs double layers structures on Si substrate at Frequency 5.8 GHz

The maximum absorption value of the RAM of MgO and MgO/AlAs single and double layers structure on Si substrate in frequency of 5.8 GHz where absorption values close to 99% in all cases in are observed. The absorption values have been showed as attenuation in dB in our work which reflect the real behavior of RAM as shown in Figures (6) and (7). These data confirm the dependence of attenuation with the number of layers which mean the increased of the sheet resistive of structure and thus, the increasing in the reflection losses.

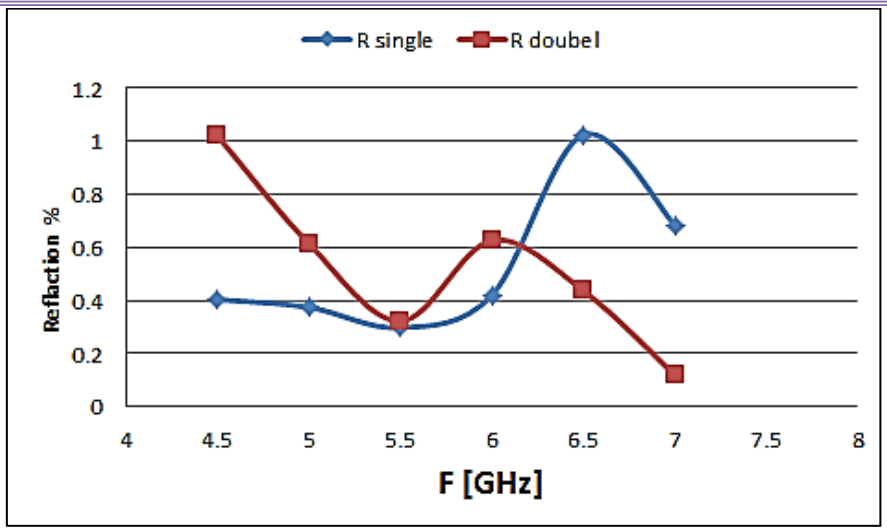

Fig. (6) Reflectance spectra as a function of the wavelength for MgO single layer and MgO/AlAs double layers structures on Si substrate at Frequency

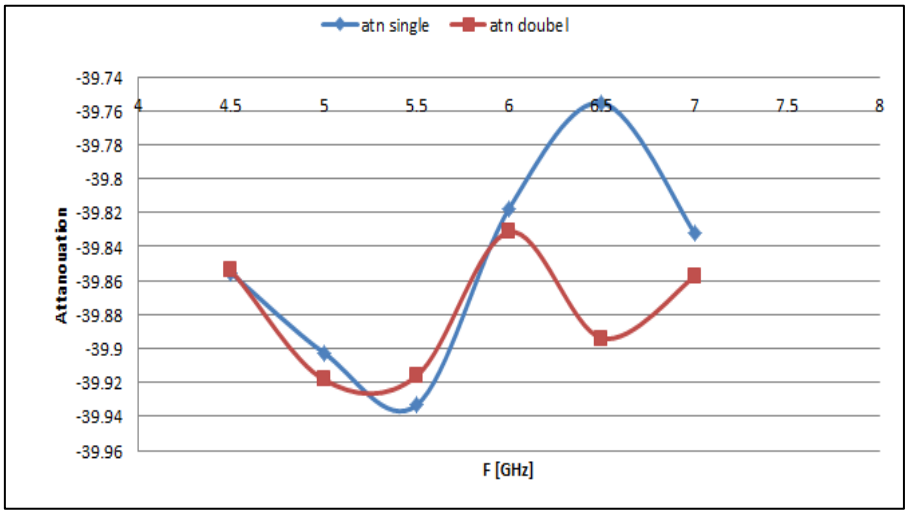

Fig. (7): Attenuation as a function of the wavelength for MgO single layer and MgO/AlAs double layers structures on Si substrate at Frequency 5.4 GHz

From these results in Figures (6) and (7), it is possible to use MgO and MgO/AlAs single and double layers structure on Si substrate as materials to RAM in frequency of 5.8 GHz with high effectively. The results calculated in this work have been summarized in Table 1.

Table (1): Theoretical and calculated values of refraction and translation of single, and double MgO/AlAs/Si on Si substrate at Frequency range 10 and 5.8 GHz

For 10 [GHz]			
Structure	Reflectance	Transation	
Si substrate	29		Th.
MgO/Si	1	1.75	Calc.
MgO/AlAs/Si	0.3	1.3	Calc.

For 5.8 [GHz]			
Si substrate	29		Th.
MgO/Si	0.57	1.3	Calc.
MgO/AlAs/Si	0.37	1.2	Calc.

3. Conclusions

There are several main and important conclusions in this work could summarized in many points as following:

MgO and MgO/AlAs single and double layers structure on Si substrate are suitable materials to RAM applications in frequency range from 8 GHz to 12 GHz. Low value of transmittance at design frequency of 10 GHz and fluctuation values over all range of frequencies. Low value of reflectivity at design frequency of 10 GHz and fluctuation values over all range of frequencies. High RAM attenuation value of -39 dB at design frequency in broadband of 8-12 GHz. It is possible to use MgO and MgO/AlAs single and double layers structure on Si substrate as materials to RAM in frequency of 5.8 GHz with high effectively.

Reference

1. Knott, Eugene F., Tuley, Michael T., Shaeffer, John F., Radar Cross Section (Scitech Radar and Defense), (2004) Paperback Paperback, 1, 1709

2. McGraw-Hill, Yearbook of Science and Technology (McGraw-Hill's Yearbook of Science & Technology), (2007), 1st Edition.

3. Vladimir Díaz Charris, José Manuel Gómez Torres, Analysis of radar cross section assessment methods and parameters affecting it for surface ships, Ship Science & Technology - Vol. 6 – No. 11 - (91-106) (2012) - Cartagena (Colombia).

4. C. G. Jayalakshmi, A. Inamdar, A. Anand, B. Kandasubramanian, 2019. Polymer matrix composites as broadband radar absorbing structures for stealth aircrafts, Journal of applied polymer sciences, J. APPL. POLYM. SCI. 2019, 47241-47262.

5. Yang Liu, Wenlong Zhang, Jianhang Sun, Baige Xingm and Leo Ligthart, Radar Cross Section Near-Field to Far-Field Prediction for Isotropic-Point Scattering Target Based on Regression Estimation, Sensors 2020, 20, 6023; doi:10.3390/s20216023.

6. Y. Naito; K. Suetake, Application of Ferrite to Electromagnetic Wave Absorber and its Characteristics, IEEE Transactions on Microwave Theory and Techniquesm Volume: 19, Issue: 1, Jan. (1971).

7. Won Ho Choi, Woon Hyung Song,Won-Jun Lee, Broadband Radar Absorbing Structures with a Practical Approach from Design to Fabrication, Journal of electromagnetic engineering and science, vol. 20, no. 4, 254~261, oct. 2020.

8. Xiaohu Ren, Huiqing Fan, Yankui Cheng, Carbonyl iron and ferrite powders such as barium hexaferrite have been popular as magnetic RAMs, Applied Physics A, 122(5), (2016).

9. Sang-Ha Hwang, Young-Bin Park, Kwan Han Yoon and Dae Suk Bang.
Smart Materials and Structures Based on Carbon Nanotube Composites, Carbon Nanotubes - Synthesis, Characterization, Applications, Intech open publisher, 2011.

10. Jing Tian, Hongyu Shi, Haoquan Hu, Bo Chen, Yongfang Bao, Pu Tang, Implementation of Atomically Thick Graphene and Its Derivatives in Electromagnetic Absorbers, Applied Sciences, Vol. 9, Issue 3, 10.3390/app9030388, *Appl. Sci.* 2019, *9*(3), 388; https://doi.org/10.3390/app9030388.

11 Gi-Won Jeong Yeong-Hoon Noh, Won-Ho Choi, Joon-Hyung Shin, Jin-Hwe Kweon, Jong-Gwan Yook, Young-Woo NamElectromagnetic-mechanical repair patch of radar-absorbing structure with electroless nickel–plated glass fabric damaged by lightning strike, Journal of composite material, Volume: 55 issue: 7, page(s): 989-1002, 2021.

Structural and Optical Properties of Lithium Doped Titanium Oxide Thin Films Prepared by Chemical Spray Pyrolysis

Jenan Abdullah Khlati
Department of Physics, College of Education, Mustansiriyah University, Baghdad, Iraq.

Abstract:
Undoped TiO_2 and TiO_2: Li thin films were deposited on glass substrates using chemical spray pyrolysis technique CSPT. UV- UV-Visible and X-ray diffraction (XRD) were used to investigate the effect of Lithium Doping on the Optical and Structural Properties of Titanium Oxide Thin Films spectroscopy respectively. XRD anaylsis assures that TiO_2 films are polycrystalline structure with recognized peak at (121). Grain size increases from 9.69 nm to 10.84 nm as Lithium concentration increase. The transmittance is more than 52% in the visible range for for all the films. The optical bandgap of Undoped TiO_2 and TiO_2: Li film has been decreased from (3.46 to 3.35) eV. The optical absorption coefficient, refractive index and extinction coefficient are affected via Lithium content.
Keywords:: TiO_2:Li, thin films, chemical spray pyrolysis, structural and optical properties.

الخصائص التركيبة والبصرية لأغشية اوكسيد التيتانيوم الرقيقة المشوب بالليثيوم المحضرة بواسطة الترسيب الكيميائي الحراري

جنان عبد الله خلاطي
قسم الفيزياء، كلية العلوم التربية، الجامعة المستنصرية

المستخلص
حضرت اغشية اوكسيد التيتانيوم النقية والمشوبة بالليثيوم المرسبة على القواعد الزجاجية باستخدام طريقة الترسيب الكيميائي الحراري، تم استخدام الأشعة فوق البنفسجية المرئية وحيود الاشعة السينية لمعرفة تأثير التشويب بالليثيوم على الخواص البصرية والتركيبية لأغشية اوكسيد التيتانيوم الرقيقة على التوالي. فحوصات حيود الاشعة السينية بيت بأن أغشية اوكسيد التيتانيوم المحضرة ذات تركيب متعدد البلورات باتجاه سائد هو (121) ويزداد الحجم الحبوبي من 9.69 نانومتر إلى 10.84 نانومتر مع زيادة تركيز الليثيوم، تكون النفاذية أكثر من 52٪ في النطاق المرئي لجميع الأفلام، فجوة الطاقة البصرية لاغشية اوكسيد التيتانيوم النقية والمشوبة بالليثيوم قلت من (3.46 إلى 3.35) فولت، يتأثر معامل الامتصاص البصري، معامل الانكسار ومعامل الخمود بالتشويب بالليثيوم.
الكلمات الافتتاحية: اوكسيد التيتانيوم، الليثيوم، أغشية رقيقة، الترسيب الكيميائي الحراري الخصائص التركيبة والبصرية.

Introduction

Titanium dioxide (TiO_2)is considered by some researchers that it is, it was, and it will be the best photocatalyst, due to its transparency in the visible domain, low cost, non-toxicity, excellent chemical, high oxidation potential, and mechanical stability in unfriendly environment, or in a large number of solvents, etc. [3-7]. A direct energy bandgap ranging from 3.0 to 3.4 eV [1-4]. Besides, TiO2 is chemical stability, non-toxic, a refractive index and high optical transmittance, between 2.4 - 2.9 [5-10]. Titanium dioxide is employed in many dye sensitised solar cells, optical devices and biomedical applications, [5, 6, 11]. Many methods were employing for the deposition of Titanium dioxide films, sputtering [12], radio-frequency (RF) sputtering [13], hydrothermal[14], chemical vapor deposition [15, 16], precipitation[17], sol–gel [18], electron-beam evaporation [19], anodic oxidation[20], spray deposition [21],. pulsed laser deposition [22], and chemical spray pyrolysis [23]. In present work costless and easy chemical method is utilized to deposited Undoped TiO_2 and TiO_2: Li thin film. This work aims is to study physical properties of TiO_2 film.

Experimental

Undoped TiO_2 and TiO_2: Li thin films were deposited on a glass substrate by chemical spray pyrolysis technique (SPT). These films were originated from O.1 M $TiCl_2$ that resolved in 1:1 redistilled water: ethanol. The doping material was Lithium trichloride ($LiCl_3$) resolved in redistilled water, drops of HCl were gathered the sol get it homogenous. The preparation conditions were: Substrate temperature 400 ^{O}C, space between spout and substrate was 28 cm, spraying time 10 s held by 90 s to avert refrigeration, spray average was 4ml/min, Film thickness was evaluated by weighing method, their values were 330 ± 35 nm. XRD was employed to obtain films structure. The spectra of transmission and absorption were inspection via using (UV-Vis spectrometer, T70-80), in the wavelength range from (300-900 nm).

Result and discussion

The XRD patterns of Undoped TiO_2 and TiO_2: Li thin films are graphed in the Fig. (1), Fig. (1) offers the XRD patterns of TiO_2 film. Sundry peaks at angles (25.21^o), ((30.76^o), (48.33^o) and (64.10^o) matched the (101), (121), (231) and (133) plane, which were fit with ICDD card No (29-1360), Strong peak was appear toward (121).

The Grain size(D) of Undoped TiO_2 and TiO_2: Li was estimated from Scherer's equation (1) [24]:

$$D = \frac{0.9\lambda}{\beta cos\theta} \qquad (1)$$

Where λ is wavelength of the X-rays used (0.1541 nm), β and θ are (FWHM) and the diffraction angle respectively. It can be seen from Table 1 that β decreases when Undoped TiO_2 concentration increases up to TiO_2: 3% Li, the grain size of Undoped TiO_2 and TiO_2: Li particle is about (9.69 – 10.84) nm, with Lithium concentration as listed in Table. 1.

Other structural parameters such as dislocation density (δ) is also evaluated. δ gives number of The dislocation density (δ) and lattice strain (ε) were predestined via the following equations [25, 26]:

$$\delta = \frac{1}{D^2} \qquad (2)$$

$$\varepsilon = \frac{\beta cos\theta}{4} \qquad (3)$$

We found that dislocation density (δ) of Undoped TiO_2 and TiO_2:Li film is about (9.69 - 10.84), which refers to low defects. The strain decreases via increasing Lithium concentration. The calculated structural parameters are offered in Table. 1

Figure (2) represents each of the FWHM, D, δ and ε versus doping.

Table 1. Optical bandgap, Grain size and structural parameters of the intended films.

Doping (%)	2 θ (°)	(hkl) Plane	FWHM (°)	Optical bandgap (eV)	Grain size (nm)	Dislocations density (× 10^{14})(lines/m^2)	Strain (× 10^{-4})
Undoped ZrO_2	31.35	111	0.78	5.22	10.58	89.33	32.76
ZrO_2: 2% Ti	31.32	111	0.73	5.16	11.30	78.31	30.66
ZrO_2: 4% Ti	31.29	111	0.68	5.10	12.13	67.96	28.56

The transmission (T) spectrum of Undoped TiO_2 and TiO_2: Li films was illustrated in Fig. (3). Fig.(3) offers transmittance (T) spectra of intended films. transmittance is more than 52% in the visible range for 1 to 3% Lithium (Ti) doping. The transmittance of TiO_2 film decreases by doping Lithium.

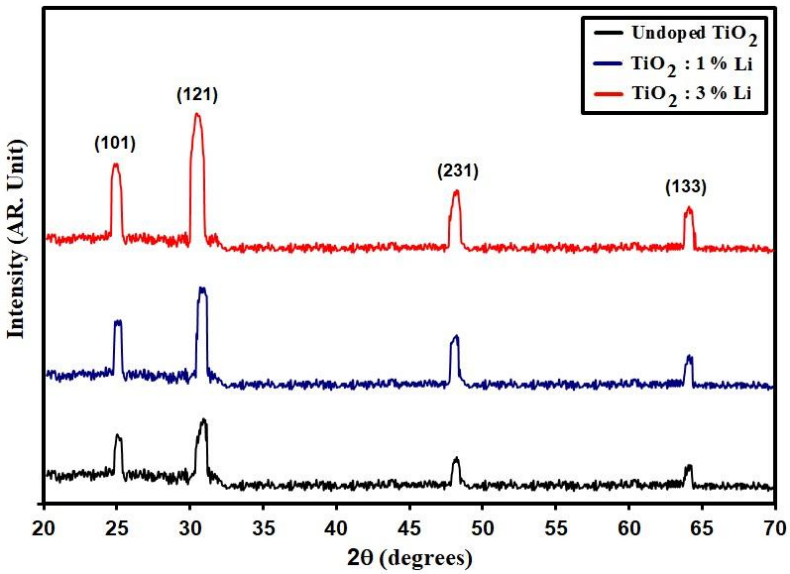

Fig.1. XRD patterns of (Undoped TiO_2 and TiO_2: Li) thin films.

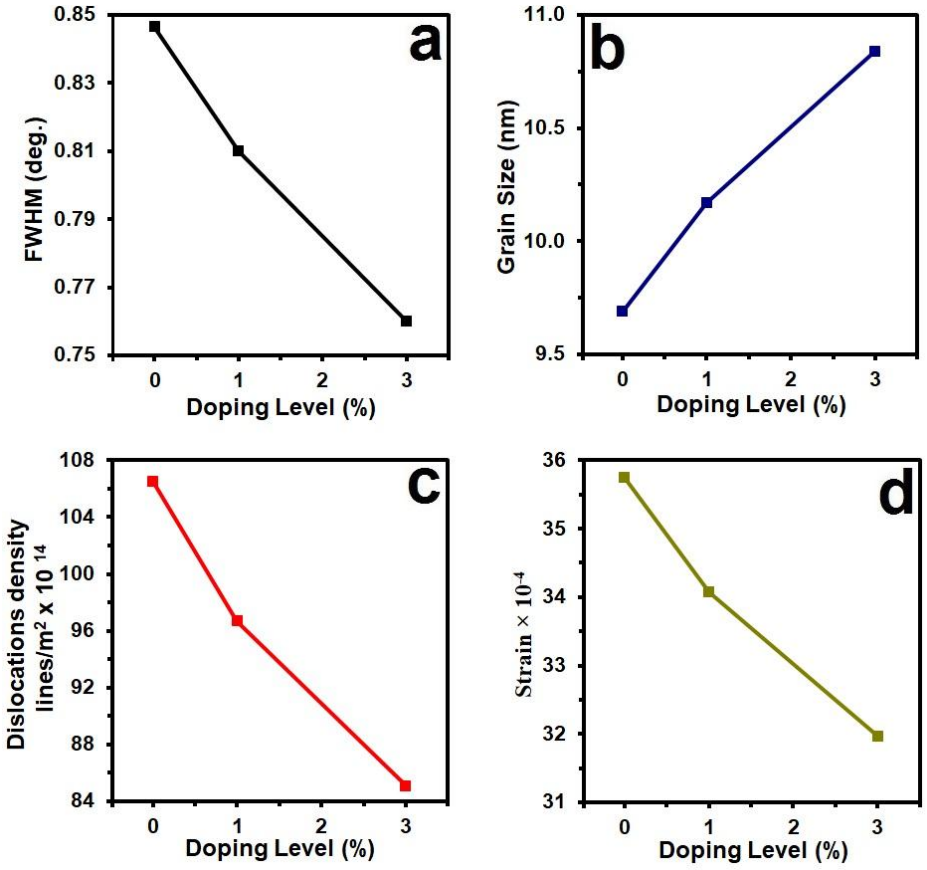

Fig.2. FWHM (a) Grain size (b) Dislocation (c) and Strain (d) of the prepared films.

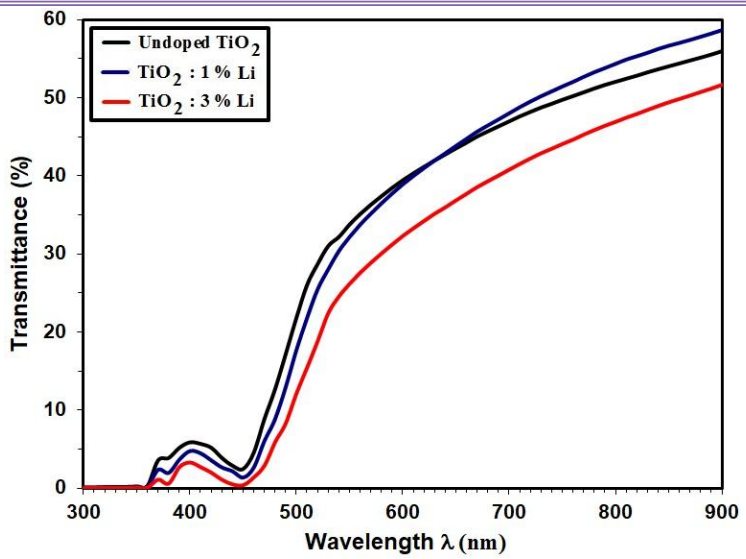

Fig. 3 Transmission spectra for the prepared films

The optical absorption coefficient (α) calculated from Eq. (4) [27]:

$$\alpha = \ln (1/T)/d \quad (4)$$

Where, d is film thickness. Fig.4 shows the absorption coefficient of Undoped TiO_2 and TiO_2: Li films decreased with an increase at 1% or 3% doping Lithium.

The energy gap E_g can be evaluated from dependence of $(\alpha h\nu)^2$ against hν utilizing Tauc formula [28]:

$$(\alpha h\nu) = A\left(h\nu - E_g\right)^{\frac{1}{2}} \quad (5)$$

Where A is the constant, Fig. (5) show the relationship between absorption edge $(\alpha h\nu)^2$ and energy of photon for Undoped TiO_2 and TiO_2: Li, energy gap is found to be about (3.46 - 3.35) eV respectively.

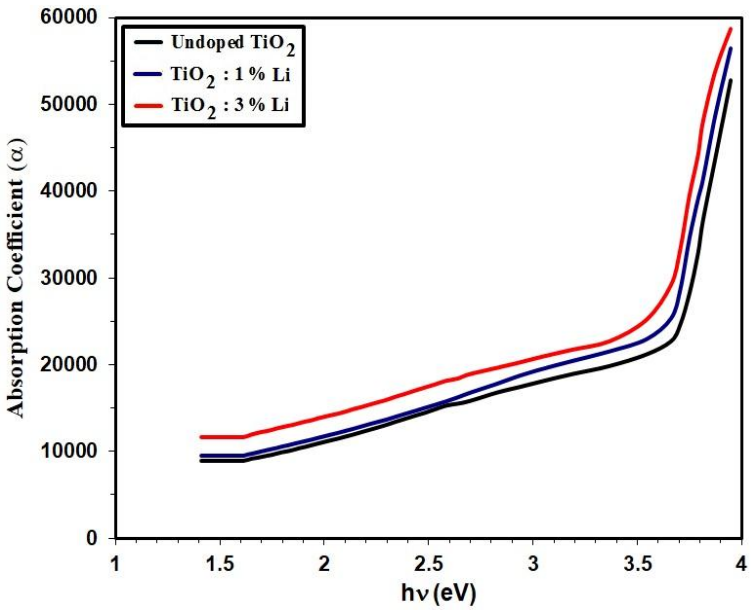

Fig. 4. the relation between absorption coefficient and photon energy for intended films.

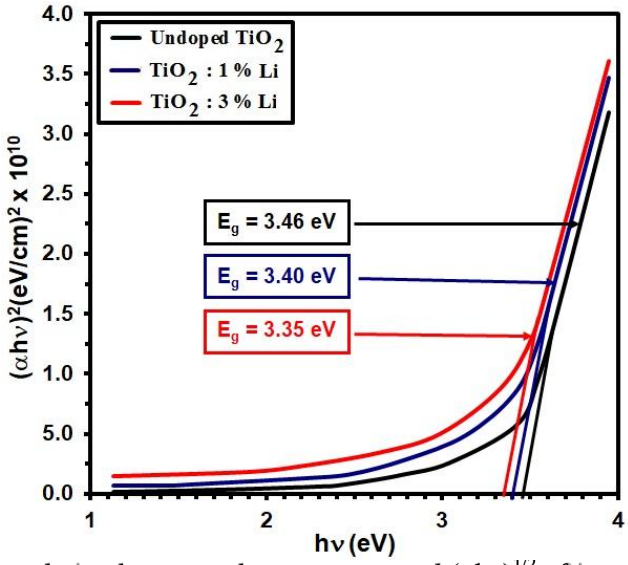

Fig. 5. The relation between photon energy and $(\alpha h\nu)^{1/2}$ of intended films.

Optical constants such as refractive index (n) and extinction coefficient (K) were evaluated according to Eqs. (6, and 7), respectively and illustrated in Figs. (6 and 7). These two factors declines with the influence of increasing Lithium doping 29, 30].

$$n = [1 + R/1 - R] + [4R / (1-R)^2 - k^2]^{1/2} \quad (6)$$

$$k = \alpha\lambda/4\pi \quad (7)$$

Where λ is the wavelength.

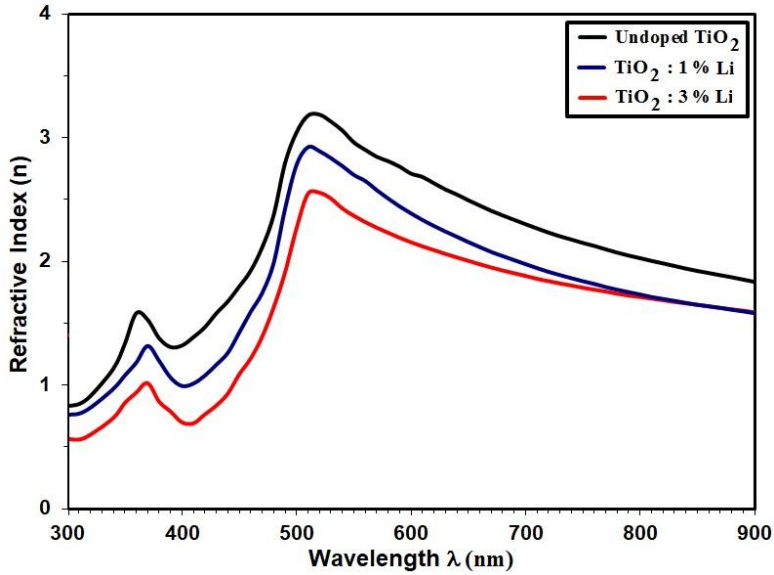

Fig. (6) The relation between refractive index and the wavelength of the intended films.

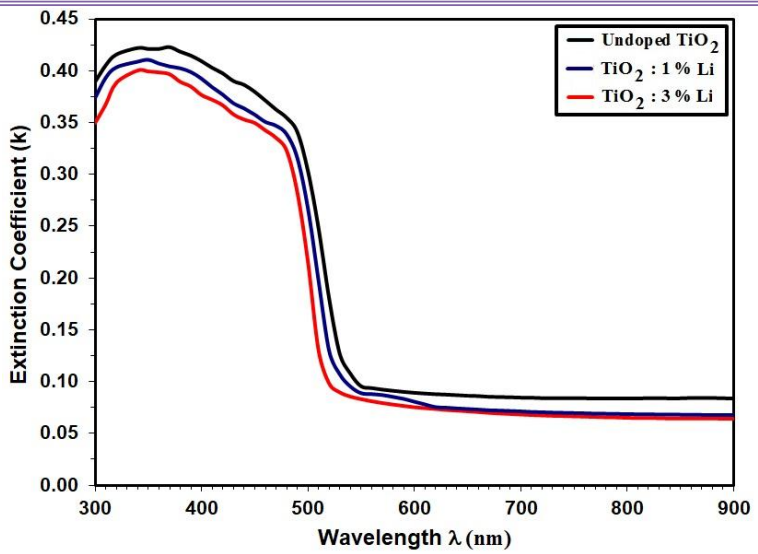

Fig. (7) the relationship between extinction coefficient and the wavelength of the intended films.

Conclusion

The effect of Lithium doped cadmium oxide thin films on some physical properties was investigated. XRD results displayed that TiO_2 films have (121) dominant peak. Crystallite size increases from 9.69 nm to 10.84 nm as Lithium concentration. The The strain (ε) of n TiO_2 films was observed in the range of (35.75), (34.07) and (31.97) nm for the (TiO_2, TiO_2:1% Li, TiO_2:3% Li) respectively. The transmittance in the visible range is more than 52 %. The optical bandgap values were decreased from 3.46 to 3.35 eV with the increment of Lithium content.

References

[1] S. Phadke, J. D. Sorge, S. Hachtmann, D. P. Birnie, "optical characterization of sol-gel TiO_2 thin film microstructure evolution with temperature", Thin Solid Films. 518(2010), p. 5467.
[2] D. H. Song, S. H. Uhm, S. B. Lee, J. G. Han, and K. N. Kim: 'Antimicrobial silver-containing titanium oxide nanocomposite coatings by a reactive magnetron sputtering', Thin Solid Films, 2011, 519(20), 7079-7085.
[3] T. Shibata, H. Irie, and K. Hashimoto: 'Photoinduced hardness change on TiO_2 single crystal surfaces', Chemical Communications, 2009(25), 3735-3737.
[4] Raoufi D, Kiasatpour A, Fallah HR, Rozatian ASH. Surface characterization and microstructure of ITO thin films at different annealing temperatures. Appl Surf Sci. 2007;9:9085–9090.
[5] J. He, I. Ichinose, T. Kunitake, and A. Nakao, "In Situ Synthesis of Noble Metal Nanoparticles in Ultrathin TiO2−Gel Films by a Combination of Ion-Exchange and Reduction Processes," Langmuir, Vol. 18, No. 25, pp. 10005–10010, 2002.
[6] Z. Tan, K. Sato, and S. Ohara, "Synthesis of layered nanostructured TiO_2 by hydrothermal method," Adv. Powder Technol., Vol. 26, No. 1, pp. 296–302, 2015.
[7] F. U. Khan, M. Zubair, I. Khan1, M. Z. Ansar, M. K. Alamgir, and S. Nadeem, "Effect of Annealing Temperature on Structural and Optical Properties of Cu-TiO_2 Thin Film," Int. J. Tech. Res. Appl. www.ijtra.com Spec. Issue, Vol. 37, No. 8, pp. 2320–8163, 2016.
[8] M. M. Yusuf, H. Imai, H. Hirashima, "Preparation of porous titania film by modified sol-gel method and its application to photocatalyst", J. Sol-Gel, Sci. Technol. 25,(2002), p. 65.
[9] S. S. Cetin, S. Corekci, M. Cakmak, and S. Ozcelik: 'Structural investigation and electronic band transitions of nanostructured TiO_2 thin films', *Crystal Research and Technology*, 2011, **46** (11),1207-1214.13.
[10] D. O. Scanlon, C. W. Dunnill, J. Buckeridge, S. A. Shevlin, A. J. Logsdail, S. M. Woodley, C. R. A. Catlow, M. J. Powell, R. G. Palgrave, I. P. Parkin, G. W. Watson, T. W.

Keal, P. Sherwood, A. Walsh,and A. A. Sokol: 'Band alignment of rutile and anatase TiO2', *Nature Materials*, 2013, **12**(9), 798-801.
[11] B. Prasai, B. Cai, M. K. Underwood, J. P. Lewis, and D. A. Drabold: 'Properties of amorphous andcrystalline titanium dioxide from first principles', *Journal of Materials Science*, 2012, **47**(21), 7515-7521.
[12] C. Shao, W. H. Wang, M. Y. Hsu, L. C. Wang, Characteristics of ion-beam-sputtered high-refractive-index TiO_2-SiO_2 mixed films", J. Opt. Soc. Am. A 16(1999), P1477.
[13] M. Torrell, L. Cunha, M. R. Kabir, A. Cavaleiro, M. I. Vasilevskiy, and F. Vaz: 'Nanoscale color control of TiO_2 films with embedded Au nanoparticles', Materials Letters, 2010, 64(23), 2624-2626.
[14] F. C. Chung, Z. Zhu, P. Y. Luo, R. J. Wu, and W. Li, "Fabrication of a Au@SnO core-shell structure for gaseous formaldehyde sensing at room temperature," Sensors Actuators, B Chem., Vol. 199, pp. 314–319, 2014.
[15] B. S. Liu, X. J. Zhao, Q. N. Zhao, C. L. Li, and X. He: 'The effect of O-2 partial pressure on the structure and photocatalytic property of TiO2 films prepared by sputtering', Materials Chemistry and Physics, 2005, 90(1), 207-212.
[16] Guo D, Ito A, Goto T, Tu R, Wang C, Shen Q, Zhang L. Effect of laser power on orientation and microstructure of TiO_2 films prepared by laser chemical vapor deposition method. Mater Lett. 2013;9:179–182.
[17] L. Lu-Lin, T. Chiau-Yiag, and W. Hui-Ping, "Morphologic Characterization of Anodic Titania Nanotube Arrays for Dye-Sensitized Solar Cells," J. Chinese Chem. Soc., Vol. 57, No. 5B, pp. 1147–1150, 2010.
[18] Sasani Ghamsari M, Bahramian AR. High transparent sol–gel derived nanostructured TiO_2 thin film. Mater Lett. 2008;9:361–364. doi: 10.1016/j.matlet.2007.05.053.
[19] Senthilkumar V, Vickraman P, Jayachandran M, Sanjeeviraja C. Structural and optical properties of indium tin oxide (ITO) thin films with different compositions prepared by electron beam evaporation. Vacuum. 2010; 84 (6):864–869.
[20] C. Zhang, W. Ding, H. Wang, W. Chai, and D. JU, "Influences of working pressure on properties for TiO2 films deposited by DC pulse magnetron sputtering," J. Environ. Sci., Vol. 21, No. 6, pp. 741–744, 2009.
[21] Nguyen-Phan T-D, Pham VH, Cuong TV, Hahn SH, Kim EJ, Chung JS, Hur SH, Shin EW. Fabrication of TiO_2 nanostructured films by spray deposition with high photocatalytic activity of methylene blue. Mater Lett. 2010;9:1387–1390.
[22] M. Walczak, M. Oujja, J. Marco, M. Sanz, M. Castillejo, Pulsed laser deposition of TiO_2: Diagnostic of the plume and characterization of nanostructured deposits. Appl. Phys. A Mater. 93(2008), P735.
[23] R. Ayouchi, C. Casteleiro, R. Schwarz, J.R. Barrado, n. F. Mart, "Optical properties of TiO_2 thin films prepared by chemical spray pyrolysis from aqueous solutions", Phys. Status Solidi C7(2010),P933.
[24] T. Rojviroon and S. Sirivithayapakorn: 'Properties of TiO_2 thin films prepared using sol–gel process', *Surface Engineering*, 2013, **29**(1), 77-80.
[25] S. H. Kang, M. S. Kang, H. S. Kim, J. Y. Kim, Y. H. Chung, W. H. Smyri, and Y. E. Sung: 'Columnar rutile TiO_2 based dye-sensitized solar cells by radio-frequency magnetron sputtering', *Journal of Power Sources*, 2008, **184**(1), 331-335.
[26] J. R. Devore: 'Refractive Indices of Rutile and Sphalerite', *Journal of the Optical Society of America*, 1951, **41**(6), 416-419.
[27] J. K. Yao, H. L. Huang, J. Y. Ma, Y. X. Jin, Y. A. Zhao, J. D. Shao, H. B. He, K. Yi, Z. X. Fan, F. Zhang, and Z. Y. Wu: 'High refractive index TiO_2 film deposited by electron beam evaporation', *Surface Engineering*, 2009, **25**(3), 257-260.
[28] H. Lee, Y. K. Park, S. J. Kim, J. H. Park, S. J. Ki, and S. C. Jung: 'TiO_2 photocatalyst film using circulating fluidised bed–chemical vapour deposition', *Surface Engineering*, 2015, **31**(2), 134-139.
[29] K. Eufinger, E. N. Janssen, H. Poelman, D. Poelman, R. De Gryse, and G. B. Marin: 'The effect of argon pressure on the structural and photocatalytic characteristics of TiO_2 thin films deposited by d.c. magnetron sputtering', *Thin Solid Films*, 2006, **515**(2), 425-429.
[30] J. G. Yu and X. J. Zhao: 'Effect of substrates on the photocatalytic activity of nanometer TiO2 thin films', *Materials Research Bulletin*, 2000, **35**(8), 1293-1301.

Monte Carlo Estimation of Total Efficiency for NaI Detectors: Point and Extended Sources

[1]Ali N. Mohammed, [2]Luma Y. Abbas
[1]Mustansiriyah University, College of Education, Department of Physics, Baghdad, Iraq
[2] Mustansiriyah University, College of science, Department of Physics, Baghdad, Iraq
[1]aliphysics2203@uomustansiriyah.edu.iq, [2]lmaphysics2203@uomustansiriyah.edu.iq
[1] Corresponding Author: aliphysics2203@uomustansiriyah.edu.iq

Abstract:
A computer simulation program based on Monte Carlo method was designed and written to be as viable tool to calculate the total gamma counting efficiency of NaI detector from point and disk sources. This Monte Carlo computer program allows us to follow, step by step, the story of a prefixed number of photons, starting from their creation in the source, up to their possible absorption in the detector or their escape from it. The program has a modular structure, to favor a wide range of possibilities in the choice of the geometry. The standard error between the present calculations and other results from previously reported literature were found, aggregate, to be less 3% at all energy regions. The current simulation is possible to calculate the total efficiency of other types of scintillation and semiconductor detectors.
Keywords: NaI detector, total efficiency, Monte Carlo Method.

المستخلص:
تم تصميم وكتابة برنامج محاكاة حاسوبي بالإستناد على طريقة مونت كارلو ليكون اداة فعالة في حساب كفاءة عد كاما لكاشف آيوديد الصوديوم NaI لمصادر نقطية واخرى بهيئة قرص. يسمح البرنامج المصمم متابعة، خطوة بخطوة، تاريخ الفوتونات بدأ من انبعاثها من المصدر ولغاية تفاعلها وامتصاصها في الكاشف او هروبها منه. اظهر البرنامج مرونة في التعامل مع اوضاع هندسية مختلفة لنظام الكشف. بعد مقارنة الحسابات الحالية مع النتائج المنشورة، وجد ان نسبة الخطأ بشكل إجمالي لا تتعدى 3%. من الممكن إستخدام المحاكاة الحالية في حساب الكفاءة الكلية لأنواع اخرى من الكواشف الوميضية والكواشف شبه الموصلة.
الكلمات المفتاحية: كاشف آيوديد الوصديوم NaI، الكفاءة الكلية، طريقة مونت كارلو.

1. Introduction:

Gamma detection techniques are widely used in gamma ray spectroscopy for nuclear physics, medical radiography **[1]**, neutron activation analysis **[2]**, well logging **[3]**, and study of cosmic rays **[4]**. In 1948, NaI(Tl) scintillation crystals came into use and provided better conditions for γ-ray detection **[5]**. Since then, scintillation counting has been extended to many other inorganic crystals [e.g. CsI(TI), $Bi_4Ge_3O_{12}$(BGO), $CdWO_4$(CWO)] and organic-based liquids and plastics. Liquid scintillations counting has found wide applications, mainly in the life sciences.

In the beginning of the 1960s, Ge(Li) and Si(Li) crystals and later intrinsic (or high purity) Ge (HPGe) crystals-revolutionized the nuclear sector because of their high energy resolution. Cadmium Telluride (CdTe) has been regarded as a promising semiconductor material for hard X-ray and γ-ray detection since the early 1970's. In the 1990's, the remarkable progress in the technology of producing a high quality single crystal of CdTe and the emergence of Cadmium Zinc Telluride (CdZnTe) has dramatically changed the situations of high resolution room temperature detectors **[6]** and thus is particularly suited for field measurements. Cryogenic detectors **[7]**, the latest generation in detector technology under development in different laboratories around the world, reach even a higher energy resolution, since they are able to register phonons, the thermal debris of the

ionizing event **[1]**. In many fields, the above-mentioned detectors apply to investigations with very low event rates. Therefore, these detectors require a low background.

Detector efficiencies as a function of, mainly, energy can be obtained experimental, empirical, semi-empirical or by modeling approaches i.e. (analytical and Monte Carlo approaches). One main reason for following Monte Carlo simulation is that, in many experimental conditions, it is impossible to use calibrated sources covering the whole relevant energy range, besides this, these sources are obviously limited as concerns their sizes and compositions. By the Monte Carlo method, on the contrary, one can hope to reproduce in a flexible way any experimental physical situation, no matter how complex.
The determination of a sample to detect absolute efficiency using experimental, empirical and the Monte Carlo approaches has been treated by several authors **[8-25]**.

This work describes and evaluates, by Monte Carlo Simulation, the total efficiency of scintillation, as NaI, detector to identify and measure low – level radioactive sources for a wide range of gamma-radiations coming from punctiform and extended sources, included energies in the range up to 10 MeV. The detector types mentioned has its own characteristics that make it suitable for individual applications. One of the two obvious advantages with this approach is the short computation time. The second advantage is the flexibility of putting various detector-related parameters such as source-detector distance, source size, detector radius, etc. as input variables into the computer algorithm. This ability males this method very versatile and can be applied to any detector system and configuration.

2. Simulation procedure:

The present Monte Carlo computer program allows us to follow, step by step, the story of a prefixed number of photons, starting from their creation in the source, up to their possible complete or partial absorption in the detector or their escape from it. The program has a modular structure, to favour a wide range of possibilities in the choice of the geometry.
Isotropic point source and cylindrical detector arrangement are shown in Fig.1, its assumes the existence of a point source, which only "sees" the front face of a cylindrical detector, place at a fixed distance. In the Fig.1, the Z-axis is the symmetry axis of the detector (oriented from the source to the detector) and the XY plane is tangent to the source at its point most remote from the detector itself. In this model, photon interactions within the source and in the container of the source are neglected and scattering of the photons from the shield and other surrounding materials back to the detector was assumed to be negligible.

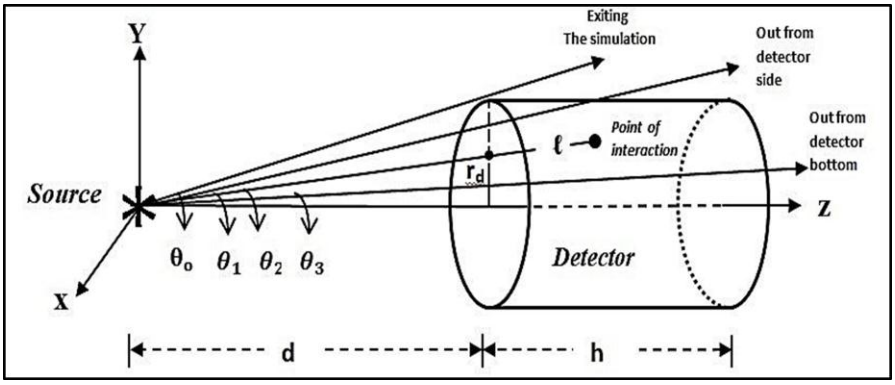

Fig. 1: The simulated geometrical configuration.

To start the program, the values of different physical and geometrical constants must be read in, such as, for example, the geometrical characteristics and positional variables of source and detector. The photons are usually assumed to be isotropically emitted, with a Gaussian energy distribution. However, it is easily possible to arrange the program to simulate preferential-emission directions and more complicate energy distributions.

The different followed steps of the program, to simulate the story of each photon, have been described detail and schematic **[26]**. But here, depending on the type of detector crystal. Viz, difference an attenuation coefficients or the probabilities of the interaction between the gamma ray and this crystal. Description of simulation, briefly, formed as follows:

Step A. each photon is emitted from a randomly chosen point inside the volume of the source, it has a random direction in the half space containing the detector. The emission point and the direction of the trajectory refer to the frame described in fig.1. The self-absorption inside the source is negligible. Otherwise the program goes on with the following step.

Step B. The photon exit path from the source is extended up to the interception point with the plane containing the front face of the detector. If the interception is outside this face, a specific counter is increased (this number allows the calculation of the solid angle) and the program starts again from *step A*. when, on the other hand, the photon goes into the detector, the "virtual" path l_d is evaluated (l_d is the distance which the photon would cover inside the detector in the case of missing interaction).

Step C. To establish the possible interaction point and the type of process which the photon actually undergoes, the relevant absorption coefficients as a function of the gamma energy *E* must be known. To this end, suitable analytical expressions have been obtained, which reproduce to a very good approximation the absorption coefficient values of **ref.27**. The whole energy range up to 20 MeV has been divided into four intervals only, in order to minimize the computing time. It is then possible to calculate the total probability that any one of the three considered processes may occur: $W = (1 - e^{-\mu l_d})$ where $\mu=\mu_{ph}+\mu_c+\mu_{pp}$. Starting from this expression for W, the program chooses first of all whether or not a photon interacts inside the detector. In the negative case a particular counter is increased and the calculation starts again from *step A*, otherwise, the probabilities concerning the various processes are separately evaluated, and the actual processes together with the coordinates of the interaction point are selected.

Step D. Each interaction process is then treated as follows:

Photoelectric effect: In this case the photon is totally absorbed, the event is recorded and a new photon is considered.

Compton scattering: The new direction and corresponding energy of the photon are calculated, on the basis of the Compton angular distribution. The so-defined new photon is followed again, with the same procedure described from *step B*.

Pair production: The energy E of the incoming photon is totally absorbed into the detector, except the energy of the Tow photons following the annihilation of the positron at rest, $E_{\gamma\gamma} = 1.022\ MeV$. Each one of these photons is then followed inside the detector, starting from *step B*, their possible energy losses were then added to the already transferred energy.

Step E. An important point is that the energy (partially or totally) transferred to the detector by each photon is separately recorded, so that all the above process has been treatment for access to the total probability of interaction.

The efficiency measures the percentage of radiation that a given detector detects from the overall yield that is emitted from the source into a solid angle of usually4π. The volume and shape of the crystal, the dimension of the source, the absorption cross section in the

crystal, the distance and position from the source to the detector determines the efficiency of the detector **[28, 29]**. The efficiency curves for the individual detectors were obtained using the following equation for each gamma-ray energy emitted by the calibration sources: **[28, 30]**

$$\text{absolute total efficiency} = \frac{\text{Number of counted photons}}{\text{Number of emitted photons by the source}}$$

$$\text{Intrinsic total efficiency} = \frac{\text{Number of counted photons}}{\text{Number of entered photons to detector}}$$

3. Results and Discussion:

In this study, the total detection efficiency of different scintillation and semiconductor detectors for different energy photons incoming from like-point and thin disk sources has been calculated by employing Monte Carlo technique using a personal computer (PC). A computer program has been designed and written to carry out these calculations. Since, it can be used for different sizes and types of gamma detectors by controlling the input parameters.

At nearby distances, for a good statistical distribution, 10^5 photons have been followed. The error on the total efficiency value was found to be ±0.0012 from repeated calculations for a certain energy value as shown in fig. 2.

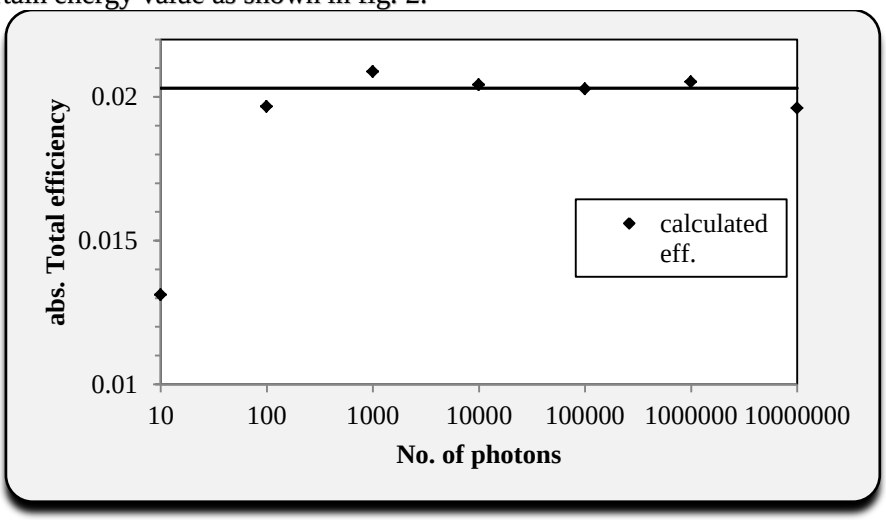

Fig.2: the statistical influence of the value of efficiency versus the number of emitted photons from source.

Total efficiency values calculated for a 3″×3″ NaI(Tl) detector for source-detector distances of d=0.001, 0.5, 10, 20 and 30 cm are given in the Tables 1-4, respectively, containing the standard error (st.er.%) between the present calculations and other results from previously reported literature.

Table 1: Absolute total efficiency values for a 3″×3″ NaI(Tl) with a axial point source at d=0.001 cm away from the front face of the detector.

E (Mev)	Absolute Total Efficiency						St.Er.%
	present work	ref.31 (2016)	ref.24 (2007)	ref.12 (1972)	ref.32 (1961)	ref.19 (1958)	
0.662	0.368280	0.3618	0.36460	0.367	0.37	0.362	-1.01
1.332	0.29367	0.3011	0.29300	0.296	0.302	0.293	-0.23
2.620	0.24216	0.2491	0.24760	0.249	0.25	0.248	2.20

Table 2: Absolute total efficiency values for a 3″×3″ NaI(Tl) with a axial point source at d=0.5 cm away from the front face of the detector.

E (Mev)	Absolute Total Efficiency				St.Er.%
	present work	ref.24 (2007)	ref.14 (1977)	ref.16 (1964)	
0.080	0.433053	0.43330	0.435	0.435	0.06
0.212	0.40167	0.40130	0.404	0.403	-0.09
1.100	0.23092	0.22810	0.229	0.228	-1.24

Table 3: Absolute total efficiency values for a 3″×3″ NaI(Tl) with a axial point source at d=10 cm away from the front face of the detector.

E (Mev)	Absolute Total Efficiency							St.Er.%
	present work	ref.25 (2010)	ref.24 (2007)	ref.14 (1977)	ref.13 (1974)	ref.12 (1972)	ref.16 (1964)	
0.320	0.025056	0.02520	0.0249	0.0251	0.025		0.0247	0.57
0.662	0.02042	0.02030	0.0202	0.0201	0.019	0.0183	0.0198	-0.57
1.330	0.01653	0.01650	0.0164	0.0165	0.0164	0.0168	0.0162	-0.17
2.620	0.01380	0.01415	0.0140			0.0132		2.46
2.750	0.01365	0.01400	0.0139		0.0141			2.53

Table 4: Intrinsic total efficiency values for a 3″×3″ NaI(Tl) with a axial point source at d=20 and 30 cm away from the front face of the detector.

E (Mev)	Intrinsic Total Efficiency								St.Er. %	St.Er. %
	d=20 cm				d=30 cm					
	present work	ref.33(1981)*	ref.33 (1981) **	ref.35 (1983)	present work	ref.33 (1981) *	ref.33 (1981) **	ref.34 (1983)		
0.514	0.755	0.784	0.746	0.76	0.799	-	-	-	3.70	
0.662	0.7121	0.720	0.700	0.72	0.76	0.78	0.739	0.77	1.09	3.40
0.835	0.6718	0.695	0.669	0.67	0.72	0.76	0.707	0.72	3.33	5.52
* Experimental values, ** Calculated values										

While total efficiency values calculated for a 3″×3″ NaI(Tl) detector for a disk source with radius 3.81 cm for the source-detector distances of d=3 and 10cm are given in the Tables 5-6, respectively, containing the standard error (st.er.%) between the present calculations and other results from previously reported literature.

Table 5: Absolute total efficiency values for a 3″×3″ NaI(Tl) with a axial disc source with radius 3.81 cm locate at d=10 cm away from the front face of the detector.

E (Mev)	Total Effeciency						
	present work	ref.25 (2010)	ref.24 (2007)	Ref.35 (1998)	ref.13 (1974)	ref.12 (1972)	ref.19 (1958)
0.050	0.029998	0.02997	0.0301	0.02744	-	-	-
0.100	0.02934	0.02940	0.0295	0.02801	-	-	-
0.500	0.02073	0.02065	0.0206	0.02087	-	-	-
0.662	0.01927	0.01920	0.0191	-	0.019	0.0183	-
1.000	0.01718	0.01700	0.0169	0.01727	-	-	-
1.332	0.01568	0.01567	0.0155	-	0.0164	0.0168	0.0156
2.000	0.01350	0.01409	0.0142	0.0144	-	-	-
2.620	0.01318	0.01349	0.0133	-	-	0.0132	0.0133
2.750	0.01309	0.01336	0.0133	-	0.0141	-	-
5.000	0.01307	0.01264	0.0127	0.01298	-	-	-

4. Conclusions:

In this paper various types of total efficiency were simulated and calculated at wide range of γ-rays energy using Monte Carlo approach, then:

1. The present work provides us with useful tool for efficiency calculations and constitutes a good procedure for the reliable computations instead of the routine of laboratory or experimental measurements. Therefore, one can economize time by averting the calibration of experimental setup for every particular geometry.
2. The results can be functioned in gamma spectroscopy and determination the activity of radioactive sources.
3. Current simulation is possible for other types of detectors, whether, scintillation [e.g.: CsI (TI), $Bi4Ge_3O_{12}$(BGO), $CdWO_4$(CWO)] or semiconductor [e.g.: HPGe, Ge(Li), CdZnTe] using appropriate data for each detector.

References:

1. Sui Shen, Gerald L. DeNardo, Ama Yuan, Diane A. DeNardo and Sally J. DeNardo, “Planar Gamma Camera Imaging and Quantitation of Yttrium-90 Bremsstrah-lung”, J. Nucl. Med. 35 (1994) 1381.
2. David Tin Win,’Neutron Activation Analysis (NAA)’, AU J.T. 8:1 (2004) 8.
3. Shipley, T. H., Ogawa, Y., Blum, P., and Bahr, J.M. (Eds.), Proc. of the Ocean Drilling Program, Scientific Results, 156 (1997) 183.
4. C. Y. Huang , S. E. Park, M. Pohl, C.D. Daniels, “Gamma-rays produced in cosmic – ray interactions and the TeV-band spectrum of RX J1713.7-3946“, Astroparticle Phys., 27 (2007) 429.
5. Heusser G., ”Low-Radioactivit, y Background Techniques“, Annu. Rev. Nucl. Part. Sci., (1995) 544.
6. Tadayuki Takahashi and Shin Watanabe, “Recent progress in CdTe and CdZnTe detectors”, IEEE Transac Nucl. Sci. 48(4) (2001).
7. Previtali E., “20 years of cryogenic particle detectors: past, present and future“, Nucl. Phys. B. Proc. Supplements 150 (2006) 3.

8. K. Debertin, B. Grosswendt, "Efficiency calibration of semiconductor detectors by primary standard sources and Monte Carlo calculations", Nucl. Instr. and Meth. 203 (1982) 343.
9. L. Moens, J. Hoste, "Calculation of the peak efficiency of high-purity germanium detectors", Int. J. Appl. Radiat. Isot. 34 (1983) 1085.
10.T. K. Wang, W. Y. Mar, T. H. Ying, C. L. Tseng, C.H. Liao, M. Y. Wang, "HPGe Detector efficiency calibration for extended cylinder and Marinelli-beaker sources using the Esolan program.", Int. J. Appl. Radiat. Isot. 48 (1997) 83.
11. K.M. Wainio, "Calculated gamma ray response characteristics of semiconductor detecto-rs", G.F. Knoll, Nucl. Instr. and Meth. 44 (1966) 213.
12. T. Nakamura, "Monte Carlo calculation of efficiencies and response functions of NaI(Tl) crystals for thick disk gamma-ray sources and its application to Ge(Li) detectors", Nucl. Instr. and Meth. 105 (1972) 77.
13. M. Belluscio, R. DeLeo, A. Pantaleo, A. Vox, "Efficiencies and response functions of NaI(Tl) crystals for gamma rays from thick disk sources", Nucl. Instr. and Meth. 118 (1974) 553.
14. A. Cesana, M. Terrani, "Gamma-ray activity determination in large volume samples with a germanium-lithium detector", Anal. Chem. 49 (1977) 1156.
15. C. Birattari, A. Salomone, "Efficiency evaluation of gamma-ray solid-state detectors", Nucl. Instr. and Meth. 174 (1980) 391.
16. R. L. Heath, 'Gamma-ray Spectrum Catalogue', Scintill. Spectrom. 1(1964) IDO-16880-1.
17. G. Haase, D. Tait, A. Wiechen, "Monte Carlo simulation of several gamma-emitting source and detector arrangements for determining corrections of self-attenuation and coincidence summation in gamma-spectrometry", Nucl. Instr. and Meth. A 329 (3) (1993) 483.
18. A. Jehouani, R. Ichaoui, M. Boulkheir, "Study of the NaI(Tl) efficiency by Monte Carlo method", Appl. Radiat. Isot. 53 (2000) 887.
19. S. H. Vegors Jr., L. L. Marsden, R. L. Heath, "Calculated efficiencies of cylindrical radiation detectors", USAEC Report IDO-16370, (1958).
20. A. Perez-Andujar, L. Pibida, "Performance of CdTe, HPGe and NaI(Tl) detectors for radioactivity measurements", Appl. Radiat. Isot. 60 (2004) 41.
21. L. Zikovsky, B. Chah, "A computer program for calculating Ge(Li) detector counting efficiencies with large volume samples", Nucl. Instr. and Meth. A 263 (1988) 483.
22. S. Komboj, B. Kahn, "Evaluation of Monte Carlo Simulation of Photon Counting Efficiency for Germanium Detectors", Health Phys. 70 (1996) 512.
23. S. H. Jiang, J. H. Liang, J. T. Chou, U. T. Lin, W. W. Yeh, 'A hybrid method for calculating absolute peak efficiency of germanium detectors', Nucl. Instr. And Meth. A 413 (1998) 281.
24. S. Yalcin, O. Gurler, G. Kaynak, O. Gundogdu, "Calculation of total counting efficiency of a NaI(Tl) detector by hybrid Monte-Carlo method for point and disk sources", Appl. Radiat. Isot. 65 (2007) 1179.
25. A. Hamzawy, "Simple analytical formula to calculate γ-ray cylindrical detectors efficiencies", Nucl. Inst. And Meth. A 624 (2010) 125.
26. Kadhim A. B., Mohammed A. N., "The Treatment of Efficiency of NaI(Tl) Detector By Using Monte Carlo Simulation", Eng. & Tech. Journal, 28 (5) (2010) 1001.
27. Berger, M. J., Hubbell, J. H., XCOM program Version 3.1. NIST Standard Reference Data Base. (1999).

28.Debertin K., Helmer R.G., "Gamma- and X-ray Spectrometry with Semiconductor Detectors". North-Holland, Amsterdam. (1988).
29.Uosif M. A. M., 'Ninth Degree Polynomial Fit Function for Calculation of Efficiency Calibrations for Ge(Li) and HPGe Detectors', Al-Azhar University, Assiut, Egypt. (2005) (Private Communication).
30. Mowlavi A. A. et al., "Calculation of Intrinsic Efficiency of NaI(Tl) Detector Using MCNP Code", Int. J. of Pure and Appl. Phys., 1,(2) (2005) 129-136.
31.Huseyin Ozan Tekin, "MCNP-X Monte Carlo Code Application for Mass Attenuation Coefficients of Concrete at Different Energies by Modeling 3×3 Inch NaI(Tl) Detector and Comparison with XCOM and Monte Carlo Data", Science and Technology of Nuclear Installations, (Volume 2016), Article ID 6547318, Hindawi Publishing Corporation.
32.Miller, W. F., Snow, W. J., "NaI and CsI efficiencies and photofractions for gamma-ray detection", Nucleonics 19:11 (1961) 174.
33.Saito K. and Moziuchi S., "Monte Carlo calculation of accurate response functions for a NaI(Tl) detector for gamma rays", Nucl. Instr. and Meth. 185 (1981) 299-308.
34.Capponi M., Massa I., Piccinini M., Poli M., 'Monte Carlo simulated detector responses to gamma radiations coming from extended sources', Nucl. Instr. And Method, 217(1983) 465-471.
35.Selim Y.S., Abbas M.I., Fawzy M.A., 'Analytical calculation of the efficiencies of gamma scintillators. PartI: Total efficiency for coaxial disk sources', Radiat. Phys. Chem. 53:6 (1998) 589.

Gamma-Ray Attenuation Properties Assessment for THA Alloys: Monte Carlo and Transmission Techniques

Firas Hashem Ahmed[1, a], Ali N. Mohammed[2,b]
[1, 2] **Physics Department, College of Education, Mustansiriyah University, Baghdad, Iraq**
[a]**firashashem@uomustansiriyah.edu.iq,** [b]**aliphysics2203@uomustansiriyah.edu.iq**
[a] **Corresponding Author: firashashem@uomustansiriyah.edu.iq**

Abstract:

In present work, a new procedure of computer simulation program based on Monte Carlo method and photon attenuation technique was designed and written to be as virtual experimental system, instead of the real experimental system. The attenuation coefficients, as well as several other properties, were determined for Heavy Tungsten Alloy to assess its use in radiation applications. The density of alloy, also, was calculated. Simulation results are useful for training and development of human resources, staff and students, in the field of application of nuclear techniques, particularly, in radiation shielding protection.
Keywords: Monte Carlo simulation, attenuation coefficients, Heavy Tungsten Alloy.

المستلخص:

في العمل الحالي، تم تصميم وكتابة إجراء جديد لبرنامج محاكاة الحاسوب على أساس طريقة مونت كارلو وتقنية التوهين الفوتوني ليكون نظامًا تجريبيًا افتراضيًا، بدلاً من النظام التجريبي الحقيقي. تم تحديد معاملات التوهين، فضلا عن خصائص اخرى، لسبائك التنجستن الثقيل لتقييم استخدامها في تطبيقات الإشعاع. كما تم حساب كثافة السبيكة. نتائج المحاكاة مفيدة لتدريب وتطوير الموارد البشرية والموظفين والطلاب، في مجال تطبيق التقنيات النووية، ولاسيما في الحماية من الإشعاع.
الكلمات المفتاحية: محاكاة مونتي كارلو، معاملات التوهين، سبائك التنجستن الثقيل.

1. Introduction

Many human activities such as nuclear reactors, nuclear research institutions, radiation therapy clinics, factories that use radio isotopes, and nuclear weapons lead to exposure, directly or indirectly, to gamma-ray hazards. Therefore, it is necessary to take precautions because of these risks, by using shields and increasing their efficiency.

Tungsten heavy alloys were invented by McLennan in 1935, after that, these alloys were manufactured to use as alternatives to lead as shields against radiation. These alloys have a host of properties that make them possible to be used as radiation shields. These properties are plasticity, high density, impact strength, and high strength [1].

When there is a need to use a material in the shielding industry, an important factor must be studied and calculated, which is the linear attenuation coefficient. As determining its value accurately is important to know the possibility of using the material in radiation physics, radiation dosimetry, radiography, crystallography, spectrometry, biology, medicine, environment, agriculture and industry.

Computer simulation can be defined as: "The use of a computer to mimic events in the actual world according to a properly developed assumption takes shape of logical, statistical, or mathematical relationships that are formed into a model " [2]. The results can be managed by adjusting a set of input parameters to assist the analyst to understand the basic system's dynamics. The model is usually evaluated numerically via simulation periods and data are collected to assess real-world system properties. In general, these data are described with statistics like any experiment. Thus simulation is considered as an

experiment [3], or a computer experiment, when considering the similarity of traits with laboratory experiments.

The Monte Carlo method is a stochastic numerical simulation technique that deals with all geometrical and physical states of the problem. Simulations of the transmissions of neutrons, photons, and electrons, especially in irregular geometrical systems, can be done using this technique. The transfer details of single particles are formed by random sampling of particles as they move through the geometry. Then these transfer details are interpreted to present information on amounts of interest, such as detector response or particle influence. The Monte Carlo method is useful in solving difficult-to-solve problems with common deterministic techniques. This method also presents an answer with a statistical uncertainty, so that a level of conviction in the results can be ascertained.

The attenuation or transition of particles is simply the amount of change in count rate detection from a source when a substance, with a particular thickness, is entered in between.

In the current research, a new computer simulation program was designed and implemented based on the Monte Carlo method and the photon attenuation technique to be used as a conceptual experiment system instead of the actual experiment system.

2. Simulation procedure

The suggested design for the present simulation is shown in Fig.1 which include a radio-active source, a NaI(Tl) detector and a THA as sample with various thickness values. The distance between the source-alloy and the alloy-detector can be varying.

We have developed a Monte Carlo simulation to study the interaction occurred when the photons beam hit the alloy. Only photons transmitted within a solid angle covered by the detector are to be counted.

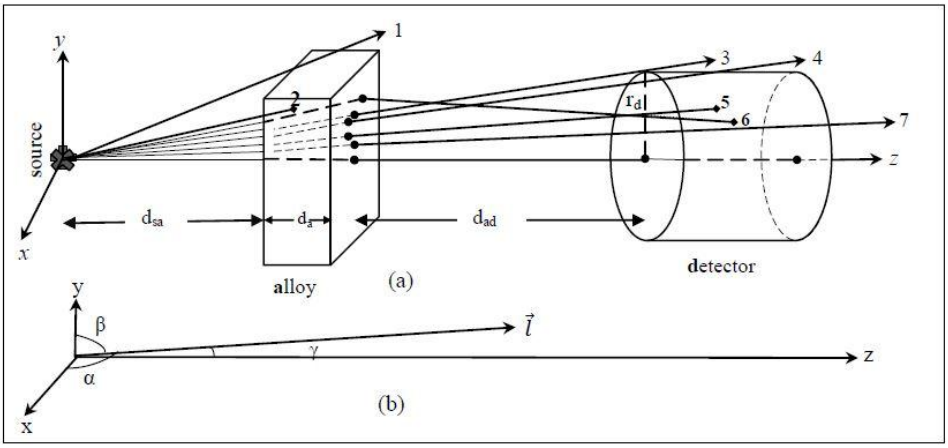

Fig.1: The suggested design for the present simulation of source-alloy, alloy-detector systems by present Monte Carlo computer program. (a) Fixed dimensions system and (b) reference dimensions system.

All interactions based on physical and mathematical considerations. According to the following steps:

(1) Every photon is emitted from a random point (xo, yo, zo) from the source.
It has a random direction (α ,β,γ). Emission point and direction of trajectory are described in fig.1.

(2) Parametric equations were used to estimate the location of photons as follows:

$$x = x_o + l\cos\alpha \cdots\cdots\cdots (1)$$
$$y = y_o + l\cos\beta \cdots\cdots\cdots (2)$$
$$z = z_o + l\cos\gamma \cdots\cdots\cdots (3)$$

(3) When the photon hit the alloy the virtual path *pl* is evaluated. It is the distance which the photon passes inside the detector in the case of missing interaction. According to an exponential distribution using the equation [4]:

$$p_l = -\frac{1}{\mu_l} ln(1 - R_n) \cdots\cdots\cdots (4)$$

where *Rn* is the random number ($0<R_n< 1$), and μl is the linear attenuation coefficient of γ-radiation. XCOM program [5] used to calculate the mass attenuation coefficients (μ_l), where ρ is the bulk density of the element. The weighting equation [6] can be used, since:

$$(\mu_l)_c = \sum_{i=1}^{n} w_i (\mu_l)_i \cdots\cdots\cdots (5)$$

where: (μl) is the linear attenuation coefficient of compound or mixture, and (w_i) the weighting factor and linear attenuation coefficient of *ith* element in compound respectively.

(4) Putting the parameter *pl* of eq. (4) instead of the parameter *l* in eqs. (1), (2) and (3) with particular new values of random direction (α, β, γ) determines either the photon completely absorbed within alloy material (i.e. trajectory 2) or penetrates the alloy forward of the detector (i.e. trajectories 3-7).

(5) Carrying out the steps from 2 to 5 to determine either the photon don't collide the front face of the detector (i.e. trajectory 3) or collides (i.e. trajectories 4-7). These photons either escape from side or bottom of the detector (i.e. trajectories 4 and 7) or registered as directly (i.e. trajectory 5) or as indirectly (i.e. trajectory 6).

3. Results and Discussion:

By estimating the linear attenuation coefficient (μl) and mass attenuation coefficients (μm) for a particular material the attenuation properties of photons in this material can be known. In our procedure, 10^8 gamma photons (monoenergetic) were sent towards the attenuator. These photons emitted from virtual radioactive sources with energies are 662 keV and 1250 keV.

The attenuators in our simulation are manufactured of high-density tungsten heavy alloys. Table 1 state the composition of tungsten heavy alloys (THAs) used for present research. A virtual NaI(Tl) detector was used to detect these photons. This method simulates actual practical experience.

Table 1. Compositions of tungsten heavy alloys (THAs) used in present research.

Sample	Composition weight				Density (g/cm^3)
	W (%)	Ni (%)	Fe (%)	Co (%)	
THA-1	90.8	6.2	1.2	1.8	17.4
THA-2	96.2	2.8	0.8	0.2	18.44
THA-3	98.2	1.4	0.4	0	18.53

Table 2. Mass attenuation coefficients of tungsten heavy alloys (THAs) used for present research.

Sample	Mass Attenuation Coefficients ($g.cm^{-2}$)	
	662 keV	1250 keV
	XCOM	XCOM
THA-1	0.09051	0.05415
THA-2	0.08993	0.05417
THA-3	0.09189	0.05417

The semi-logarithmic calculated distributions of registered counts versus energy (Attenuation graph) for particular gamma energy are shown in Fig.2.

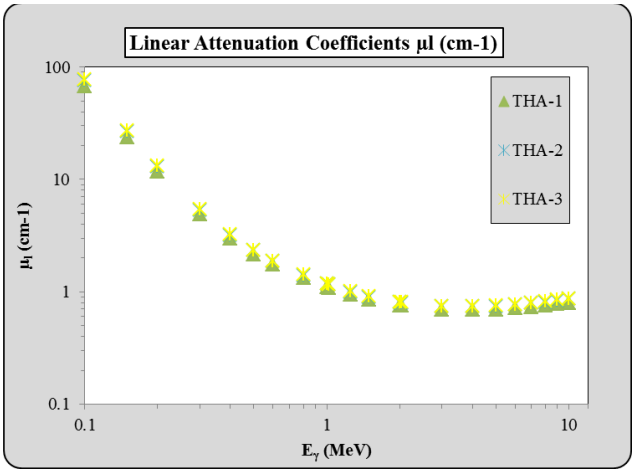

Fig. 2. Linear attenuation coefficients of tungsten heavy alloys (THAs) used for present research.

The transmission for a gamma source of energy E through d [cm] of shielding material was estimated indirectly by determining the dose imparted to a thin cylinder of air of length 0.1 cm, centered behind the shield on the z-axis. Fig.3 and Fig.4 show Tungsten heavy alloys (THAs) transmition comparisons at 662 keV and 1250 keV of gamma-ray energy respectively.

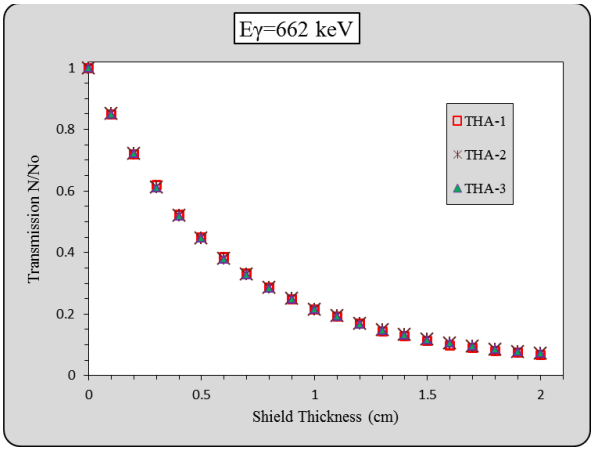

Fig.3: Tungsten heavy alloys THAs Transmition Comparison at 662 keV of gamma-ray energy.

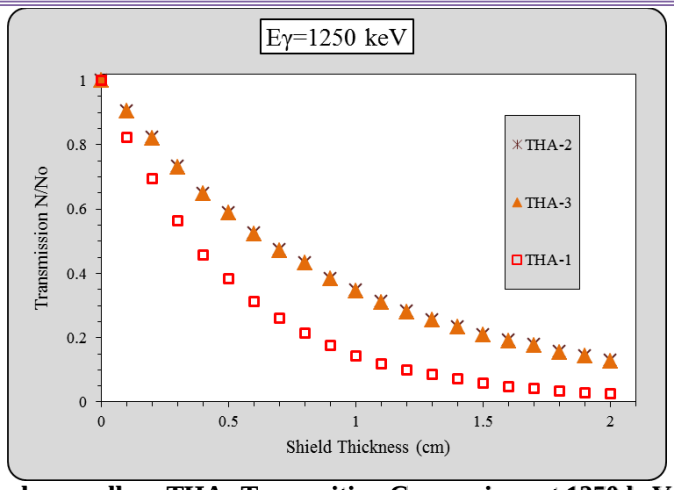

Fig.4: Tungsten heavy alloys THAs Transmition Comparison at 1250 keV of gamma-ray energy.

4. Conclusions:

i. Gamma attenuation method can be effective tool for knowing some properties of alloys as agamma ray shield.
ii. The present computer program was a Monte Carlo method and gamma attenuation technique can be used as virtual experiment instead of the real experimental set up.
iii. The present program can be quantified of various types of alloy.
iv. The present simulation program can be used to design different experimental geometries.

References

[1] Paweł Skoczylas, Zbigniew Gulbinowicz and Olgierd Goroch, Microstructure and Properties of Tungsten Heavy Alloy Connections Formed during Sintering with the Participation of the Liquid Phase. Materials (Basel), (2020), 13(21): 4965.
[2] McHaney, Roger, Understanding Computer Simulation. Ventus Publishing Aps. (2009).
[3] Dagpunar, J. S., Simulation and Monte Carlo: With applications in finance and MCMC. John Wiley & Sons, Ltd. (2007).
[4] Dunn William L., and J. Kenneth Shultis, Exploring Monte Carlo Methods. Elsevier B.V., Oxford, UK. (2012).
[5] Berger, M. J., and Hubbell, J. M., XCOM Program V.3.1: Photon Cross Sections Database. NIST standard reference database. (1999).
[6] Martin, James E., Physics for Radiation Protection. Weinheim: Wiley-VCH, (2006).

Jordan Generalized (σ,τ)-Reverse Derivation on Semirings

Salah Mehdi Salih [(1)] **Marwa Riyadh Salih** [(2)]
Department of Mathematics College of Education Mustansiriyah University. Baghdad, Iraq.
[(1)] dr.salahms2023@gmail.com, [(2)] nzj72hd@gmail.com

Abstract

The propos of this paper are preset the concepts of generalized (σ,τ)-reverse derivation, Jordan generalized (σ,τ)-reverse derivation and Jordan generalized triple (σ,τ)-reverse derivation on semiring. We prove that every Jordan generalized (σ,τ)- reverse derivations on semiring S with additive inverse and identity associated with Jordan (σ,τ)-reverse derivation d on S, where σ, τ are automorphism on S is generalized (σ,τ)-reverse derivation on S.

المستخلص

الهدف من هذا البحث تقديم المفاهيم التالية تعميم المشتقات العكسية -(σ,τ)، تعميم مشتقات جوردان العكسية (σ,τ) وتعميم مشتقات جوردان الثلاثية العكسية -(σ,τ) وقد برهنا بان كل تعميم مشتقه جوردان العكسية -(σ,τ)على شبه الحلقه S التي تمتلك المعكوس والعنصر المحايد مع عملية الجمع والمرتبطة مع مشتقة جوردان الثلاثية العكسية -(τ,σ) على S، اذ τ,σ دوال تماثل من S الى S تكون تعميم المشتقة العكسية -(σ,τ).

1. Introduction

The notion of semirings was first introduced in 1934 by H. S. Vandiver. [1]

A semiring is an algebraic structure, consisting of a nonempty set S on which we have defined two associative binary operations, addition (usually denoted by +) and multiplication (usually denoted by · or by concatenation) such that the multiplication is distributive over addition. A natural example of semiring which is not a ring is set of Natural numbers N, under usual addition and multiplication of numbers.[2],[3]

A semiring S is said to be prime if $xSy=0$ implies $x=0$ or $y=0$ for all $x,y\in S$, a semiring S is said to be semiprime if $xSx=0$ implies $x=0$ for all $x \epsilon S$, a semiring S is said to be 2-torsion free if $2x=0$ implies $x=0$ for all $x \epsilon S$. [3], [4].

The semiring $(S,+,.)$ is said to be semiring with additive identity 0 such that $x+0 = x = 0+x$ for all $x \epsilon S$. A semiring $(S,+,.)$ is said to have an identity element 1,if $1\neq 0$ such that $1.x= x = x.1$ for all $x \epsilon S$. A semiring $(S,+,.)$ is said to be an additive commutative if x+y = y+x, for all x,y∈S, and is said to be commutative with multiplication if $(S,.)$ is commutative. The set $C(S)=\{x \epsilon S, xy=yx$ for all $y \epsilon S\}$is called the center of the semiring S. A semiring S is called with additive invertible if S with additive identity and for all x∈S there exist -x∈S such that x+(-x)=0= (-x)+x, and S is called with multiplicative invertible if S with multiplicative identity such that for all x∈S there exist x^{-1}∈S and $x.x^{-1}=1=x^{-1}.x$.

S. M. Salih in [6] present the concepts of (σ,τ)-reverse derivation, Jordan (σ,τ)-reverse derivation and Jordan triple (σ,τ)-reverse derivation on semiring. For more informations see [7,8].

In this paper we generalization [6] by introduce the concepts of generalized (σ,τ)-reverse derivation, Jordan generalized (σ,τ)-reverse derivation, Jordan generalized triple (σ,τ)-reverse derivation and prove that: Every Jordan generalized (σ,τ)-reverse derivation

on 2-torsion free semiring S where σ,τ are automorphism on S is Jordan generalized triple (σ,τ)-reverse derivation on S.

2. Generalized (σ,τ)-Reverse Derivations on Semirings

In this section we present the concepts and properties of generalized (σ,τ)-reverse derivations, Jordan generalized (σ,τ)-reverse derivation and Jordan generalized triple (σ,τ)-reverse derivation on semiring S. We begin with the following definition:

Definitions 2.1: let S be semiring and σ, τ are automorphism on S, an additive map f on S is called generalized (σ, τ)-derivation associated with (σ,τ)-reverse derivation d on S if and only if for all a,b∈S

f(ab) = f(b)$\sigma(a)$+τ(b)d(a)

f is called Jordan generalized (σ,τ)-reverse derivation on S associated with Jordan (σ,τ)-reverse derivation d on S if for all a,b ∈S

$f(a^2) = f(a)\sigma(a) + \tau(a)d(a)$

f is called Jordan generalized triple (σ,τ)-reverse derivation on S associated with Jordan triple (σ,τ)-reverse derivation d on S if for all a,b∈S

f(aba) = f(a)σ(b)σ(a) + σ(a)d(b)τ(a) + τ(a)τ(b)d(a)

Example 2.2: Let $A=\left\{\begin{pmatrix} n & 0 \\ 0 & m \end{pmatrix} : n, m \in Z\right\}$ be a semiring and f be generalized (σ,τ)-reverse derivation of A associated with (σ,τ)-reverse derivation d on A, and let $S = A \times A$. We use the usual addition and multiplication on matrices of S. Then S is a semiring. We define F be an additive mapping of S such that $F(a, b) = (f(a), f(b))$ then F is generalized (σ,τ)-reverse derivation on S associated with (σ,τ)-reverse derivation D on S such that D(a,b)=(d(a), d(b)) for all (a,b) ∈S.

Lemma 2.3: Let f be Jordan generalized (σ,τ)-reverse derivation on additive commutative, identity and inverse semiring S associated with Jordan (σ,τ)-reverse derivation d on S, where σ,τ are automorphuism on S then for all a,b ∈S

f(ab+ba) = f(b)σ(a) + τ(b)d(a) + f(a)σ(b) + τ(a)d(b)

Proof: f((a+b)(a+b)) = f(a+b)σ(a+b)+ τ(a+b)d(a+b)

= (f(a)+f(b))(σ(a)+σ(b))+ (τ(a)+τ(b))(d(a)+d(b))

= f(a)σ(a)+f(a)σ(b)+f(b)σ(a)+f(b)σ(b) + τ(a)d(a)+

τ(a)d(b) + τ(b)d(a)+τ(b)d(b) …(1)

On the other hand

$f((a+b)(a+b)) = f(a^2+ab+ba+b^2)$

$= f(a^2) + f(b^2) + f(ab+ba)$

= f(a)σ(a) + τ(a)d(a) + f(b)σ(b) + τ(b)d(b) + f(ab+ba) …(2)

Comparing (1) and (2) we have

f(ab+ba) = f(b)σ(a)+ τ(b)d(a)+ f(a)σ(b)+ τ(a)d(b)

Definition 2.4: Let S be semiring with additive inverse. If f is Jordan generalized (σ,τ)-reverse derivation on S associated with Jordan (σ,τ)-reverse derivation d on S, we define φ from S×S into S by

φ(a,b) = f(ab)- f(b)$\sigma(a)$-τ(b)d(a), for all a,b∈S

In the following lemma we present the properties of φ(a,b):

Lemma 2.5: If S is semiring with additive inverse and f is Jordan generalized (σ,τ)-reverse derivations on S associated with Jordan (σ,τ)-reverse derivation d on S, where σ and τ are automorphism on S then for all a,b,c ∈S

i) φ(a,b)= -φ(b,a)

ii) φ(a+c,b)= φ(a,b)+ φ(c,b)

iii) φ(a,b+c)= φ(a,b) + φ(a,c)

Proof:

i) f(ab+ba) = f(b)σ(a)+ τ(b)d(a)+ f(a)σ(b)+ τ(a)d(b)
f(ab)+f(ba)= f(b)σ(a)+ τ(b)d(a)+ f(a)σ(b)+ τ(a)d(b)
f(ab)- f(b)σ(a)- τ(b)d(a)= -f(ba)+ f(a)σ(b)+ τ(a)d(b)
φ(a,b)= -φ(b,a)

ii) φ(a+c,b) = f((a+c)b)- f(b)$\sigma(a+c)$-τ(b)d(a+c)
= f(ab + cb) –f(b)(σ(a)+σ(c)) - τ(b)(d(a)+d(c))
= f(ab)+f(cb) –f(b)σ(a) –f(b)σ(c)- τ(b)d(a) - τ(b)d(c)
= f(ab) –f(b)σ(a) - τ(b)d(a) + f(cb) –d(b)σ(c) - τ(b)d(c)
= φ(a,b)+ φ(c,b)

iii) φ(a,b+c)= f(a(b+c))- f(b+c)$\sigma(a)$-τ(b+c)d(a)

= f(ab+ac) – (f(b)+f(c))σ(a) - (τ(b)+τ(c))d(a)
= f(ab)+f(ac) –f(b)σ(a)- f(c)σ(a) –τ(b)d(a)-τ(c)d(a)
= f(ab) –f(b)σ(a) –τ(b)d(a)+ f(ac) - f(c)σ(a) -τ(c)d(a)
= φ(a,b) + φ(a,c)

Remark 2.6: If S is semiring with additive identity then f is generalized (σ,τ)-reverse derivations on S associated with (σ,τ)-reverse derivation d on S, where σ and τ are automorphism on S if and only if φ(a,b) =0, for all a,b∈S.

3. The Main Results

The propose results of this paper introduce in this section. We begin with the following lemma.

Lemma 3.1: If S is semiring with additive inverse, identity and commutative. f is Jordan generalized (σ,τ)-reverse derivation on S associated with Jordan (σ,τ)-reverse derivation d on S, where σ,τ are automorphism on S then:

φ(a,b)=0, for all a, b ∈ S,

Proof: By Lemma 2.3 we get:

f(ab+ba) = f(b)σ(a) + τ(b)d(a) + f(a)σ(b) + τ(a)d(b) …(1)

Now we have

Since f is additive mapping of the semiring S we have

f(ab+ba) = f(ab)+ f(ba)

= f(ab) + f(a)σ(b) +τ(a)d(b) …(2)

Comparing (1) and (2) we get

f(ab) – f(b)σ(a) - τ(b)d(a) =0

φ(a,b)=0

Theorem 3.2: Every Jordan generalized (σ,τ)- reverse derivations on semiring S with additive inverse, identity and commutative associated with Jordan (σ,τ)-reverse derivation d on S, where σ,τ are automorphism on S is generalized (σ,τ)-reverse derivation on S.

Proof: Let f be Jordan generalized (σ,τ)- reverse derivations on semiring S

Then by Lemma 3.1 we get

φ(a,b)=0

Now by Remark 2.6 we get

f is generalized (σ,τ)-reverse derivations on semiring S.

Proposition 3.3: Every Jordan generalized (σ,τ)-reverse derivation on 2-torsion free semiring S where σ,τ are automorphism on S is Jordan generalized triple (σ,τ)-reverse derivation on S.

Proof: Since f Jordan generalized (σ,τ)-reverse derivation on S associated with Jordan (σ,τ)-reverse derivation d on S

Replace ab+ba by b in lemma 2.3 we get

$f(a(ab+ba)+(ab+ba)a) = f((aa)b+(ab)a+(ab)a+(ba)a)$

$= f(b)\sigma(a)\sigma(a) + \sigma(b)d(a)\tau(a) + \sigma(b)\tau(a)d(a) + f(a)\sigma(b)\sigma(a) + \sigma(a)d(b)\tau(a) + \tau(a)\tau(b)d(a) + f(a)\sigma(b)\sigma(a) + \sigma(a)d(b)\tau(a) + \tau(a)\tau(b)d(a) + f(a)\sigma(a)\sigma(b) + \sigma(a)d(a)\tau(b) + \tau(a)\tau(a)d(b)$ …(1)

On the other hand

$f(a(ab+ba)+(ab+ba)a) = f(aab+aba+aba+baa)$

$= f(b)\sigma(a)\sigma(a) + \sigma(b)d(a)\tau(a) + \sigma(b)\tau(a)d(a) + f(2aba) + f(a)\sigma(a)\sigma(b) + \sigma(a)d(a)\tau(b) + \tau(a)\tau(a)d(b)$ …(2)

Comparing (1) and (2) we get

$f(2aba) = f(a)\sigma(b)\sigma(a) + \sigma(a)d(b)\tau(a) + \tau(a)\tau(b)d(a) + f(a)\sigma(b)\sigma(a) + \sigma(a)d(b)\tau(a) + \tau(a)\tau(b)d(a)$

Since S is 2-torsion free we get

$f(aba) = f(a)\sigma(b)\sigma(a) + \sigma(a)d(b)\tau(a) + \tau(a)\tau(b)d(a)$

Thus f is Jordan generalized triple (σ,τ)- reverse derivation on S.

Corollary 3.4: Every generalized (σ,τ)- reverse derivation on 2-torsion free semiring S is Jordan generalized triple (σ,τ)- reverse derivation on S.

Proof: Assume that f is generalized (σ,τ)- reverse derivation on S, by Definition 2.1 f is Jordan generalized (σ,τ)- reverse derivation on S and by Proposition 3.3 f is Jordan generalized triple (σ,τ)- reverse derivation on S.

References:

1) H. S. Vandiver 1934. Note on a simple type of algebra in which the cancellation law of addition does not hold, bull. Amer. Math. Soc., Vol. 40, 916- 920.

2) M. Chandramouleeswaran, 2010, "On Derivations of Semirings", Advances in Algebra Volume 3, Number 1, pp. 123–131.

3) D. Mary Florence, 2018, "On Right Centralizers of Semiprime Semirings" Advances in Algebra, Volume 11, Number 1, pp. 19-28.

4) S. P. Nirmala Devi1, V. Thiruveni, 2015, "BI-Derivationson Ideals in Semiprime Semirings" International Journal of Pure and Applied Mathematics, Volume 98 No. 5, pp. 1-7.

5) N. Sugantha Meena1, M. Chandramouleeswaran, 2015, "Reverse Derivations on Semirings" International Journal of Pure and Applied Mathematics Volume 104 No. 2, pp. 203-212.

6) S. M. Salih, 2020, "Jordan (σ,τ)-Reverse Derivations on Prime Semirings", Academic J. for Engineering and Science, Vol. 2, No. 4, pp. 27-30.

7) S. M. Salih and M. R. Salih, 2014, "On Jordan Generalized Higher Reverse Derivations on Γ- rings", IOSR Journal of Mathematics, Volume 10, Issue 5 Ver. IV, pp. 25-33.

8) S. M. Salih and M. R. Salih, 2014, "Ideal of Prime Γ-Rings with Right Reverse Derivations", IOSR Journal of Mathematics, Volume 10, Issue 5 Ver. III, pp.83-85.

Subject Review on Different Steganography Methods

Donia Fadil Chalob[1], Ameer Badr Khudhair [2], Zainab Mohammed Essa[3]
Department of computer Science, Collage of education, Mustansiyiah University, Iraq1,[3]
Al-Mansour University College[2]

Abstract
Different Steganography methods are introduced to provide security. Data is typically presented as text, audio, video and image files that can be hidden using steganography algorithms. The hide of undisclosed information in video and image file is known as video steganography and image steganography, respectively. This paper have been reviewed different steganography techniques like transform domain, spatial domain, vector embedded and statistical techniques.
Keywords: Steganography, Security, LSB, DCT, DNA.

المستخلص:
يتم تقديم طرق إخفاء المعلومات المختلفة لتوفير الأمان. يتم تقديم البيانات عادةً على هيئة ملفات نصية وصوتية وفيديو وصور يمكن إخفاؤها باستخدام خوارزميات إخفاء المعلومات. يُعرف إخفاء المعلومات غير المكشوف عنها في ملفات الفيديو والصور باسم إخفاء المعلومات وإخفاء الصور على التوالي. استعرضت هذه الورقة تقنيات إخفاء المعلومات المختلفة مثل مجال التحويل، والمجال المكاني ، والمتجه المدمج ، والتقنيات الإحصائية.
الكلمات الرئيسية: إخفاء المعلومات، الامنية، LSB, DCT, DNA.

1. Introduction

The World Wide Web now allows for the unlimited and simple transmission of digital data: text, audio, video, image, network, etc. over the internet (WWW). Meanwhile, such unrestricted admission to enormous amounts of information has attracted serious threats to secure and privacy protected communication over WWW, making securing information over non-secured networks makes a challenge. Adversaries be able to frequently damage information by trying to manipulate the message, producing ethical or financial damage. As a result, many information cipherment and concealment techniques have been established in order to achieve secure data communication [1, 2].

There are two types of information hiding domains which are steganography and watermarking, both of which are utilized to conceal the private message. Furthermore, while these two techniques are closely related, each has its own set of goals [3, 4].

The purpose of watermarking is to preserve the integrity of the confidential data by preventing outsiders from learning of its existence, whereas steganography is the practice of hiding information by placing a covert message in a public medium with no indication of its presence. The secret message is disordered so that it appears to eavesdroppers as ciphered communication during the information encryption process known as cryptography. An encrypted message, on the other hand, is frequently ineffective, attracting opponents' attention or making it evident to them. [3].

Steganography is a data concealment technique in which the media containing the hidden message has secret data integrated in the cover media such that is impossible to detect and noticed by the intruder. The message will be meaningless even if it is noticed. In the digital world, both steganography and cryptography aim to store and shield the hidden message from intruders. These methods can be used composed or separately. Their mixture produces exceptional results; however multiple layers are required to ensure the highest level of security. Text, image, DNA, network, audio and video data formats are currently used with digital steganography [4].

The layout of this study is as follows: Types of steganography are covered in Section 2. The steganography research methodologies are presented in Section 3. Section 4 also covers the conclusion.

2. Steganography Types

In steganography, a variety of cover objects types are employed. They include text, image, audio, video, and protocol. Steganography methods were classified according on the kind of cover item utilized [5]:

I. Text Steganography

Information can be concealed in text using general methods such the quantity of tabs, white space, capital letters, and each n^{th} letter of a word.

II. Image Steganography

Steganography is referred to as image Steganography if the cover object is an image. The pixel intensity is typically employed in this technique to hide.

III. Audio Steganography

Steganography is referred to as audio Steganography when an audio signal is employed as a cover object. This approach uses digital audio formats like wav, mp3, and others.

IV. IP Steganography

The term "IP" stands for Internet Protocol. Network protocols including User Data Protocol (UDP), Stream Control Transmission Protocol (SCTP), Transmission Control Protocol (TCP), Internet Protocol (IP), and others are utilized in this technique for the cover object. Unused TCP/IP header bits can be used for steganography.

V. Video Steganography

The video indication is utilized as a cover in video steganography. Videos are typically made up of images and sounds. As a result, a large amount of data can be concealed using video signal as a carrier. As cover objects, H.264, MPEG, AVI, and others.

3. Literature Survey

Many methods related to steganography have been studied over the years. Some of these studies are discussed in this section.

Instead of pursuing high PSNR, **Yang** et al. [6] developed a novel RDH technique for enhancing the detail information's visual quality in medical photographs. To enhance texture area contrast and image quality, the suggested method preferentially embeds data into the texture area utilizing the histogram shifting (HS) and contrast enhancement methods.

Vardhan et al. [7] after eliminating the rounding error utilizing mapping integer with cumulative distribution function, an Integer Wavelet Transform (IWT)-based technique for concealing revocable data in cipher pictures is provided. A new reversible data hiding technique is used by ciphering one of the four IWT bands using a fractal as the key and histogram shifting. Additional methods of cipherment and data concealment are being developed, such as logistic map and embedding of Least Significant Bit. The proposed method generates a random sequence using King's dream fractal. only a portion of the image is Low Low (LL) is encrypted. At this stage, the data is simultaneously hidden by combining all three of the unencrypted bands with high frequency coefficients into a single image, or i2. The image histogram of i2 is examined and two threshold standards are selected as (T1, T2). It is necessary to generate a calculated number of random generated message bits; this amount can be obtained by counting the number of accurate available threshold planes. By lowering the histogram's center peak and shifting the values to both sides of the selected threshold levels, the proposed method seeks to hide data. To do this, if

the embedding bit is 1, the coefficients of i2 will be multiplied by 1, otherwise the coefficients of i2 will remain unaltered, from the randomly generated message bits consisting of 0s and 1s. This process is repeated until the message bits are exhausted. The histogram's peak is shifted to together parts of the threshold value, obscuring the original image.

Manikandan et al. [8] improved the standing reversible data concealing method using a new cipher operation to rise the bit error rate without losing the embedding rate by a factor of 3. The proposed approach allows for the insertion of three bits of information into a single image block of size B B pixels. Similarly to the existing method, the source and destination in the proposed method only need to share 3 cipherment/ decipherment keys. This manuscript proposes an improved reversible data concealment method via cipherment. The bit error rate is increased by a factor of three without compromising the current reversible data hiding strategy using cipherment. The key management overhead remains identical as it was in the previous scheme. However, the cipherment operation has been slightly changed; the selection of a pseudorandom order for the cipherment operation of a particular block is identified by 3-bits sequence that to embedding in the particular block. Because there be able to 8 different combinations of bits when dealing with 3-bit data, defining nine different pseudorandom sequences, with one used if no requirement to embed data in a certain block. As a final point, an experiment study on thistechnique demonstrates that the suggested work will be more beneficial in uses such as transmission of medical image.

Elharrouss et al. [9] offered a k-LSB- based method based on LSB coding to hide the image using k least bits. Before decoding the secret image, the blocks that contain it are identified using a region detection procedure. A steganography's resolution may be impacted; to improve the resolution, an image quality improvement technique is utilized. The three least significant bits (LSB) are used to incorporate a text message within a concealing image. However, To embed an image into an image, the three least significant bits are insufficient. The content of a pixel can be represented by its first four bits. n order to do so, continue by blending this image into another. The feature of the concealment images and steganographic images may be affected. Use a method for improving the image quality after removing the embedded image to improve its quality. The extraction of the steganography uses the identical methods as the encoding portion, which involves removing the first four pixels' worth of information.

Bangera et al. [10] proposed a technique implemented using MATLAB, First, the RSA cryptographic algorithm converts the message to encrypted text. Using the LSB audio steganography technique, the encrypted text is concealed in audio media. The acquired output audio is utilized as the input audio in the second round of audio steganography. At the destination direction, The audio steganography decoding algorithm extracts the encrypted text from the audio cover twice. The original message is decrypted using RSA decipher.

Kar et al. [11] presented a DNA-based method for transmitting information concealed inside a video file. Image frames are first created from the video file. Data is hidden using the Least Significant Bit replacement method in random frames at random places. Assess the peak signal-to-noise ratio (PSNR) and mean squared error (MSE), which are calculated from the original and stenographic files and averaged over the whole video frame, for the proposed architecture. The result shows that the stenographic file video has suffered only minor degradation. (ACTGGTCACGTAGTAG, for example), and applying three separate procedures on the selected DNA strand.

Huang & Tang [12] introduced a novel spatial steganography technique for voice over internet protocol (VoIP) covert communication, solving the challenge of expanding covert VoIP bands' capacity without endangering the channels' audibility. The model introduced two concepts to covert VoIP communications, orthogonal data concealment characteristics and data concealment vectors, based on Orthogonal Modulation Theory in communications. By taking into account the variation characteristics of the VoIP audio stream in the time domain, a hidden vector negotiation technique was presented to achieve dynamic self-adaptive steganography in media streams.

Deepika & Saravanan [13] introduced a hash-based data hiding method in which the frame data is used to create the hash array after the speech stream has been collected from the UDP protocol. The hash array needs to be refreshed for each new frame. The secret data is then chopped, and the hash function is used to determine the proper bit position to embed the secret data. The value of the hash array is set to 0 once the secret data has been properly implanted. The receiver receives the hash array and audio samples as a VoIP frame, after which the secret message can be extracted using the hash array flag value. On both sides of the sender and receiver, In terms of undetectability, computational complexity, and speech quality, the method fared well. The issue is the hash array's increased bandwidth usage during VoIP communication operations.

Yasir Hamza et al. [14] has been recommended to use visual cryptography in conjunction with an enhanced image steganography technique. A secret logo “binary image” of size 128 x 128 is ciphered using visual cryptography two out of two share to produce two secret shares. Through the embedding operation, a (512 x 512) cover RGB image is separated into 3 bands: red, green and blue. To obtain the coefficients of the blue band, Discrete Shearlet Transform (DST) is used. To gain a stego image, The coefficients of the modified blue layer are where the first secret share is set. The plain secret logo is created by extracting the first secret share from the coefficients of the blue layer of the stego image and XORing it with the second secret share. According to the outcomes of the experimentations, the suggested method Using a payload capacity of 1 bpp, improves the stego image's imperceptibility. Furthermore, Using two out of two share visual cryptography and the second secret share as a private key, the secret logo is enhanced.

Mansoor Fateh et al [15] proposed a method where only one change, Two pixels contain the secret message's two hidden bits. However, This method doesn't offer a technique to conceal a message with multiple bits. Only n - 2 bits can be used with this technique, where n is the number of bits in a secret message block. An improved version of the LSB matching revisited method that is suitable for $n > 2$ is described in this study. The proposed method is divided into two parts:embedding and message extraction. The secret message is transformed into a bit-stream and then separated into a series of blocks with n bits in each block during the embedding stage. Afterward, choose 2n-1 pixels to mask those n bits of the secret message. The following step is to decide which operations will be used to create this message. Lastly, applying the achieved processes to the coefficients in order to conceal the conceal message. When $n > 2$, this method requests less alterations than LSB MR. This approach has a capacity that is $(((2^n - 1)/2^{n-1}) 1) 100\%$ greater than F5 technique when $n > 2$ is greater than 75%. For n - 3 the capacity of this system is 75% larger than that of F5. The suggested method can be applied in the first step of any steganography process to lessen the change in the stego image.

Dalia and Loay [16] proposed a method based on LSB inversion and arithmetic operations. The LSB values of cover pixels are not replaced with secret bits; they are reversed.. This improves the image quality of the stego. As a result, To define which bits are flipped, a flag is utilized. Finding the minimum and maximum numbers, as well as

subtraction and division, are arithmetic operations. By using these arithmetic processes, the amount of embedded data is reduced while capacity is increased. Division operations produce quotients and remainders, which are kept in arrays of quotients and remainders, respectively. The maximum size for each quotient is 3 and 2 bits, respectively, due to the use of the divisors 32 and 8, and the remainder is 3 bits. The conceal image is divided into two identical sections. By inverting the pixel LSBs, the first section is utilized for embedding quotients. In addition, In order to enhance the outcomes, several inverted LSBs will be inverted once more in this part. The second section is used to embed leftover data by flipping pixel LSBs. This section lists which inverted bits are inverted again as well as the number of bits utilized to embed each pixel in the first half.

K. Rosemary and M. Mary [17] focuses on data hiding in DCT-based JPEG images to improve storage capacity and security. It was suggested to the researcher to use a modified quantization table and matrix encoding technique to embed the secret message inside a JPEG image. A matrix encoding was used to eliminate distortion, and the conventional quantization table was changed to enhance storage space.

Ambika et al. [18] presented an encryption-based steganography technique. The cover image was separated into RGB components individually. Over the image's transformed components, multi-level DWT has been applied. The Multi-Objective Whale Optimization was utilized to choose the finest pixels. The RGB components of the private image have been separated. Encryptions using the DES, AES algorithms were performed on the divided levels R, G and B. The image that has been inserted into the cover image at the specified pixel location.

Amal and Iman [19] proposed a mechanism in 3 phases. The first stage involves grey image values are mixed up using a set of keys produced by a quantum chaotic map. The 2nd stage creates mixture keys combining a Zaslavsky and 3-D Henon map, which are utilized to cipher the scrambled grey image. The third phase, a new algorithm for hiding the ciphered grey image at arbitrary positions inside a speech file is suggested. This method combines the LSB technique for determining concealed bits and the zero- crossing K-means technique for mining locations in a dispersed way so that intruders cannot simply regain any hacked person's hidden data. Additionally, magnitude value was chosen as a specific piece of data to conceal encoded image data using a fractional Fourier transform. The measurements MSE, PSNR, NSCR and UACI are utilized to evaluate the effectiveness in the encipherment algorithm and the measurements SNR, PSNR and MSE are utilized to evaluate the effectiveness of the hidden method.

Hazim Noman [20] For information security, a cryptography and steganography method was proposed. By XORing the secret message and the QR code, cryptography was used to get the encrypted message. The LSB method was used in steganography to embed the encrypted message into the cover image. The QR technique was used in this study, and the ciphered message was concealed in locations chosen via the bat algorithm. To verify the effectiveness of the suggested approach, secret messages of various sizes were tested with numerous cover images. Finally, following the embedding procedure, the quality of the cover picture was evaluated using conventional criteria.

4. Conclusion

This article examined several steganography techniques, with a particular emphasis on steganography and comprehensive classification. Additionally, numerous forms of digital steganography and steganography review publications were explored. Each of the plans examined has some benefits and some drawbacks. Based on what the references indicated, it can be concluded that the if the developed technique combines the spatial and frequency

domains, the image steganography scheme will be more reliable and secure, in addition to creating the secret text with a new encryption technique to add an additional layer of protection. Furthermore, the pixels in the image should be selected at random. Taking into account the advantages and disadvantages of each methods examined, it is critical to develop a forceful and effective algorithm capable of data embedding, obtaining a high payload, and data.

References

[1] Anupriya Arya and Sarita Soni, "A Literature Review on Various Recent Steganography Techniques", International Journal on Future Revolution in Computer Science & Communication Engineering, Vol. 4(1), pp. 143 – 149, January 2018.
[2] Donia Fadhil Chalob, Zynab M. Jasim, Zainab Mohammed Essa, and Ziad M. Abood, "Subject Review: Image Encryption Techniques based on Chaotic Systems", International Journal of Engineering Research and Advanced Technology (IJERAT), Vol. 7(7), July - 2021.
[3] Sonali K. Powar, H. T. Dinde and Radhika. M. Patil, "A Study and Literature Review on Various Image Steganography Techniques", International Research Journal of Engineering and Technology (IRJET), Vol. 7(8), Aug 2020.
[4] Amal Abdulbaqi Maryoosh, Zahraa Salah Dhaief and Raniah Ali Mustafa, "Subject Review: Information Steganography Based on Different Methods", International Journal of Advances in Scientific Research and Engineering (ijasre), Vol. 7(3), March – 2021.
[5] S. Nanda Kishor, G. N. Kodanda Ramaiah, S. A. K. Jilani, "A Review On Steganography Through Multimedia", IEEE International Conference on Research Advances in Integrated Navigation Systems (Rains -2016), April 06-07, 2016, R. L. Jalappa Institute of technology, Doddaballapur, Bangalore, India.
[6] Yang, Yang, Weiming Zhang, and Nenghai Yu., "Improving visual quality of reversible data hiding in medical image with texture area contrast enhancement", 2015 international conference on intelligent information hiding and multimedia signal processing (IIH-MSP). IEEE, 2015.
[7] Vardhan, M. Vishnu, B. Rama Krishna, and V. Thanikaiselvan, "IWT Based Data Hiding in Encrypted Images", 2018 Second International Conference on Electronics, Communication and Aerospace Technology (ICECA). IEEE, 2018.
[8] Manikandan, Vazhora Malayil, and Vedhanayagam Masilamani. "An improved reversible data hiding scheme through novel encryption", 2019 Conference on Next Generation Computing Applications (NextComp). IEEE, 2019.
[9] Elharrouss, Omar, Noor Almaadeed, and Somaya Al-Maadeed. "An image steganography approach based on k-least significant bits (k-LSB)," 2020 IEEE International Conference on Informatics, IoT, and Enabling Technologies (ICIoT). IEEE, 2020.
[10] Bangera, Kripa N., et al. "Multilayer security using RSA cryptography and dual audio steganography", 2017 2nd IEEE International Conference on Recent Trends in Electronics, Information & Communication Technology (RTEICT). IEEE, 2017.
[11] Kar, Nirmalya, Kaushik Mandal and Baby Bhattacharya, "Improved chaos-based video steganography using DNA alphabets", ICT Express 4.1 (2018): 6-13.
[12] Huang, Yong Feng, and Shanyu Tang. "Covert voice over internet protocol communications based on spatial model", Science China Technological Sciences 59.1 (2016): 117-127.

[13] Lei, Tim, Jeremy Straub, and Benjamin Bernard, "Lightweight Network Steganography for Distributed Electronic Warfare System Communications", Advances in Security, Networks, and Internet of Things. Springer, Cham, 2021. 437-447.
[14] Yasir Ahmed Hamza, Nada Elya Tewfiq and Mohammed Qasim Ahmed, "An Enhanced Approach of Image Steganographic Using Discrete Shearlet Transform and Secret Sharing", Baghdad Science Journal, Vol. 19(1), pp. 197-207, 2022.
[15] Mansoor Fateh, Mohsen Rezvani, and Yasser Irani, "A New Method of Coding for Steganography Based on LSB Matching Revisited", Hindawi, Security and Communication Networks, Vol. 2021.
[16] Dalia Nashat and Loay Mamdouh, "An efficient steganographic technique for hiding data", Journal of the Egyptian Mathematical Society, 27:57, 2019.
[17] K. Rosemary Euphrasia and M. Mary Shanthi Rani, "Steganography in DCT-based compressed images through Modified Quantization and Matrix Encoding", International Journal of Computer Science and Information Security (IJCSIS), Vol. 15, No. 2, February 2017.
[18] Ambika, Rajkumar L. Biradar and Vishwanath Burkpalli, "Encryption-based steganography of images by multiobjective whale optimal pixel Selection", International Journal of Computers And Applications, 2019.
[19] Amal Hameed Khaleel and Iman Qays Abduljaleel, "Secure image hiding in speech signal by steganography-mining and encryption", Indonesian Journal of Electrical Engineering and Computer Science, Vol. 21(3), pp. 1692~1703, March 2021.
[20] Hazim Noman Abed, "Robust and Secured Image Steganography using LSB and Encryption with QR Code", Journal of AL-Qadisiyah for computer science and mathematics, Vol. 9(2), 2017.

Nonlinear Dynamics of Semiconductor Lasers with Optoelectronic Feedback and Modulation

Raghad Ismail Ibrahim[1], Wasmaa A. Jabbar [2]
[1,2] **Mustansiriyah University /College of Education/Physics Department, Baghdad, Iraq**
[1]**raghedismail@yahoo.com,** [2]**wasmaajabbar@gmail.com**

Abstract

In this work the dynamics of chaotic behavior and attractor selection in semiconductor laser utilizing optoelectronic feedback and direct current modulation have been studied experimentally .The effect of the external perturbation is presented and showed modulation in the chaotic system.

The study has begins from the generation of chaotic spiking in the semiconductor laser by optoelectronic feedback, Then studying the chaotic spiking characteristics and determining the control parameters which lead to various effects on the behavior of the system output, periodic, and quasi-periodic to chaos. The dynamics of the laser output are analyzed by Fast Fourier Transformation, attractors and bifurcation Diagram.

Keywords: Chaos, Chaos-based communications, frequency modulation, amplitude modulation.

1. Introduction

Significance of chaotic dynamics in semiconductor lasers receive great attention in the near past decades, due to the applicability of chaotic synchronization of such systems in the field of optical secure communication. This theory was proven by several research groups [1, 2, 3].Semiconductor lasers are generally very stable systems when operated with only a Dc bias current. By inclusion additional degrees of freedom to the system dynamic instabilities are induced. Involving external optical injection to the system produce different chaotic outputs [4, 5]. Producing optical feedback [6], direct current modulation [7]. And delayed optoelectronic feedback are the methods of generation chaotic optoelectronic feedback [8]. The conventional method of producing ultra-short pulses is positive delayed optoelectronic feedback [9] from semiconductor lasers. The dynamics of semiconductor lasers with direct current modulation widely studied [10]. It has already been proved that the effect of mode gain reduction occurring due to nonlinear processes is suppression of chaotic dynamics [11]. Production chaotic dynamics by using bidirectional coupling configuration between two such lasers is found [12]. A strong current modulation combined with positive delayed optoelectronic feedback is found to generate chaotic dynamics and bi stability in semiconductor lasers [13].The effect of such a combination in inducing chaotic dynamics through a quasi-periodic route in quantum-well lasers also has been studied [14]. The directly modulated semiconductor lasers with GHz modulation are the most preferred light source in the optical communication systems. A widely investigated topic is chaotic synchronization of two such lasers because of its applicability in optical secure communication [15]. The nonlinear gain reduction for (InGaAsP) lasers used in optical communication systems is very strong and its direct consequence on the dynamics of such lasers suppress of chaotic outputs. A significant role in modeling semiconductor laser dynamics is that the dynamic response of semiconductor laser strongly model is established in terms of dynamical time series, frequency spectrum and phase portraits; the influence of amplitude modulation on the nonlinear behaviors of the considered system is investigated in detail. depends on the nonlinear gain [16]. The results

of numerical investigations on the effect of a delayed optoelectronic feedback on the dynamics of lasers Diode was illustrated [13]. The study was undertaken to find out the possibility of obtaining chaotic outputs from Laser Diode under small values of perpetrated modulated amplitudes. The optoelectronic feedback scheme has the advantage of ease of implementation, as it is insensitive to the optical phase of the output intensity. Therefore the effects of negative delayed optoelectronic feedback schemes were investigated. The results reveal that in the range of normal estimates of nonlinear gain reduction factor for such lasers as suggested by Agrawal [10], only a strong negative delayed optoelectronic feedback is efficient in producing chaotic output.

In this study, an experimental setup was implemented for studying the control and modulation of chaos in SL with ac coupled optoelectronic delay feedback. Modulation is an important characteristic of the chaotic systems that enable encrypting data in chaos communication, in which data could be encoded and modulated in chaos carrier. Finally, this work will show hidden and appeared frequencies by changing the amplitude or frequency of the modulating signal.

2. Experimental work

2.1 Modulation on Chaotic dynamic

In this setup, a function generator (Model UTG9002C, Range 2MHz) is used to enhance the generated chaotic behavior. The Voltage Controlled Generator (VCG) is the basic component of the function generator. The VCG produces the precision sine, square wave, and triangle wave over a frequency range of 20 Hz to 2 MHz with coarse and fine tuning. Figure 1 shows the experimental setup of chaos modulation.

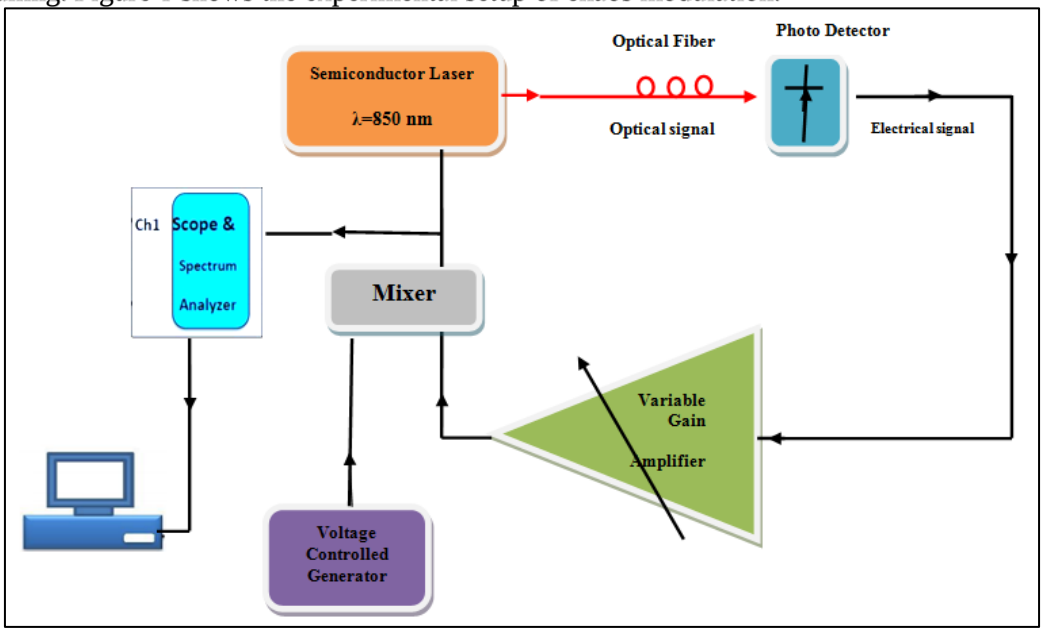

Figure 1 Experimental setup with optoelectronic feedback for investigating chaos modulation.

The system is comprised of a closed-loop optical system equipped with a semiconductor laser with AC and nonlinear optoelectronic feedback. The laser light produced by the system is sent to a photodetector which converts the optical signal to an electrical signal using an optical fiber. This process results in the generation of an electrical signal which is amplified by a variable gain amplifier and added to the bias current of SL. The output signal from the variable gain amplifier was modulated by external perturbation

through a periodic signal with two control parameters frequencies. The modulated frequency could be seen from the FFT. Different time series could be obtained by changing either the frequency or amplitude of perturbation. The bifurcation diagram was drawn for each parameter to see the differences between them.

2.2 External Chaotic Modulation

The experimental setup of SL and signal generator for satisfying chaotic modulation to study the resonance phenomena are shown in Figure 1. The experimental include the following procedure : the amplifier gain of the entire feedback loop and the dc-pumping current have been fixed, the output signal from the amplifier modulated by external perturbation which is sinusoidal signal that has two control parameter amplitude and frequency. Adding amplitude changes from (0.08-0.86Volt) to the system's dynamical state while frequency is fixed at 167 Hz, after that the output signal is observed with digital oscilloscope. The results have been analyzed with origin program software.

2.2.1 Frequency hiding in Chaos

In this experiment, one can introduce the method of hide frequency in the chaotic dynamic of the laser. Some frequencies could be hidden whereas others appeared, when the frequencies are hidden, the communication link considered as secure. It uses the same experimental setup in Figure 1.

The SL bias current changing causes the variation of nonlinear dynamics of the system. It was accomplished that a time series for each observed set of data from the chaotic signals. In this, The SL value power considered as a control parameter of chaotic spike evolution as shown in Figure 2. The analysis of the time series and their FFT of chaotic systems show the maximum value of frequencies in chaotic region. The maximum value of frequencies incited by this Figure are a good candidate for the modulated frequency. The amplitude of time series are studied for the best modulation in chaotic region.

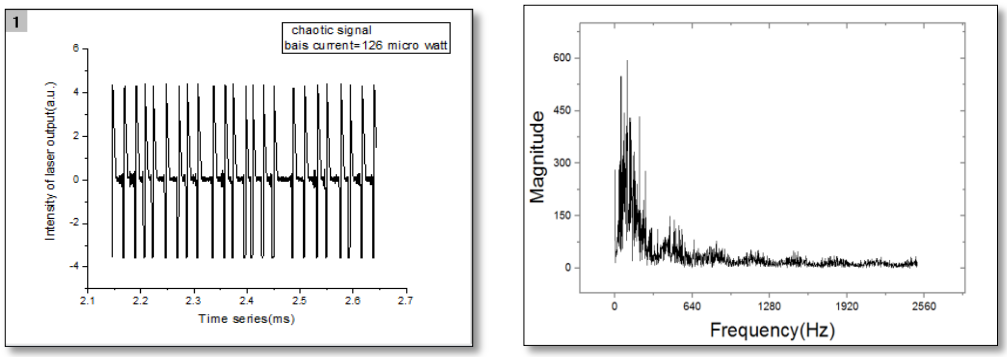

(a) (b)

Figure 2: The chaotic carrier signal (a) time series and (b) FFT of Chaotical spiking.

The chaotic carrier signal must have a much higher amplitude and frequency than the message signal, therefore the ratio of the massage signal to the carries chaos signal are calculated. The FFT frequency range is limited (0- 2500) Hz, this lead to the 10% of 2500Hz is 250 Hz and 20% from 2500Hz is 500Hz and so on. The amplitude of the chaos is 800 mv, the 10% of 800mv is 80mv and 20% from 800mV is 0.16 V and so on respectively.

We report the experimental and numerical study of hiding frequency in chaos in two stats, first, when the amplitude of the external perturbation is varied, secondly, when the frequency of this perturbation is changed.

We begin with amplitude modulation, the amplitude of the single wave is varied in proportion to that of the carrier signal being transmitted. The sinusoidal signal message that has two control parameter amplitude and frequency. First we observe the dynamical sequence where the frequency has been fixed at 166 Hz (7%from chaos signal). By gradually increasing in the amplitude of the perturbation (0.06, 0.08, 0.1… 0.6) volt will hid the frequency in the first step, then the frequency begin to appear and increasing in appearing. Then the frequency fixed at (50, 275, 300, 325,…2500)Hz and changing amplitude.

Second, Frequency modulation, when the amplitude of perturbation has been fixed with gradually increasing in the frequency. The amplitude of perturbation is fixed at 0.08 (10% from chaos carrier Amplitude) and changing frequency (166, 191, 216, 241… 1725) Hz. Then experimental has been repeated when the amplitude is fixed at (0.12, 0.16, 0.2, 0.25, 0.32, 0.5…0.8) Volt and changing frequency (166, 191, 216, 241…1725)Hz until frequency appear.

2.2.2 External chaotic modulation

External chaotic modulation is an important method to control chaos. In our study, the modulation applied on the source by a function generator as mentioned in the experimental part. Figure 3 includes the time series of different amplitude where the modulation frequency has been fixed at 167Hz which represent the minimum values of the frequency added which is convert the behavior of the system while the amplitude is changing.

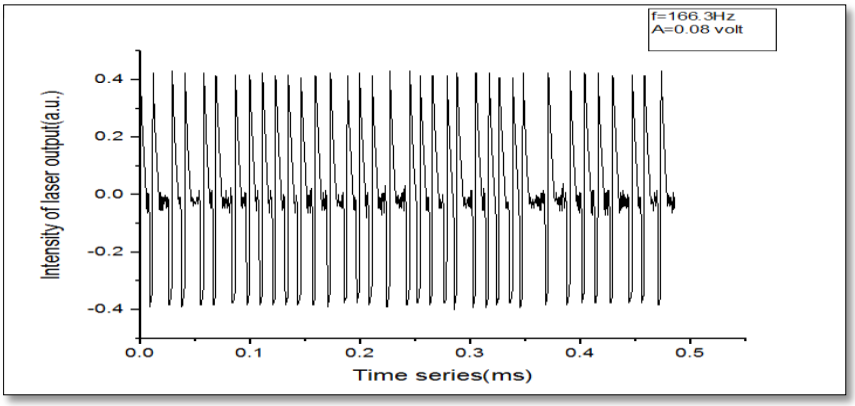

(a)

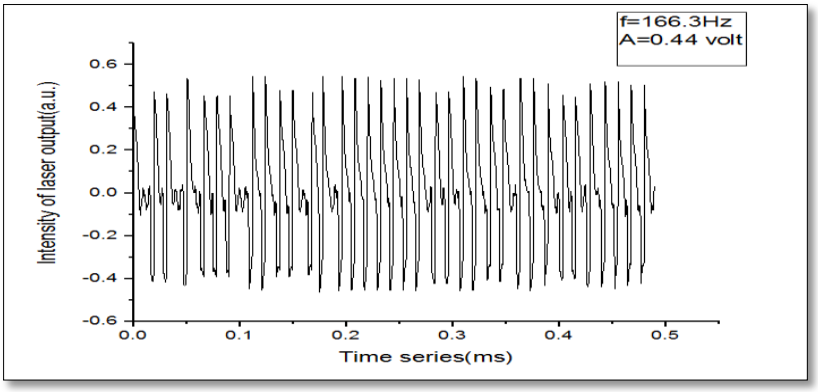

(b)

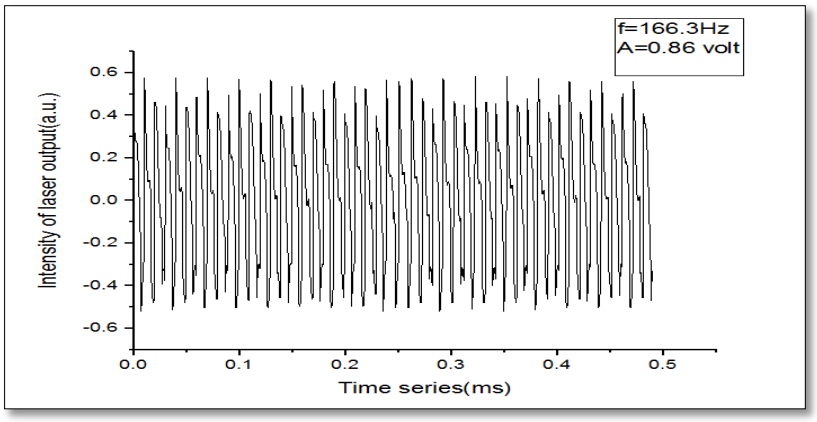

(c)

Figure 3 : Time series at fixed frequency 167Hz and amplitude values (a) 0.08 v, (b) 0.44v, (c) 0.86 v.

This Figure shows the system transition from chaotic to regular state. The regularity of nonlinear dynamic system is related to the optimal amount of frequency and increment of the amplitude.

The results indicate that the amplitude could be considered as a parameter at optimal amount of frequency (167 Hz) which control the system's collective dynamics, the different amplitudes have been controlled the chaotic system from chaos to quasi periodic and then to periodic. So, very interesting results have been obtained regarding to the effect of the chaotic resonance by adding the amplitude on the chaotic systems. This phenomenon was named as resonance in excitable nonlinear dynamical systems.

2.2.3 Frequency hiding in Chaos

The aim of this experiment is to indicate the encryption region. Previously, the amplitude of the single wave is varied in proportion to that of the carrier wave being transmitted. The frequency has been fixed at166Hz (7%from chaos signal).By gradually increasing in the amplitude of the perturbation (0.06, 0.08, 0.1, 0.12, 0.14, 0.16, 0.18, 0.2, 0.22, 0.24,..0.6) Volt will hid the frequency, then at 0.48 Volt the frequency begin to appear and at 0.62 Volt increasing in appearing as shown in Figure 4.

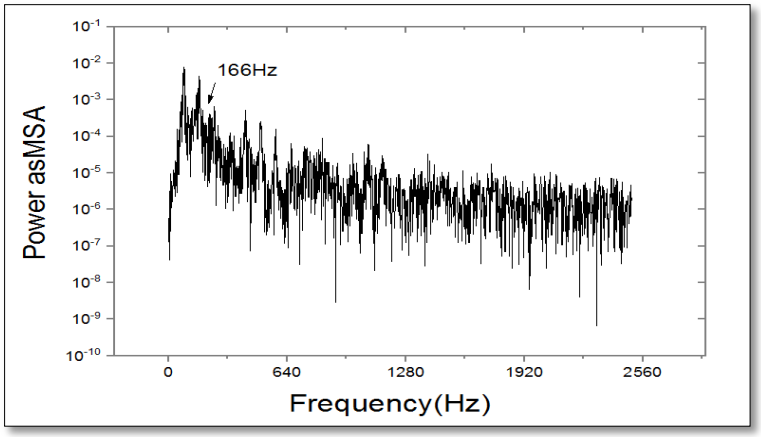

(a)

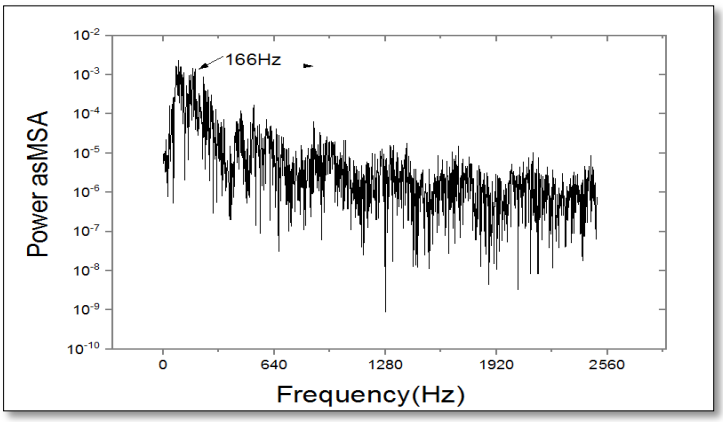

(b)

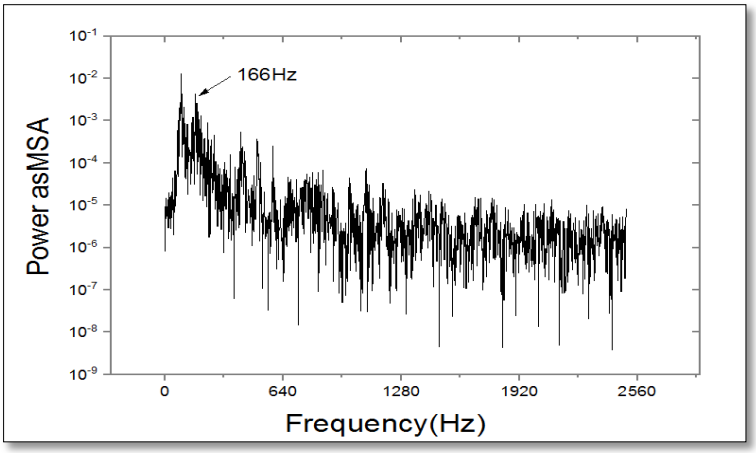

(c)

Figure 4 Power spectra with different modulation amplitude
(a) 0.08v, (b) 0.48v (d) 0.62 v.

This Figure shows the sinusoidal starts to appear in the spectrum when the external amplitude is increased; three types of the power spectrum analysis exist, hidden spike frequency, low spike frequency and a spike frequency.

Then frequency is fixed at 250 Hz(10% from chaos carrier signal) and changing amplitude until frequency appear, then frequency fixed at (275, 300, 325, 350, 375, 400, 425, 450, 475, 500…2500) Hz and changing amplitude.

Second, The amplitude of perturbation is fixed at 0.08Volt (10% from chaos carrier Amplitude) and changing frequency (166, 191, 216,2 41, 266, 291, 316, 341, 366, 391, 416 …1725) Hz, all the values of frequency are hidden.

The experiment has been repeated when the amplitude is fixed at 0.12Volt (15% from chaos carrier Amplitude)) and with gradually increasing in the frequency from (166, 191, 216, 241, 366, 391, 416…1725) Hz until frequency appear at 1750Hz as demonstrated in Figure 5.

Figure 5 shows that frequency is hidden until 170 Hz begin to appear and increasing in appearing at 250 Hz. Then the amplitude is fixed at (0.08, 0.12, 0.16, 0.2, 0.25, 0.28, 0.32, 0.36, 0.4, 0.44, 0.48…0.8) Volt and changing frequency (166, 191, 216, 241…1600)Hz until frequency appear.

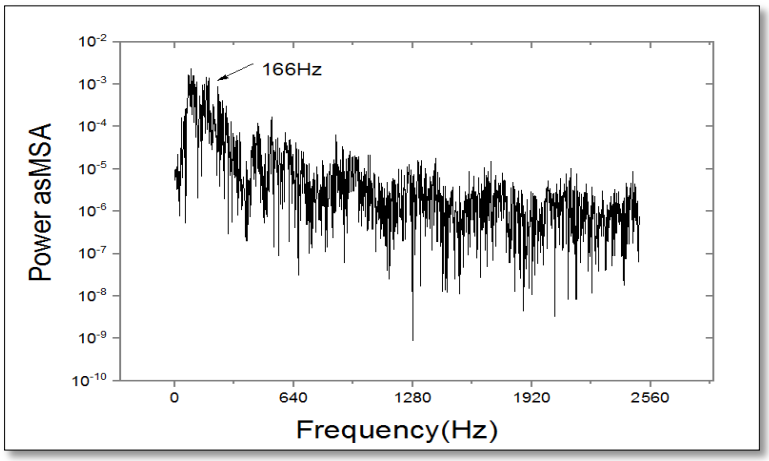

(a)

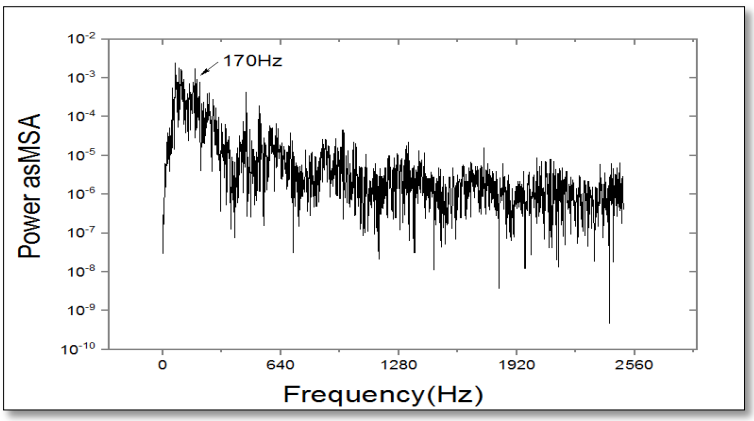

(b)

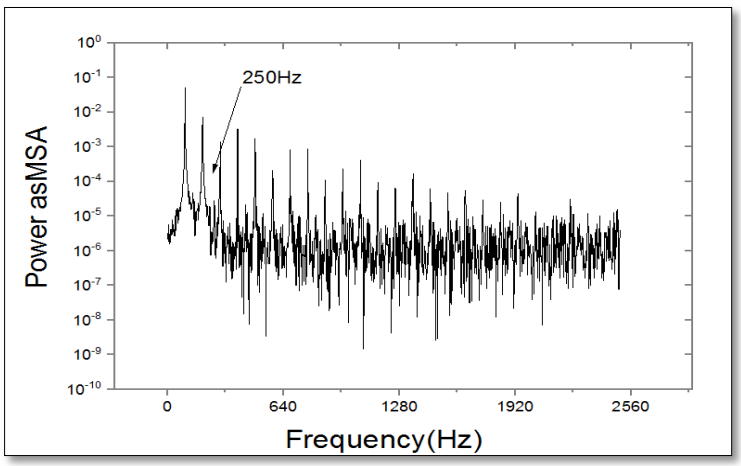

(c)

Figure 5: Power spectra with different modulation frequency (a) 166Hz, (b) 170Hz, (c) 250Hz.

The amplitude is fixed as mentioned previously and changing frequency until frequency appears. The results indicate that the frequency could be considered as a parameter at optimal amount of amplitude which control the system's collective dynamics, the different frequencies have been controlled the chaotic system from chaos to quasi periodic and then to periodic. So, very interesting results have been obtained regarding to the effect of the chaotic resonance by adding the frequency on the chaotic systems.

Conclusions

Depending on the results, the conclusions could be summarized that, the effect of the external perturbation is presented and showed modulation in the chaotic system. When the output chaotic signal under the effect of external perturbation, the different frequencies have been controlled. The control of modulation can be achieved by changing in the amplitude or frequency of perturbation signal. It is clear that the Chaotic dynamics are a good candidate for hiding information, which is an important part to encrypt the data in optical communications. Different frequencies have been applied as control parameters, appearance and hidden of these frequencies are achieved for the security of chaos communication. So, appearing and hiding of these frequencies are achieved for the security of optical communication. From the results we notice that we can not use some frequencies for security communication because we can not hide these frequencies in both states high and low amplitude.

References

[1] J. P. Goedgebuer, L. Larger, H. Porte, "Optical cryptosystem based on synchronization of hyper chaos generated by a delayed feedback tunable laser diode", Physical Review letter", 80, (2249-2252), (1998).
[2] I. Fischer, Y. Liu, and P. Davis, Synchronization of chaotic semiconductor laser dynamics on sub nanosecond time scales and its potential for chaos communication", "IEEE Journal OF Quantum Electronic", 62,(4), (2000).
[3] S. Tang, H. F. Chen, S. K. Hwang, J. M. Liu, "message encoding and decoding through chaos modulation in chaotic optical communication", "IEEE Transactions on circuits and system",49,(163-16),(2002).
[4] V. Kovanis, A. Gavrielides, T. B. Simpson, J.M. Liu, "Instabilities and chaos in optically injected semiconductor lasers", "Journal of Applied Physics.",67, (2780- 2782), (1995).
[5] T. B. Simpson, J. M. Liu, A. Gavrielides, V. Kovanis, P. M. AL sing, "Period-doubling Cascades and chaos in a semiconductor laser with optical injection", "Journal of Physical Review",51,(4181-4185), (1995).
[6] Y. Cho., T. Umeda, "Observation of chaos in a Semiconductor laser with delayed feedback", "Journal Optical Communication", 59, (131-136), (1986).
[7] H. G. Winful, Y. C. Chen, J. M. Liu, "Frequency locking, quasi periodicity, and chaos in modulated self-pulsing semiconductor lasers' 'Journal of Applied Physics", 48, (616-618), (1986).
[8] F. Y. Lin, J. M. Liu, "Nonlinear dynamics of a semiconductor laser with delayed negative optoelectronic feedback", "IEEE Journal of Quantum Electron.", 39 (562-568), (2003).
[9] T. C. Damen, M.A. Duguay, "An Opto electronic Regenerative pulser", "Journal of Electronic Letter" 16,(166-167), (1980).
[10] G. P. Agrawal, "Effect of gain nonlinearities on period doubling and chaos in directly

modulated semiconductor lasers", " Journal of Applied Physics Letter"', 49, (1013-1015), (1986).
[11] T. Kuruvilla, V. M. Nanda Kumaran, "Suppression of chaos through reverse period doubling in coupled directly modulated semiconductor lasers", "Journal of Physics Letter A", 254, (59-64), (1999).
[12] S. Rajesh, V. M. Nanda Kumaran, "Suppression of chaos in a directly modulated semiconductor laser with delayed optoelectronic feedback", Journal of Physics Letter A General atomic and Solid State Physics, 319,(340-347),(2003).
[13] K. AL-Naimee and F. T. Arecchi, "Chaotic spiking and incomplete homo clinic scenarios in semiconductor lasers with optoelectronic feedback", New Journal Of Physics, 11, (11pp), (2009).
[14] C. Juang, S. M. Chang, N. K. Hu, C. Lee and W. W. Lin, "laser chaos induced by delayed feedback and external modulation"," Japanese journal of applied physics", 44, (7827-7831), (2005).
[15] V. Bindu, V.M. Nandakumaran, "Numerical studies on bi directionally coupled directly modulated semiconductor lasers.", "Journal of Physics. Letter. A", 34, (345-351) (2000).
[16] R. S. Tucker, "High speed modulation properties of semiconductor laser", "Journal of Light wave Technology.", 3, (1180-1192), (1985).

Subject Review: On Different Cryptography Algorithms

Zainab Mohammed Essa, Donia Fadhil Chalob, Doaa Mohsin Abd Ali Afraji Ameer Badr Khudhir
Collage of Education, Mustansiyiah University, Iraq

Abstract
Due to the magnificent evolutions in transmission networks exclusively in the Internet network, which utilize to interchange various kinds of data via numerous people. Data security has come to be a major discussion. For that reason, there is a growing heed in the use of encryption and decryption techniques. Lots of encryption techniques have been evolute to maintain data security. One of these techniques that commonly used in recent is chaotic encryption systems. Where numerous techniques were suggested to encrypt text using a chaotic map because their features such as sensitivity to initial conditions and unpredictability of random behaviors etc... In this paper, we attempt to review and describe numerous techniques used to encrypt text and make a comparison among these techniques.
Keywords: Cryptography, Decryption, Text Encryption.

1. Introduction
Securing information is, and will remain an important goal, require interchanging and storing numerous kinds of data such as text, video, audio and image over the Internet, an environment in which it is uncomplicated to penetrate the information interchanged, cryptographic methods have been utilized to safeguard the confidentiality of data from unauthorized access [1]. Text encryption is the generality additional benefit method to protect the confidentiality when storing or transmitting text through a network. [2] Lately, cryptography depend on chaotic systems has been find out and is fetching recurrently utilize in image encryption techniques. In fact, chaotic systems display pseudorandom behavior and have substantial features such as unpredictability of the orbital growth, high sensitivity to parameters and initial conditions, guide the simplicity of implementation of software and hardware to increase the encryption rate, etc... These features and another make from chaotic depend cryptography are related with most significant properties of cryptography like confusion, diffusion. [3] Cryptography and cryptanalysis are two terms need to be clearly defined to give wide comprehension for the work in progress. Cryptography mathematically encrypts and decrypts information so that the user becomes capable of storing and transmitting information that is sensitive within insecure networks. This information is viable to the public except the specified recipients. As for cryptanalysis, it is defined as a process to analyze and break down secure communication. Encryption is a process in which an algorithm is used to make the transformed information is un-readable by unauthorized users. Therefore, cryptographic method is simply based on encoding and transforming information into unreadable cipher text to protect a sensitive data such as credit card number. The encoded data may only be decrypted or turned readable by a key. Both of symmetric-key and asymmetric-key encryptions are considered as primary types of encryption. [4]

2. Literature Survey
There are numerous techniques that associated to text encryption has been studied. In this section we debate some of these researches.
R Thanuja and S Dilip Kumar [5] utilized a Novel Cryptographic architecture that utilize IDEA & BLOWFISH procedure for encryption purposes and utilizing of SHA-I for

creating hash value for cipher text so as to make available a robust cryptographic architecture.

Unnikrishnan Menon et al. [6] used a novel 2D chaotic function that shows a uniform bifurcation above a large range of parameters and displays high levels of chaotic behavior to create a random sequence that is utilized to encrypt the input data. The suggested technique utilize a genetic algorithm to optimize the parameters of the map to improve security for any given textual data. Several analyses demonstrate an adequately big key space and the existence of multiple global optima representative the requisite of the suggested technique and the security providing via it.

M. Y. T. Irsan and S. C. Antoro [7] used the nature of the chaotic map via utilizing the MS map as a key stream generator. The cipher text discover via the determined algorithm is overly hard to be cracked via the bruce-force attack and known-plaintext attack. The decryption method has been tested using 3 different secret keys (that is overly similar with the secret key on the encrypted procedure), and resulting the decrypted text is the similar with plaintext only if the input is exactly the similar secret key as in encrypted procedure.

Siham Oleiwi Tuam et al. [8] presents a hybrid method of the chaotic map as well as DNA computation to Text encryption. Two logistic maps are employed for key generation to be used in permutation process, and 1D logistic map is used for generating index permutation. DNA computation coding rules and addition operation are used to frame the final result of the encryption process to produce encrypted text.

Riyadh Bassil Abduljabbar et al. [9] used fast method for text encryption based on genetic algorithm is presented. Method of encryption is reached via the genetic operators Crossover and mutation. The encryption suggestion method depend on dividing the plain text characters into pairs, and applying the crossover operation between them, followed via the mutation process to obtain the encrypted text. The exploratory results display that the suggestion supply a significant enhancement in encryption rate with comparatively great-speed treating.

Zahraa K. Taha [10] utilizes method to complete step via step execution of Advanced Encryption Method, i.e. encrypting 128 bit data utilize the modification AES-2Keys. The encryption method contains of the mixture of many classical procedures such as substitution, rearrangement and transformation encoding methods.

Mohammed Amin Almaiah et al. [11] mixture between elliptic curve cryptosystem and hill cipher (ECCHC) is proposed called Novel hybrid encryption, so as to change Hill Cipher from symmetric technique (private key) to asymmetric One (public key) and growth its security and efficiency and resist The hackers. Thus, no want to share the secret key between sender and receiver and both can create it from the private and public keys. Thus, the suggested methodology presents a new contribution via its ability to encrypt every character in the 128 ASCII table via utilizing its ASCII value direct without wanting to assign a numerical value for every character.

Ahmed Steef, M. N. Shamma and A. Alkhatib [12] utilize a technique to encrypt and decrypt the message text according to the ASCII(American Standard Code for Information Interchange) and RSA algorithm via altering the message text into binary representation and dividing this representation to bytes(8s of 0s and 1s) and applying a bijective function between the group of those bytes and the group of characters of ASCII and then utilizing this tool to be compatible with using RSA procedure, lastly, Java application was built to put in this method directly.

R. Venkateswaran and V. Sundaram [13] used chance of exploiting the properties of Genetic Procedure with poly substitution approaches in a linear method, to create ASCII values of the given text and then applying conversion, transposition with the properties of

Cryptography. In polyalphabetic substitution ciphers the plaintext letters are enciphered dissimilarity based upon their location in the text. As the name polyalphabetic proposes this is attained via utilizing several two, random keys and three keys mixtures in place of just one, as is the situation in most of the simpler crypto schemes. utilizing two keys, we take 2 keys e1, e2 and let the ASCII values of e1 be 1 and e2 be 2 and take the text, add ASCII values of e1 to first character and ASCII values of e2 to second character. As another option add the value of e1 and e2 to consecutive characters. can utilize Poly substitution process combining the properties of cryptography for text encryption via 2 keys and 3 keys and even more then 3 keys to create the decryption procedure extra complicated.

Dr. Ekhlas Abbas Albahrani and Tayseer Karam Alshekly [14] used mixture between Self-Synchronizing Stream Cipher and chaotic map; the procedure encrypts and decrypts text files of dissimilar sizes. Initially, the corresponding ASCII values of the plain text are act as input to the permutation action which diffuses the positions of these values via utilizing hyper-chaotic map. Next, the outcome values are input to substitution process via1D Bernoulli map. Lastly, the resultant vales are XOR feedback with the key.

M. A. Murillo-Escobar et al. [15] chaos encryption utilize a 128 bit secret key, two logistic maps with optimized pseudorandom sequences, plain text characteristics, and only one permutation diffusions round, is a method in a novel symmetric text cipher procedure. Numerous security analysis are offered as secret key size, secret key sensitivity, frequency with histograms, autocorrelation analysis, information entropy analysis, differential analysis, classic attacks analysis, and encryption/decryption time. Depended on numerical simulation results.

Narendra K. Pareek et al. [16] used a novel chaotic block cipher in which a logistic map, Henon map, and secret key are utilized. The chaotic cipher that suggested applies; the confusion and diffusion are reached respectively with the help of chain block ciphering and secret key depending on permutation boxes. Because of the privilege confusion and diffusion characteristic, the suggested chaotic cipher is extremely robust.

Mina Mishra and V. H. Mankar [17] utilized pseudo random number generator (PRNG) and non-Linear functions. PRNG utilized in the work are matlab random number generator (RNG) and Linear congruently generator (LCG). The developed procedures are named with reference to PRNG utilized in it. State of PRNG is assuming as secret key of the cipher. The encryption systems have been cryptanalyzed for four dissimilar approaches to examination its power like key space analysis, plaintext and key sensitive examination. Famed plaintext attack is also executed via taking into consideration a lesser series of plaintext and the complete cipher text for lesser text. The analysis is achieved on diverse keys chosen randomly from key for several texts and files. Key sensitivity up to 50 % and plaintext sensitivity ranging from 3% to 50 % have been gotten in the progressive ciphers. It is concluded that suggested encryption procedures. Have strength against linear, differential and statistical attacks.

Qusay S. Alsaffar et al. [18] research chains between numerous phases of encryption Procedures: DNA encryption process, GZIP algorithm, AES cryptography and image steganography. This paper suggested multiplying via a factor along the latest phase of DNA encryption, and the outputs of this operation are compressed utilizing the GZIP process, where the message is altered to a new form and its size summary to (75%), then after the message is encrypted utilizing the AES encryption Procedure to increase the grade of security. Moreover, LSB image Steganography technology is used to hide the encrypted message in a high-quality image.

Samsul Arifin et al. [19] square key matrix in the Hill Cipher approach essential have a reverse modulo. The unimodular matrix is one of the rare matrices that necessity has an inverse. A unimodular matrix can be used as a key in the encryption method. These study goals to show that there is additional method to guard text message data. Symmetric cryptography is the sort of encryption used. A Bernoulli Map is utilized to generate a unimodular matrix. To begin, the academics utilize an identity matrix to create a unimodular matrix. The Bernoulli Map series of real values in (0, 1) is interpreted to integers between 0 and 255. The numbers are then inserted into the unimodular matrix's top triangular entries. To obtain the full matrix as the key, the academics use Elementary Row Operations. The data is then encrypted utilizing modulo matrix multiplication.

3. Conclusion

This work reviewed diverse method for text encryption within the period (2010-2021). Text encryption turns out very important especially when the transferring will have done thought open network. These encryption patterns are studied and analyses fully to improvement the efficiency of the encryption approaches and to guarantee the security performance. This study summarizes, each scheme is unique in its own technique, which may be suitable for several applications. The new encryption technology is growing every day, thus the fast and secure traditional encryption technology will always accomplish a high security rate. All technologies have particular benefits and drawbacks and thus new technologies have been developed.

References

1. Krasimir Kordov, “Text Encryption Algorithm for Secure Communication”, 2021, international journal of applied mathematics, vol. 34 no. 4.
2. Muhammed Jassem Al-Muhammed And Raed Abu Zitar, ”Dynamic Text Encryption”, 2017, International Journal of Security and its Applications, vol. 11, no. 11.
3. Amal Abdulbaqi Maryoosh, Raniah Ali Mustafa and Zahraa Salah Dhaief,” Review: Image Encryption Techniques Based on Chaotic Map,” September -2019, International Journal of Engineering Research and Advanced Technology, vol. 5, issue 9.
4. Omar Farook Mohammad et al., ”A Survey and Analysis of the Image Encryption Methods”, International Journal of Applied Engineering Research, Volume 12, Number 23 (2017).
5. R. Thanuja and S. Dilip Kumar,” A Novel Cryptographic Architecture”, Journal of Theoretical and Applied Information Technology, April 2012. Vol. 38 No.1.
6. Unnikrishnan Menon et al, “A Novel Chaotic System for Text Encryption Optimized with Genetic Algorithm”, International Journal of Advanced Computer Science and Applications, Vol. 11, No. 10, 2020.
6. M. Y. T. Irsan and S. C. Antoro,” Text Encryption Algorithm based on Chaotic Map”, Journal of Physics: Conference Series, 2019.
7. Siham Oleiwi Tuam et al.,” Text Encryption Approach using DNA Computation and Chaotic Indexing”, International Journal of Emerging Trends in Engineering Research, August 2020.
8. Riyadh Bassil Abduljabbar et al.,” Features of genetic algorithm for plain text encryption”, International Journal of Electrical and Computer Engineering, Vol. 11, No. 1, February 2021.
9. Zahraa K. Taha, ” Text Encryption using Modified AES-2 Keys”, International Journal of Computer Applications, vol. 149, No.4, September 2016.

10. Mohammed Amin Almaiah et al.," A new hybrid text encryption approach over mobile ad hoc network", International Journal of Electrical and Computer Engineering, Vol. 10, No. 6, December 2020.
11. Ahmad Steef et al., "Rsa Algorithm with a New Approach Encryption and Decryption Message Text by Ascii", International Journal on Cryptography and Information Security, Vol. 5, No. 3/4, December 2015.
12. R. Venkateswaran and V. Sundaram," Information Security: Text Encryption and Decryption with Poly Substitution Method and Combining the Features of Cryptography", International Journal of Computer Applications, vol. 3, No.7, June 2010.
13. Ekhlas Abbas Albahrani and Tayseer Karam Alshekly," A Text Encryption Algorithm Based on Self-Synchronizing Stream Cipher and Chaotic Maps", 2017 IJSRSET Volume 3 Issue 5, Themed Section: Engineering and Technology.
14. M. A. Murillo-Escobar et al.," A novel symmetric text encryption algorithm based on logistic map", international conference on communications, signal processing and computers, 2014.
15. Narendra K Pareek et al., "Block cipher using 1D and 2D chaotic maps", Int. J. Information and Communication Technology, Vol. 2, No. 3, 2010.
16. Mina Mishra and V. H. Mankar, "Text Encryption Algorithms based on Pseudo Random Number Generator", International Journal of Computer Applications, vol. 111m No 2, February 2015.
17. Qusay S. Alsaffar et al., "An encryption based on DNA and AES algorithms for hiding a compressed text in colored Image", IOP Conf. Series: Materials Science and Engineering (2021).
18. Samsul Arifin et al. "Unimodular matrix and bernoulli map on text encryption algorithm using python", Al-Jabar: Jurnal Pendidikan Matematika, Vol. 12, No. 2, 2021, Hal 447 – 455.

تصنيع ودراسة الخصائص التركيبية والبصرية لكاشف ضوئي لمادة جرمانيوم -نحاس والمحضرة بطريقة التبخير الحراري الفراغي

ا.د. زياد طارق الدهان* ا. د. عبد الكريم حسين داغر** ندى ضمد ماذي**
* جامعة بغداد
** الجامعة المستنصرية- كلية التربية- قسم الفيزياء

الخلاصة
تم تصنيع كواشف من الجرمانيوم (Ge) بواسطة عملية تطعيم الجرمانيوم نوع (n-type) بعد طلاءه بمادة النحاس بطريقة التبخير الحراري في الفراغ وذلك بقصف سطح الجرمانيوم بنبضات ليزر (Nd–YAG) بطاقات مختلفة وهي (40,60,80) mJ. تم دراسة أثر التطعيم على الخصائص التركيبية والبصرية لسطوح العينات. الخصائص البصرية للنماذج تم دراستها من خلال قياس طيفي النفاذية والامتصاصية. الاستجابية الطيفية التي من خلالها المنطقة الطيفية التي يعمل بها الكاشف ضمن المدى الطيفي للمنطقة تحت الحمراء IR تم تحديدها، أفضل استجابية طيفية حصلنا عليها هي (0.36 A/W) للشريحة التي قصفت بطاقة قدرها (80mJ) عند الطول الموجي (808nm). الكشفية والكشفية النوعية كدالة للطول الموجي الساقط تم قياسها، اعلى كشفية هي 1.6×10^{-10} W^{-1}

Fabrication and Studying of Ge-Cu Photodetector structure and Optical Properties prepared by Vacuum evaporation method

Dr. Z. T. Al-Dahan Dr. Abdul K. H. Dagher Nada Dhamed Mathi

Abstract
Fabrication of Ge detector of n- type by doping Ge with Copper material in vacumm evaporation method, where the surface of Ge is projected by Nd-YAG Laser pulses of different energies (40, 60, 80) mJ. Studying the effects of doping on the structure and optical properties models Surface. Optical properties of models have been studied through measuring transmittance and absorpance. Spectral responsivity in which the spectral area of detector is doing at the spectral range IR region is determined, optimum responsivity is 0.36 A/W for sample which is projected by 80mJ at wavelength 808 nm. Detection and the specific detection as a function of incedent wavelength have been measured, high detection is 1.6×10-10 W-^{1}.

المقدمة (Introduction)

الجرمانيوم متحسس للأشعة تحت الحمراء القريبة ومعامل امتصاصه $(\alpha \approx 10^4)cm^{-1}$ ضمن المدى (1.5 – 1.0) (μm) (1) وانعكاسية عالية يمكن تلافيها بطلاء السطح بمادة مضادة للانعكاس لتحسين عملة ككاشف (2) لذا الجرمانيوم مهم في صناعة الكواشف الفوتونية التي تعمل على امتصاص الفوتونات الساقطة على الكترونات مادة الكاشف مما ينتج عنة تهيج الالكترونات وبالتالي تحولها إلى أشارة كهربائية. تعد الكواشف الفوتونية النوع الا فضل لكون الاستجابية الطيفية ضمن مدى محدد من الاطوال الموجية ويمكن استخدامها للكشف عن الاطوال الموجية في مدى (UV و VIS وIR) ولصغر حجمها وذات ضوضاء قليلة (3). تتوهن شدة الضوء الساقط على الجرمانيوم اسيا مع المسافة (4).

$$I = I_{\circ} \exp^{(-\alpha t)} \quad ...(1)$$

اذ ان I شدة الضوء النافـذ، α معامل الامتصاص ولحساب الامتصاصية A

$$A = \log \frac{I_{\circ}}{I} \quad ...(2)$$

لتحديد اداء الكاشف لابد من معرفة وقياس الاستجابية الطيفية (R_λ) هي النسبة بين الكمية الخارجة من الكاشف إلى الكمية الداخلة للكاشف وتقاس الاستجابية الطيفية بوحدات (V/W)أو (A /W) (5):

$$R_\lambda = \frac{S}{P_{in}} \quad ...(3)$$

S تمثل الإشارة الخارجة وتكون تيار ضوئي أو فولتية، P_{in} قدرة الأشعة الضوئية الداخلة. الاستجابية الطيفية تحدد المنطقة الطيفية لعمل الكاشف والتي تميزه عن بقية الكواشف وتحدد كفاءته وقدرته. تعرف الكفاءة الكمية (η) بأنها عدد أزواج الإلكترون - فجوة المتولدة عن كل فوتون ممتص ساقط على الكاشف (6,7).

$$\eta(\%) = 1.24\frac{R_\lambda}{\lambda} \quad \dots (4)$$

الفترة الزمنية اللازمة التي تحتاجها الإشارة الكهربائية الخارجة من الكاشف لكي ترتفع من (10%) إلى (90%) من قيمتها تسمى زمن الاستجابة وتعطى بالعلاقة الآتية (6):

$$\tau = \frac{1}{\Delta f_{det}} \quad \dots (5)$$

اذ أن Δf_{det} عرض حزمة الكاشف ويقاس بوحدة(Hz) يعتمد زمن الاستجابة على مساحة الكاشف ويحدد بمقدار ثابت الزمن (RC) وعلى مقدار مقاومة الحمل. الإشارة الكهربائية غير مرغوب بها في الكاشف التي تظهر بالرغم من عدم وجود أشعة ساقطة وتمثل أقل قدرة أشعاعية يستطيع الكاشف إن يتحسسها تدعى بالضوضاء اذ تفرض حدودا على نقل المعلومات. وهناك عدة أنواع من الضوضاء المتولدة في الكاشف التي تعتمد على نوعه، وفي الكاشف التوصيلية الضوئية يعطي تيار الضوضاء بالعلاقة الآتية (7):

$$I_{n.pc} = 4q\left[q\,\lambda AG^2\phi_B + qG^2g_{th} + \frac{K_BT}{qR_D}\right]\Delta f \quad \text{----(6)}$$

g_{th} معدل التولد الحراري، R_D مقاومة الظلام، Δf عرض النطاق الترددي، ϕ_B كثافة قدرة الإشعاعات المحيطة، G عامل الربح.

اذ يظهر نوعان من الضوضاء في الكواشف التوصيلية الضوئية، الحد الا ول من المعادلة (6) يمثل النوع الأول وهي ضوضاء

التولد- أعادة الاتحاد (g - r) تظهر هذه الضوضاء نتيجة التذبذب الحاصل في معدل التولد الحراري والاتحاد لحاملات الشحنة الحرة في اشباه الموصلات وهذا يسبب حدوث تذبذب في تركيز الحاملات ويظهر هذا النوع في الكواشف الحرارية أيضا. أما النوع الثاني من الضوضاء فهو ضوضاء جونسون (Johnson Noise) يظهر هذا النوع من الضوضاء في المقاومات نتيجة الاهتزازات الحرارية العشوائية لحاملات الشحنة وعندما يكون الكاشف في حالة توازن حراري مع المحيط ويدعى هذا النوع أيضا بالضوضاء الحرارية (Thermal Noise). أما الضوضاء في الكواشف لفولتائية الضوئية تعطي تيار الضوضاء بالعلاقة (7):

$$I_n^2 = \left[I_p + \frac{I_{sat}}{\beta}e^{(qv|\beta K_BT)} + \frac{K_B\,T}{qR_D}\right]\Delta f \quad \text{-----(7)}$$

I_{sat}تيار الإشباع العكسي.الحد الأول من المعادلة (7) يدعى بضوضاء الإشعاع (Radiation Noise)، اذ استطعنا ان نلغي كل انواع الضوضاء لا نستطيع ان نلغي هذا النوع لانه ناتج من الإشعاعات المحيطة وان تيار ضوضاء الإشعاع يعطى بالعلاقة الآتية (7):

$$I_{p=AGQN\emptyset_B} \quad \dots(8)$$

أما الحد الثاني فيدعى بضوضاء الصدمة Shot Noise. والحد الثالث في المعادلة (7) يمثل ضوضاء جونسون (Johnson Noise)

القدرة المكافئة للضوضاء هي كمية الضوء الساقط الذي يساوي مستويات الضوضاء الذاتية للكاشف، فإذا كان (I_n) يمثل تيار الضوضاء و (R_λ) يمثل أستجابية الكاشف، فتعطى بالمعادلة الآتية (8):

$$NEP = \frac{I_n}{R_\lambda} = \frac{P}{S/N\sqrt{\Delta f}} \quad \dots(9)$$

$\frac{S}{N}$: نسبة الإشارة الخارجة إلى الضوضاء. وبهذا فان NEP تمثل أقل قدرة يمكن إن يكشف عنها الكاشف بمعنى اخر الكاشف الذي يمتلك أعلى قابلية كشف يجب أن يمتلك أوطأ قدرة مكافئة للضوضاء وتقاس بوحدات (W). تعرف الكشفية بأنها النسبة بين الاستجابية الطيفية (R_λ) إلى تيار الضوضاء (I_n) للكاشف ويعطى بالعلاقة الآتية (9):

$$(W^{-1})\ \frac{R_\lambda}{I_n} = D = \frac{1}{NEP} \dots(10)$$

أن الكشفية النوعية Specific Directivity تتناسب مع مساحة الكاشف وعرض حزمة الضوضاء وتعطى بالعلاقة الآتية (9):

$$D^* = \frac{(A\Delta F)^{1/2}}{NEP} \quad \dots(11)$$

تقاس الكشفية (D) بوحدات (W^{-1}) والكشفية النوعية (D^*) تقاس بوحدات $\left((cm \cdot Hz)^{1/2} \cdot w^{-1}\right)$.

الجزء العملي

تم تقطيع شريحة الجرمانيوم التي تمتاز بسهولة الكسر الى عدة شرائح باستخدام قرص ماسي بعد ذلك نجري عمليتي الصقل والتلميع لشرائح الجرمانيوم لازالة الاضرار والتشوهات التي حصلت جراء عملية التقطيع. وبعدها تم أجراء عملية الحفر الكيميائي لأجراء الفحوصات الخاصة بالسطوح البلورية وذلك بأجراء المعالجة الكيميائية للسطوح باستخدام $(1:1:1:NHO_2:HF:CH_3COOH)$ اذ تم غمر الشرائح بالمحلول وبعد اخراج الشرائح من المحلول يتم

غسلها بالماء المقطر وتجفيفها بورق الترشيح. لغرض تطعيم شرائح (Ge) تم استخدام (2gm) من مادة(Cu) بنقاوة (99.99%) وذلك بترسيب طبقة سمكها(1μm) على الشرائح وقد استخدامت طريقة التبخير الحراري في الفراغ لترسيب (Cu) على مادة (Ge) باستخدام منظومة التبخير الحراري في الفراغ من نوع (Edward Speedvan Unit) وقبل البدء بعملية التبخير يتم تنظيف المنظومة من الداخل تنظيفا" جيدا" لتجنب تلوث الشرائح الشوائب التي تم ترسيبها سابقا وبعدها يتم وضع المادة المراد ترسيبها داخل مسخن مقاوم مصنوع من مادة التنكستن على شكل حويض درجة انصهار عالية يربط الحويض مع قطبين متصلين بمصدر للتيار الكهربائي داخل المنظومة تستخدم لتسخينه وتوضع النماذج المراد الترسيب عليها داخل حامل بصورة عمودية على الحويض وعلى مسافة (10cm) منه ثم نبدأ بزيادة التيار الكهربائي المسلط على أقطاب الحويض تدريجيا حتى تبدأ المادة بالانصهار وبزيادة التيار بالتدريج تبدأ المادة بالتبخير ويبدأ ترسيب(Cu) على مادة (Ge) وبعد الانتهاء من ترسيب المادة يتم تقليل التيار بصورة تدريجية تتم عملية التبخير الحراري تحت ضغط منخفض جداً (10^{-5} Torr) إذ تحتوي منظومة التبخير على مضختين وهي مضخة الميكانيكية (الدوار) (Rotary Pump) وتقوم بإيصال الضغط إلى (10^{-3} Torr) ومضخة الانتشار Diffusion (Pump) وتقوم بإيصال الضغط الى (10^{-5} Torr) كما يلتحق بالمنظومة نوعان من مقاييس الضغط هما (Piraning Gage) ويقيس الضغط العالي ومقياس (Penning Gage) يقيس الضغط الواطئ. تم قصف شرائح شبه الموصل (Ge) المرسب عليها مادة (Cu)، قصفت كل شريحة من الشرائح الثلاثه بأربع نبضات ليزرية وبطاقات مختلفة هي (40,60,80) mJ لغرض اجراء التطعيم، اذ صهرت مادة شبه الموصل الجرمانيوم باستخدام حزمة من ليزر – (Nd YAG) بوجود الشوائب المرسبة فأنتشرت الشوائب ضمن المنطقة المنصهرة تم استخدام تقنية حيود الأشعة السينية لدراسة البنية التركيبية للمادة ولتبيان صحة ما تم أجراءه من تطعيم بالليزر للسطوح البلورية، بواسطة جهاز حيود الأشعة السينية من نوع (Shimadzu) موديل (XRD6000) تم الفحص بالمجهر الضوئي لسطوح (Ge) المطعمة وغير المطعمة بمادة (Cu) وذلك لمعرفة مدى تأثير عملية القصف للشرائح من خلال الرؤية البصرية للتغير الحاصل في السطوح البلورية قبل وبعد التطعيم، ويتكون المجهر المستخدم في الفحص من مصدر ضوئي وعدسات ذات قوة تكبير(X 100-50-25-10) ويربط المجهر بألة تصوير (Camera) خاصة وبدورها تكون مربوطة بحاسوب الكتروني من خلاله يمكن رؤية الصورة على الشاشة ويكون الحاسوب مزود ببرنامج خاص لإظهار الصور لسطوح الشرائح. تم تسجيل قيم التيار المار عبر الكاشف وبفولتية (5V) وبقدرة (100 mW) وتم تعريض الكواشف لأشعة الليزر وقد استخدمت عدة ليزرات وبأطوال موجية مختلفة لقياس الاستجابية الطيفية (10).

المناقشة والنتائج

يبين الشكل (1) بان الجرمانيوم قبل التطعيم ذو تركيب أحادي التبلور وذلك لظهور قمة واحدة ذات شدة عالية في طيف الحيود والتي تمثل الانعكاس عند المستوي (111) ولكن لتأكسد العينة نلاحظ انحراف القمة عند المستوي (220)وقد أظهرت النتائج بعد تطعيم الجرمانيوم بمادة النحاس كما موضح بالشكل (2) وجود تأثير واضح على التركيب البلوري يمكن ملاحظة ذلك أذ تزداد قيمة زوايا الحيود بشكل طفيف مما يؤدي الى زحف القمة نحو الاطوال الموجية العالية وزيادة في عرض المنتصف للمنحني وان المسافات البينية قد قلت بشكل طفيف وهذا يؤكد وجود تأثير واضح للتطعيم كما تظهر النتائج انخفاض في ارتفاع القمة وذلك لنقصان درجة التبلور بسبب التطعيم والنتائج مقاربة لما توصل الية الباحث (11) تم قياس اطياف الامتصاصية والنفاذية (الاشكال 4,3) كدالة للطول الموجي لشرائح الجرمانيوم المطعمة وغير المطعمة ضمن المدى من الاطوال الموجية (2.5 -22 μm)انتشارشائبة النحاس زاد نفاذية الجرمانيوم وقلل الامتصاصية وهذا الاختلاف في قيم النفاذية والامتصاصية يبين نجاح عملية التطعيم السطحي وانتشار النحاس على سطوح الجرمانيوم. والنتائج مقاربة لما توصل الية الباحث (11).

الشكل (5) يوضح عدد من الصور التي تم الحصول عليها باستخدام كاميرا رقمية مربوطة بين المجهر الضوئي والحاسوب لسطوح الشرائح البلورية (Ge) المطعمة وغير مطعمة بمادة (Cu).

الشكل (6) يبين تغير الاستجابية الطيفية مع الطول الموجي عند الأطوال الموجية القصيرة معامل الامتصاص عالي تحدث استجابية عالية ويزداد تهيج الالكترونات من حزمة التكافؤ الى حزمة التوصيل الى ان تصل أعلى استجابية عند طول موجي معين ولكن عند الأطوال الموجية الطويلة (تمتص في المناطق العميقة للجرمانيوم (وينخفض بذلك معامل الامتصاص بسبب اقتراب الفوتونات الساقطة من قيمة فجوة الطاقة ($hv=E_g$) فان الاستجابية ستقترب من التلاشي. وتتفق هذه النتائج مع ما توصل اليه الباحث (12). الشكل (7) يوضح الكفاءة الكمية كدالة للطول الموجي الساقط ومن ليزرات مختلفة على الكواشف الثلاثة من (Ge:Cu)، فكانت أقصى قيمة للكفاءة الكمية عند الطول الموجي(808 nm) هي (56%) وهو الطول الموجي ذاتة الذي كانت عنده أعلى قيمة للأستجابية الطيفية. ان قيمة الكفاءة الكمية تزداد مع زيادة الطول الموجي تبعا لزيادة الاستجابية الطيفية الى ان تصل أعلى قيمة لها وبعد ذلك تهبط الكفاءة الكمية مع هبوط الاستجابية الطيفية والنتائج مقاربة لما توصل اليه الباحث (13).

الشكل (8) يوضح القدرة المكافئة للضوضاء كدالة للطول الموجي الساقط من أشعة الليزر وبأطوال موجية مختلفة لشرائح الكاشف الثلاثة تشير الى أن اقل قدرة مكافئة للضوضاء للكواشف وهي $10^{-10} \times$ (W 0.1, 0.14, 0.6) عند

الطول الموجي نفسه الذي تقع عنده أعلى كفاء كمية وأعلى استجابية طيفية هذه النتائج تتفق مع ما توصل اليه الباحث (11).

يوضح الشكل (9) الكشفية كدالة لطول الموجي التي تعطي أعلى كشفية للكواشف الثلاثة $(0.9, 0.7, 1.6) \times 10^{10}$ W^{-1} عند الطول الموجي (808nm) ويتم قياس الكشفية لغرض تحديد قدرة الكاشف على الكشف وهذه النتائج تتفق مع ما توصل الية الباحث (14). ويوضح الشكل (9) الكشفية النوعية كدالة للطول الموجي الساقط، اذ نلاحظ زيادة في الكشفية النوعية مع الطول الموجي وذلك لانها دالة للاستجابية الطيفية فأنها تتغير مع تغير الاستجابية حتى تصل إلى أفضل كشفية نوعية عند الطول الموجي $(0. 8, 0. 4, 0.3) \times 808nm)$ $(10^{10}cm\,.\,Hz^{1/2}.W^{-1}$ وهو الطول الموجي الذي تم الحصول على أعلى استجابية طيفية وأعلى كفاءة واقل قدرة مكافئة للضوضاء

الاستنتاجات:

1. شرائح (Ge) قبل وبعد التطعيم بمادة النحاس (Cu)هي ذات تركيب أحادي التبلور وأدى التطعيم الى زيادة عرض المنحني لمنتصف القمة في منحني حيود الاشعة السينية مما يعني نقصان المسافات البينية بين السطوح البلورية.
2. كما اظهرت الصور لسطوح الجرمانيوم قبل وبعد التطعيم وجود تغاير لوني واضح على السطوح وهذا بسبب اختلاف التركيب البلوري لسطح الجرمانيوم عند القصف بالليزر.
3. تبين من قياسات الكشفية للكاشف Ge:Cu انه يعمل ضمن مدى طيف الاشعة تحت الحمراء القريبة وان اعلى قمة للاستجابية الطيفية عند الطول الموجي 808 nm وللكواشف الثلاث وان افضل كاشف الذي قصف بشدة طاقة 80 mJ اذ يمتلك اعلى استجابية واعلى كفاءة.

المصادر

[1] J. E. Roth, O. Fidaner, R. K. Schaevitz, E. H. Edwards, Y. H. Kuo, T. I. Kamins, J. S. Harris, D. A. B. Miller, "Optical modulator on Siemploying Ge quantum wells, "Frontiers in Optics 2007, SanJose, CA (2007).
[2] M. A. Gren," Solar Energy Materials & Solar Cells" 92(2008) 1305.
[3] D. Porker, Optical Detectors., Research to Reality, Physics World, Vol.3, No.3, P.52-54 (1990).
[4] S.O.Kasap, "Principles of Electronic Materials and DevicesSnd Ed, Mc. Graw –Hill, New York, (2002).
[5] A. Rogalski, "Quantum well Photoconductors in Infrared Detector Technology ", J. Appl, Phys, 43, (2003).
[6] B. Levine, "Quantum-well Infrared Photodetectors ", Appl. Phys. Pp. (74-81), (1993)..
[7]A. Roglaski," IR Physics and Technology " 45,187,(2002).
[8] M. Razeghi,"Long wavelength infrared detectors", Gordonand Breach science publishers, (1996).
[9] Amoon Yoriv," Optical Electronic", 4th ed, Sunderss College Publishing adivision of Holt, Rinchart and Winston, Inc, 1991
[10] Nada Dh. Mathi,"Fabrication and studying photodetector properties for Garmainum material prepaed by technical thermal evaporation vacancy" MsC Thesis. University of Al. Mustansiriyah (2011).
[11] B. A. Hasan "The Properties of Optical, Electrical AndFabrication of Ge-Au Photoconductor in IR Region" PH.D.THESIS. University of Baghdad (2003).
[12] B. C. Hsu, S. T. Chang P. S. Chen, Z. Pei, and C.W. Liu "A High Efficient 820 nm MOS Ge Quantum Dot Photodetector", IEEE Electron Device Letters, Vol. 24, No. 5, (2002).
[13] Ozcan Bazkir and A. Kamuran Turkoglu, "Determination of Ge photodiode based near infrared detection elementsoptical Responsively ", V. 24, P.56-63 (2010).
[14] A. K. Okyay, Current C. O. Chui, and K. C. Saraswat, " Effective Dark Suppression with Asymmetric MSM Photodetectorsin Group IV Semiconductors," IEEE Photon. Technol. Appl. Phys. Lett. Vol. 88, 063506, (2005).

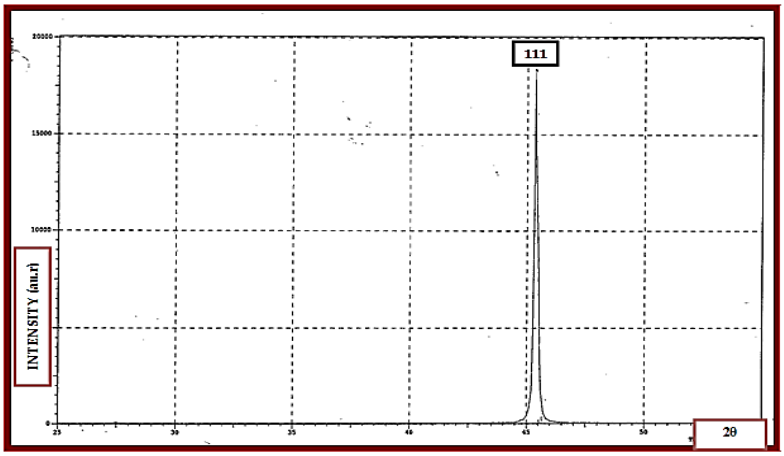

الشكل (1) مخطط حيود الاشعة السينية لشريحة (Ge) الغير مطعمة

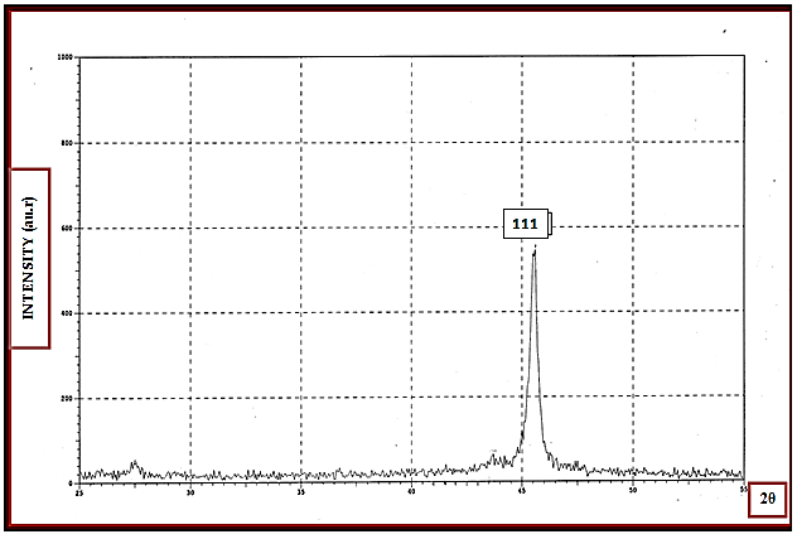

الشكل(2) مخطط حيود الاشعة السينية لشريحة (Ge:Cu) التي قصفت بشدة طاقة (40 mj)

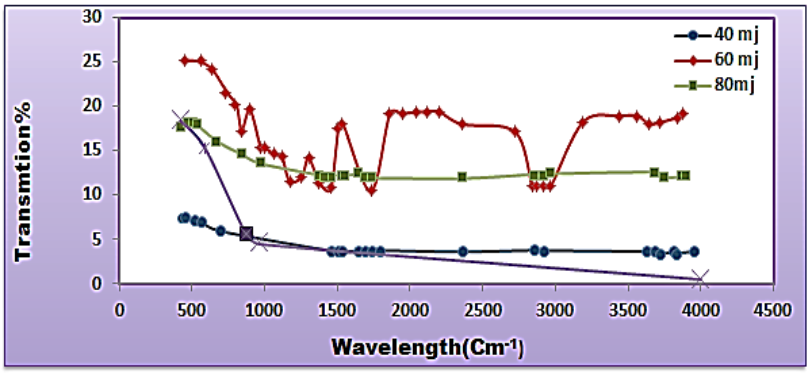

الشكل (3) النفاذية كدالة للعدد الموجي لنماذج Ge المطعمة والغير المطعمة بمادة Cu

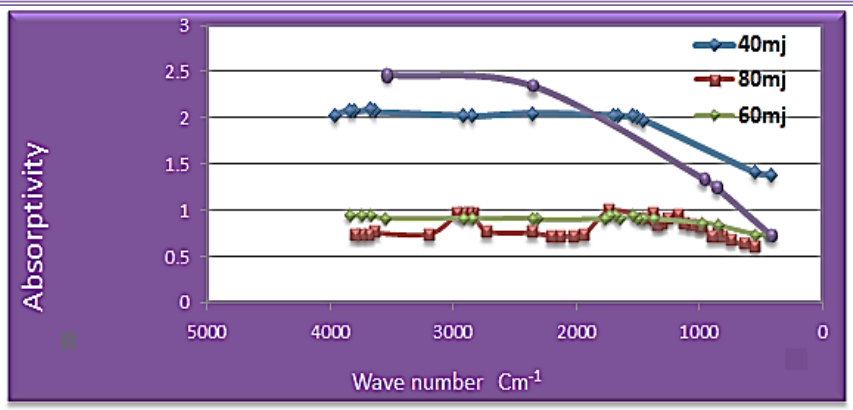

الشكل (4) الامتصاصية كدالة للعدد الموجي لشرائح Ge المطعمة والغير المطعمة Cu

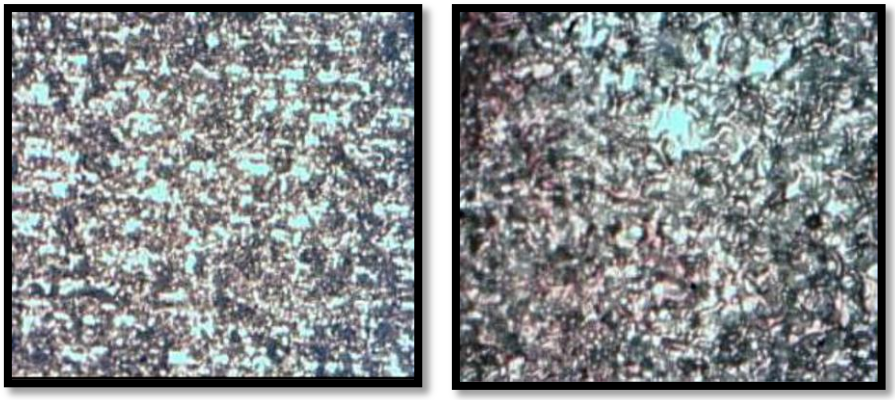

(Ge: Cu: 40mJ) 20x 20x (Ge)

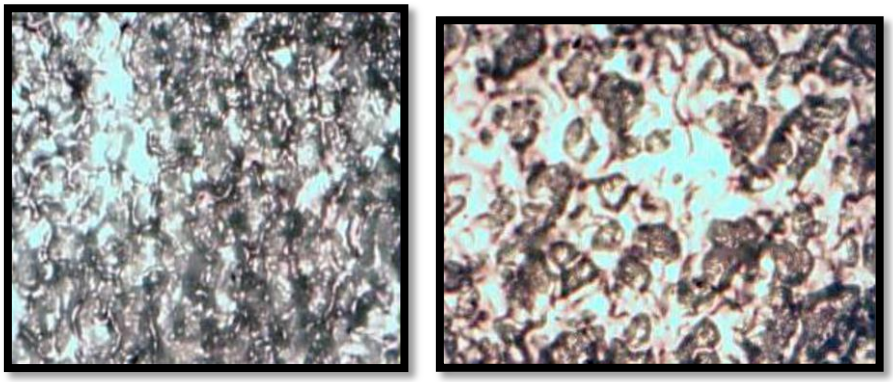

(Ge: Cu: 80mJ) 20x 20x (Ge: Cu: 60mJ)

الشكل (5) صور المجهر الضوئي لسطوح الشرائح البلوري (Ge) قبل وبعد التطعيم

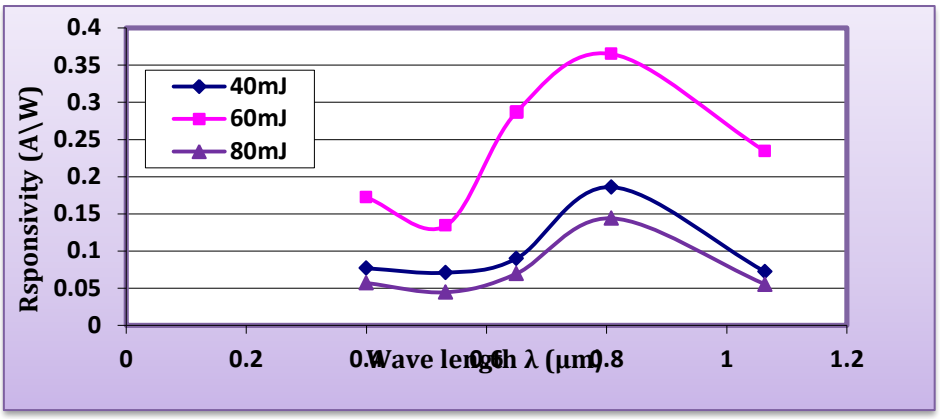

الشكل (6) العلاقة بين الاستجابية والطول الموجي وللكواشف (Ge:Cu) الثلاثة

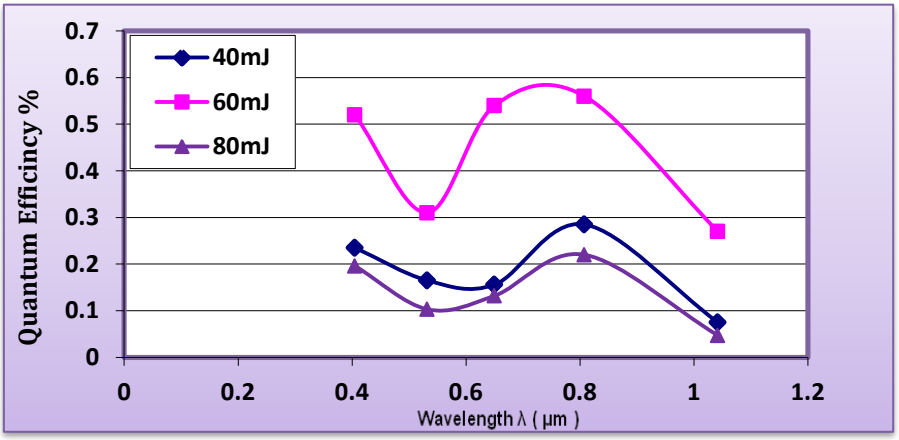

الشكل (7) العلاقة بين الكفاءة الكمية والطول الموجي

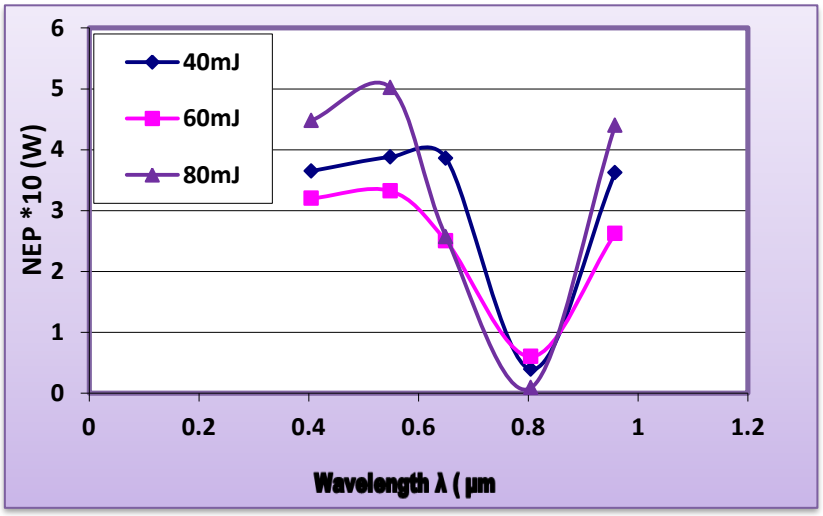

الشكل (8) العلاقة بين القدرة المكافئة للضوضاء والطول الموجي

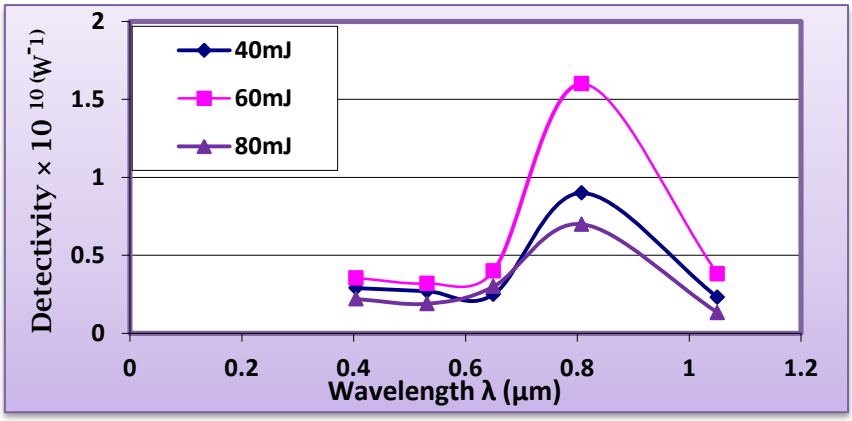

الشكل (9) العلاقة بين الكشفية والطول الموجي للكواشف Ge:Cu

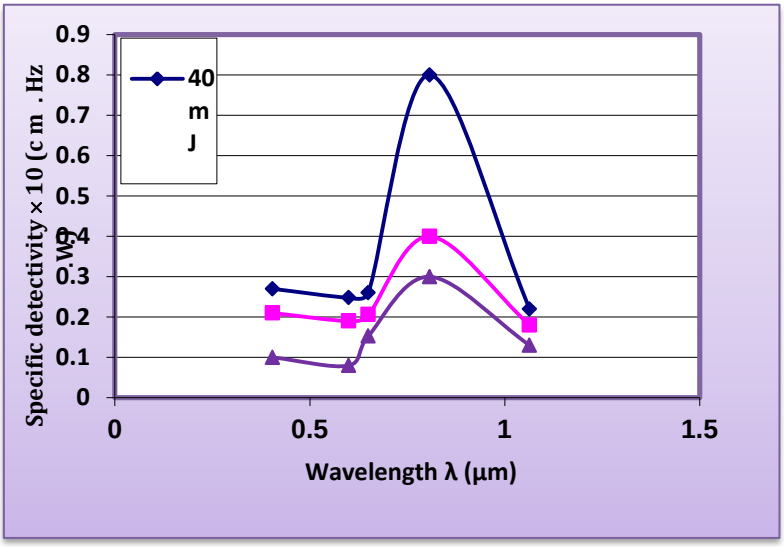

الشكل (10) العلاقة بين الكشفية النوعية والطول الموجي للكواشف Ge:Cu